

**ANALYSIS OF NON-NEWTONIAN BEHAVIOR OF
CRUDE OIL: EXPERIMENTAL STUDY AND
NUMERICAL MODELING USING COMPUTATIONAL
FLUID DYNAMICS (CFD) TECHNIQUE**

By:

Amirabbas Mohammadi

In fulfillment of the requirements of the Doctor of Philosophy in the field
of Chemical Engineering, School of Engineering, College of Agriculture,
Engineering and Science, University of KwaZulu-Natal, Durban, South
Africa

March 2020

Supervisor: Dr Ntandoyenkosi Malusi Mkhize

PREFACE

The investigation or study presented in this thesis was undertaken at the University of KwaZulu-Natal in the School of Engineering, Howard College Campus, Durban, South Africa. This thesis has been submitted as the full requirement for the award of the Doctor of Philosophy (Ph. D) degree in Chemical Engineering. The study presented in this thesis is my original work unless otherwise stated. The thesis has not previously been submitted for a degree or examination at any other tertiary institute or university.


Amirabbas Mohammadi

Signed: 

Date: 03/07/2020

As the candidate's supervisor, I agree to the submission of this thesis.

Dr Ntandoyenkosi Malusi Mkhize

Signed: 

Date: 07 March 2020

DECLARATION 1: PLAGIARISM

I, Amirabbas Mohammadi declare that:

1. The research reported in this thesis, except where otherwise indicated, is my original research.
2. This thesis has not been submitted for any degree or examination at any other university.
3. This thesis does not contain other persons' data, pictures, graphs or other information unless specifically acknowledged as being sourced from other persons.
4. This thesis does not contain other persons' writing unless specifically acknowledged as being sourced from other researchers. Where other written sources have been quoted, then:
 - a. Their words have been re-written but the general information attributed to them has been referenced.
 - b. Where their exact words have been used, then their writing has been placed in italics and inside quotation marks and referenced.
5. This thesis does not contain text, graphics or tables copied and pasted from the Internet, unless specifically acknowledged, and the source being detailed in the thesis and the References sections.

Signed: 

Date: 03/07/2020

DECLARATION 2: PUBLICATIONS

1. An Insight into Waxy Crude Oils Flow Curves Using Shear-Rotary Rheometric Experiments and Power-law Model.
2. Experimental Analysis of Viscosity, Thermal Conductivity and Specific Heat Capacity of Waxy Crude Oil and a Computational Fluid Dynamics (CFD) Study.
3. Numerical Modeling of Simultaneous Distributions of Velocity, Pressure, and Temperature in Waxy Crude Oil Flow Using Computational Fluid Dynamics (CFD) Technique.

Signed: 

Date: 03/07/2020

ACKNOWLEDGMENTS

All thanks to the God of heaven, sovereign Lord over all the nations, for granting me the grace and strength to complete this thesis.

First, I would like to thank my supervisor Dr. Ntandoyenkosi Malusi Mkhize who has been an essential part of my studies at the University of KwaZulu-Natal. Without his invaluable guidance, inspiration, and support, this research would never have come to fruition.

In addition, I am grateful to the experts of Novin Ehya Company in Iran that their guidences, made it possible for me to use their laboratory equipment and facilities in order to obtain the required experimental results. I never forget them and their kindness.

Thanks are also due to all my friends, students and staff members at the University of KwaZulu-Natal, and, in particular, in the Chemical Engineering, for their assistances, supports and collaborations.

Finally, I am sincerely thankful to my beloved parents, wife and children for their tremendous supports, and encouragements throughout my life and especially during these years of studying abroad. Without their love and faith in my abilities, I would never have got to where I am.

ABSTRACT

In modern transmission processes delivering crude oils from the reservoir to refineries and between processing units, because of ambient temperature decrease and heat transfer between the fluid and the pipeline wall and increase in paraffin content, the crude oil may exhibit non-Newtonian behavior. In these cases, engineers and equipment designers need to compensate for the velocity and pressure decrease by optimizing the transmission power, which includes pumps, transmission networks, and heat exchangers. This objective requires the correct prediction of the rheological behaviors of crude oils and the estimation of the distribution of velocity, pressure, and temperature of the flow.

Previous studies on heat transfer and distribution of velocity, pressure, and temperature of non-Newtonian fluids in pipes, channels and between parallel plates, take into account mass and heat transfer phenomena separately. Moreover, these studies ignore the heat loss and merely consider a fully developed flow for the fluid, so that the proposed models do not have the integrated capabilities to calculate the velocity, pressure, and temperature of the fluid, additionally; calculating each of these parameters is limited to a specific area of the flow path.

The main purpose of this study was to present a suitable numerical model to offset the limitations and weaknesses of the proposed models in the literature. The desired numerical model is introduced based on the thermophysical and rheological properties of the Power-law crude oil and considering the heat loss and the dependence of mass transfer and heat transfer.

Taking into account the certain initial and boundary conditions and by a Computational Fluid Dynamics (CFD) technique, the numerical model is simultaneously capable of calculating the distributions of all three variables of the flow including velocity, pressure, and temperature of the Power-law crude oil at different sections of the pipeline.

In this model, shear stresses exerted on crude oil are assumed to be in the 100–600 s^{-1} range. Based on the available samples, two types of paraffinic crude oils with different paraffin contents (7 and 25 wt.%) have been studied as reference crude oils to fulfill the following objectives:

- To analyze the impact of paraffin content on the rheological behavior of paraffinic crude oil
- To present a numerical model to estimate the velocity, pressure, and temperature of paraffinic crude oil flow in a pipeline
- To analyze the effect of paraffin content on the velocity, pressure, and temperature of paraffinic crude oil in different areas of the flow path

- To investigate the numerical model validity and accuracy

Viscosity and flow curves (shear stress-strain rate curves) of each reference crude oil sample were measured in the mentioned shear rate by rheometry using Anton Paar MCR 302.

The decrease in ambient temperature in transmission processes of crude oil from reservoir to refineries and between processing units may occur in a wide range of temperature variations. In this thesis, the temperature variations are limited between 22 and 26 °C. Hence, the non-linearity of the flow curve of each of these fluids indicates that they are non-Newtonian at the temperatures 22 and 26 °C in the 100–600 s⁻¹ range.

For the flow curves approximation and the experimental data matching, the equations of Pseudoplastic fluids, such as Power-law, Herschel– Bulkley, Bingham plastic have been used. Generally, the model of Power-law is the most widely used equation in the literature, which is more suitable for modeling and engineering calculations. Accordingly, by fitting the Power-law model to experimental data of flow curves, the model indices (the consistency index and the flow behavior index) are obtained for both reference crude oils samples.

Furthermore, the thermophysical properties of each reference crude oil sample, including thermal conductivity and specific heat capacity, were measured at the two temperatures.

In the following, by considering a Power-law crude oil flow and given its flow mechanism (Reynolds number), the governing equations including continuity, momentum, and energy equations are nondimensionalized. This numerical model is solved under dimensionless initial and boundary conditions and by a CFD technique at different points of the pipe by MATLAB coding.

In the end, the obtained numerical results for the reference crude oil are compared with those obtained from the models reported in the literature for the same system. The comparison is suggestive of the acceptable accuracy of the numerical model. Besides, the numerical model has the integrated capabilities of the proposed models in the literature.

EXTENDED ABSTRACT

During crude oil transmission from the reservoir to consumers, refineries and between processing units, reduction in ambient temperature, heat transfer between the fluid and the pipeline wall and increase in paraffin content, result in non-Newtonian behavior in the crude oil and decrease of velocity and pressure along the pipe. The non-Newtonian behavior is more pronounced in crude oils with high contents of paraffin, such as heavy crude oils.

To compensate for the velocity and pressure decrease, engineers and processing equipment designers would have to optimize the transmission power, which includes pumps, transmission networks, and heat exchangers. This objective requires the rheological behaviors of crude oils to be predicted correctly along the pipe followed by estimating the distribution of velocity, pressure, and temperature at different pipeline sections. The obtained results can help the processing engineers optimize the transmission equipment and regulate the pipelines.

On the other hand, a review of previous studies on heat transfer and distribution of velocity, pressure, and temperature of non-Newtonian fluids in pipes, channels and between parallel plates reveals the proposed models suffer from serious common weaknesses:

- Considering mass and heat transfer as separate phenomena
- Ignoring heat loss
- Considering a fully developed flow for the fluid

Therefore, the proposed models do not have the integrated capabilities to calculate all three variables of velocity, pressure, and temperature of the fluid flow. Based on these models, calculating each of these parameters is limited to a specific area of the flow path. Additionally, in some of the models that have calculated the fluid flow velocity, only the maximum or average velocity is discussed.

This study was an attempt to present a reliable numerical model based on the rheology of crude oil and solving it by a Computational Fluid Dynamics (CFD) technique to calculate and analyze the distribution of velocity, pressure, and temperature of the fluid along the pipe. The pipe wall temperature is assumed to be mainly affected by the decrease in ambient temperature.

Based on the available samples, two types of paraffinic crude oils with different paraffin contents (7 and 25 wt.%) were studied as reference crude oils to fulfill the followings:

- To analyze the impact of paraffin content on the rheological behavior of paraffinic crude oil

- To present a numerical model to estimate the velocity, pressure, and temperature of paraffinic crude oil flow in a pipeline
- To analyze the effect of paraffin content on the velocity, pressure, and temperature of paraffinic crude oil in different areas of the flow path
- To investigate the numerical model validity and accuracy

The pipe wall temperature and the temperature of the input paraffinic crude oil upon entering the pipe (at the inlet) are, respectively, assumed 22 and 26 °C. Furthermore, shear stresses exerted on the reference crude oil are assumed to be in the 100–600 s⁻¹ range.

In the first step, using Anton Paar MCR 302 rheometer, flow curves were obtained in the said shear rate range for both reference crude oils samples at 22 and 26 °C. The non-linearity of the flow curve of each of these fluids indicates that they are non-Newtonian at the temperatures 22 and 26 °C in the 100–600 s⁻¹ range.

For the flow curves approximation and the experimental data matching, the equations of Pseudoplastic fluids, such as Power-law, Herschel– Bulkley, Bingham plastic are used. Generally, the model of Power-law is the most widely used equation in the literature, which is more suitable for modeling in engineering calculations. Accordingly, by fitting the Power-law model to experimental data from flow curves, the model indices (the consistency index and the flow behavior index) were obtained for both reference crude oils samples at the two temperatures discussed.

Moreover, the thermophysical properties of the fluids, including their thermal conductivities and specific heat capacities, were measured experimentally.

To present the numerical model governing the flow of Power-law crude oil in the pipe, the fluid is assumed to enter a horizontally oriented pipe with length ℓ , diameter $2R$ and wall temperature T_w at uniform velocity v_{in} , pressure P_{in} , and temperature T_{in} . The pipe wall temperature is affected by ambient temperature ($T_w < T_{in}$). The flow is simultaneously developing, that is, velocity and temperature gradients varies along the pipe.

As mentioned earlier, most previous models consider mass and heat transfer to be separate phenomena. In this study, the interdependence of the two is not ignored; therefore, the proposed model is based on both mass and heat transfer. Furthermore, unlike other modeling attempts, the heat loss is considered a critical parameter in calculating the temperature distribution.

The Navier–Stokes equations including continuity, momentum, and energy equations are determined by considering a Power-law crude oil flow with the consistency index k and flow behavior index n . The unknowns are velocity, pressure, and temperature, whereas the input

data (known parameters) include density, viscosity, thermal conductivity, and specific heat capacity of the fluid. Moreover, the computational domain is set in $0 \leq x \leq \ell$ and $0 \leq y \leq 2R$ range.

One difficulty of solving the governing equations is the dependence of the flow behavior index, viscosity, thermal conductivity, and specific heat capacity to temperature. Yet the fluid temperature in the pipe and the computational domain is an unknown parameter. The complexity of the problem lies in the role of temperature. The temperature of the fluid is an unknown variable in the computational domain that appears in the energy equation and must be specified. If the temperature of the fluid is known all across the computational domain, fewer unknowns would remain at hand and the parameters could be calculated at any point throughout the domain (although with some difficulty). However, that is not the case in the present problem, as the temperature distribution is not specified.

In the following, the governing equations including continuity, momentum, and energy equations are nondimensionalized. The dimensionless numbers of Reynolds, Brinkman, and Prandtl are defined based on the flow mechanism, heat loss between the interior surface and its centerline, and momentum flows entering the differential fluid volume. Moreover, dimensionless variables are also introduced, by limiting the flow variables to the 0–1 range.

The said dimensionless numbers and variables make up the dimensionless equations governing the problem. The resulting dimensionless equations are relatively complex and practically unsolvable.

Drawing on CFD techniques, the distribution of dimensionless velocity, pressure, and temperature of two reference crude oils samples can be calculated and analyzed at different points along the pipe.

The finite volume method is a standard CFD technique which is employed in the beginning to discretize the computational domain (solution field) and create a computational grid. Next, the general form of the dimensionless governing equations is considered. By integrating the general equation and discretizing its terms, a suitable algorithm is obtained for discretizing the dimensionless equations governing the problem in the computational grid. Another step in the CFD technique is to solve the system of algebraic equations (obtained by discretizing the equations), which is carried out by the iterative Tri-Diagonal Matrix Algorithm (TDMA) method due to complexity. Accordingly, the velocity and pressure of the Power-law crude oil flow are calculated for all control volumes (CVs) throughout the grid using dimensionless continuity and momentum equations. On the other hand, the flow velocity and pressure are coupled in dimensionless equations. Therefore, before taking the TDMA approach, the Semi-Implicit Method for Pressure-Linked (SIMPLE

algorithm) is used to obtain the correct correlation between flow velocity and pressure (pressure–velocity coupling algorithm).

Calculating the dimensionless temperature for each of the reference crude oils samples using the dimensionless energy equation is contingent upon knowing the dimensionless velocity in any CV of fluid. By substituting the estimated dimensionless velocity in the equation, the dimensionless temperature of the fluid is also determined in any CV of the computational grid.

The distributions of dimensionless velocity, pressure, and temperature estimated for each of the reference crude oils samples are presented by coding in MATLAB.

In the end, the obtained numerical results for the reference crude oil are compared with those obtained from the models reported in the literature for the same system. The comparison is suggestive of the acceptable accuracy of the numerical model. Besides, the numerical model has the integrated capabilities of the proposed models in the literature.

TABLE OF CONTENTS

<u>Content</u>	<u>Page</u>
PREFACE.....	ii
DECLARATION 1: PLAGIARISM.....	iii
DECLARATION 2: PUBLICATIONS	iv
ACKNOWLEDGMENTS	v
ABSTRACT.....	vi
EXTENDED ABSTRACT	viii
TABLE OF CONTENTS.....	xii
LIST OF TABLES	xviii
LIST OF FIGURES	xxi
LIST OF VARIABLES.....	xxiv
GREEK SYMBOLS	xxvii
CHAPTER 1: Theoretical Background.....	1
1.1 INTRODUCTION	2
1.2 DIFFERENT TYPES OF CRUDE OIL.....	3
1.3 PARAFFINS	3
1.4 KEY TEMPERATURES	3
1.4.1 CLOUD POINT	4
1.4.2 GELATION TEMPERATURE	4
1.4.3 POUR POINT	5
1.4.4 MELTING POINT	5
1.5 Paraffin Crystallization	5
1.5.1 Paraffin Crystallization Mechanism.....	5
1.5.1.1 Nucleation.....	5

1.5.1.2 Crystal Growth.....	6
1.5.1.3 Clustering.....	6
1.6 Flow Classification	6
1.6.1 Uniform and Non-Uniform	7
1.6.2 Steady and Unsteady.....	7
1.6.3 Steady and Uniform	7
1.6.4 Steady and Non-Uniform.....	7
1.6.5 Unsteady and Uniform	7
1.6.6 Unsteady and Non-Uniform.....	8
1.6.7 Laminar and Turbulent	8
1.6.8 Fully developed, Simultaneously Developing and Developing.....	8
1.7 Rheology of Viscous Fluids.....	8
1.7.1 Viscosity	9
1.7.1.1 Viscosity of Crude Oil	9
1.7.2 Shear and Yield Stress, Strain and Shear Rate.....	10
1.7.2.1 Stress Components	12
1.7.3 Viscous Fluids.....	13
1.7.3.1 Newtonian Fluid	13
1.7.3.2 Non-Newtonian Fluid	14
1.7.4 Non-Newtonian Crude Oil.....	17
1.7.5 Power-law Model.....	18
CHAPTER 2: LITERATURE REVIEW	20
2.1 Introduction.....	21
2.2 Studies on Flow Variables	21

2.3 Procedure of Simultaneous Determination of Distributions of Velocity, Pressure and Temperature of Flow of Crude Oil along a Pipe	26
CHAPTER 3: FLOW CURVE AND VISCOSITY-SHEAR RATE CURVE	27
3.1 Introduction.....	28
3.2 Rheological Properties of Crude Oil.....	28
3.3 Anton Paar MCR 302.....	29
3.4 Reference Crude Oils	31
3.5 Experimental Procedure.....	31
3.5.1 Experimental Outputs	34
3.5.1.1 Flow Curve and Viscosity-Shear Rate Curve at 26 °C	35
3.5.1.2 Flow Curve and Viscosity-Shear Rate Curve at 22 °C	38
CHAPTER 4: THERMAL CONDUCTIVITY AND SPECIFIC HEAT CAPACITY.....	44
4.1 Introduction.....	45
4.2 Thermal Conductivity and Specific Heat Capacity.....	45
4.3 Flucon GmbH Measuring System.....	46
4.3.1 Measuring System Components	46
4.4 Experimental Procedure.....	46
4.4.1 Experimental Results	49
CHAPTER 5: NUMERICAL MODEL, INITIAL AND BOUNDARY CONDITIONS	51
5.1 Introduction.....	52
5.2 Fluid Flow Mechanism	52
5.3 Assumptions for Measured Parameters.....	53
5.4 Numerical Model	54
5.4.1 Governing Equations	55
5.4.2 Initial and Boundary Conditions.....	61

CHAPTER 6: DIMENSIONLESS NUMERICAL MODEL.....	62
6.1 Introduction.....	63
6.2 Dimensionless Numbers	63
6.2.1 Generalized Reynolds Number	63
6.2.2 Prandtl Number	64
6.2.3 Brinkman Number	65
6.3 Dimensionless Variables.....	65
6.4 Dimensionless Form of Governing Equations	67
6.5 Modified Governing Dimensionless Equations	67
6.6 Dimensionless Initial and Boundary Conditions.....	68
CHAPTER 7: COMPUTATIONAL FLUID DYNAMICS (CFD) TECHNIQUE.....	69
7.1 Introduction.....	70
7.2 Finite-Volume Method.....	71
7.2.1 Computational Domain Discretization	73
7.3 General Equation.....	73
7.3.1 Integration of General Equation.....	75
7.3.1.1 Discretization of Convective Term Integral	75
7.3.1.2 Discretization of Diffusion Term Integral	76
7.3.1.3 Discretization of Source Term Integral	76
7.3.2 SIMPLE Algorithm.....	78
7.3.2.1 Collocated Grid	79
7.3.2.2 Non-Collocated Grid	81
7.3.2.3 Corrected Pressure and Velocity.....	82
7.3.3 Tri-Diagonal Matrix Algorithm	85
7.4 Flowchart for Solving Equations by SIMPLE and TDMA Algorithms.....	87

CHAPTER 8: VELOCITY, PRESSURE AND TEMPERATURE DISTRIBUTIONS.....	88
8.1 Introduction.....	89
8.2 Convergence and Rate of Solution.....	90
8.2.1 Optimal Number of CVs.....	90
8.3 Distributions of Velocity, Pressure and Temperature	91
8.3.1 Distribution of Flow Velocity.....	92
8.3.1.1 Dimensionless Velocity Distribution at Pipe Inlet.....	92
8.3.1.2 Dimensionless Velocity Distribution near Pipe End	94
8.3.1.3 Effect of Flow Behavior Index and Reynolds Number on Dimensionless Velocity Distribution in Inlet Region.....	97
8.3.1.4 Effect of Flow Behavior Index and Reynolds Number on Dimensionless Velocity Distribution near Pipe End	98
8.3.2. Dimensionless Pressure Distribution	99
8.3.2.1 Effect of Flow Behavior Index and Reynolds Number on Dimensionless Pressure Distribution.....	101
8.3.3 Distribution of Dimensionless Temperature.....	103
8.3.3.1 Dimensionless Temperature Distribution in Inlet Region and near Pipe Wall for Flow of Reference Crude Oil Sample B	103
8.3.3.2 Dimensionless Temperature Distribution at End and near Pipe Wall for Flow of Reference Crude Oil Sample B	104
8.3.3.3 Dimensionless Temperature Distribution in Inlet Region and near Pipe Wall for Flow of Reference Crude Oil Sample A.....	105
8.3.3.4 Dimensionless Temperature Distribution in Pipe End Region and near Pipe Wall for Flow of Reference Crude Oil Sample A.....	107
8.3.3.5 Effect of Flow Behavior Index and Reynold number on Dimensionless Temperature Distribution.....	109
CHAPTER 9: VALIDITY OF NUMERICAL MODEL	112

9.1. Introduction.....	113
9.2. Validity of Numerical Model.....	113
9.2.1. Velocity of Power-law Crude Oil.....	113
9.2.2. Temperature of Power-law Crude Oil.....	114
9.2.3. Pressure Drop in Flow of Power-law Crude Oil.....	115
CHAPTER 10: CONCLUSION AND RECOMMENDATIONS	117
10.1. Experimental Conclusions	118
10.2. Numerical Conclusions	118
REFERENCES	123

LIST OF TABLES

<u>Table</u>	<u>Page</u>
Table 1.1 Specifications of a crude oil sample under viscosity measurement	10
Table 3.1 Anton Paar MCR 302 specifications.....	30
Table 3.2 Physicochemical properties of reference crude oils	31
Table 3.3 Specifications of Anton Paar MCR	32
Table 3.4 Settings for conducting a shear-rotary test.....	33
Table 3.5 Experimental flow curves data for reference crude oils A and B at 26 °C.....	36
Table 3.6 Power-law indices for reference crude oils A and B at 26 °C	37
Table 3.7 Power-law equations for reference crude oils A and B at 26 °C	37
Table 3.8 Experimental viscosity-shear rate curve data for reference crude oils A and B	38
Table 3.9 Experimental flow curves data for reference crude oils A and B at 22 °C	40
Table 3.10 Power-law indices for reference crude oils A and B at 22 °C	41
Table 3.11 Power-law equations for reference crude oils A and B at 22 °C	41
Table 3.12 Experimental viscosity-shear rate curves data for reference crude oils A and B..	43
Table 4.1 Technical data used in experimental procedure (Using Flucon GmbH measurement system).....	49
Table 4.2 Thermal conductivity and specific heat capacity measured at temperatures 26 °C and 22 °C for reference crude oils	50
Table 6.1 Prandtl number ranges for some fluids	64
Table 6.2 Variables of relations (6.4) to (6.14).....	66
Table 8.1 Input data	89
Table 8.2 Number of CVs in calculations.....	91
Table 8.3 Calculated results for dimensionless velocity of reference crude oil B between inner surface and centerline of pipe at multiple points in inlet region	92

Table 8.4 Numerical results for dimensionless velocity of reference crude oil A between inner surface and centerline of pipe at multiple points in inlet region	93
Table 8.5 Numerical results for dimensionless velocity of reference crude oil B between inner surface and centerline of pipe at multiple points near pipe end	95
Table 8.6 Numerical results for dimensionless velocity of reference crude oil A between inner surface and centerline of pipe at multiple points near pipe end	96
Table 8.7 Comparison of numerical results for dimensionless velocities of reference crude oils A and B between inner surface and centerline of pipe at multiple points in inlet region.....	97
Table 8.8 Comparison of numerical results for dimensionless velocities of reference crude oils A and B from an area in the vicinity of inner surface to centerline at multiple points at pipe end.....	98
Table 8.9 Numerical results for dimensionless pressure of reference crude oil B near pipe wall at multiple points along pipe.....	100
Table 8.10 Numerical results for dimensionless pressure of reference crude oil A near pipe wall at multiple points along pipe.....	101
Table 8.11 Comparison of numerical results for dimensionless pressures of reference crude oils A and B in the vicinity of inner surface of pipe at multiple points along pipe	102
Table 8.12 Numerical results for temperature distribution of reference crude oil sample B near pipe wall, at multiple points in inlet region	104
Table 8.13 Numerical results for temperature distribution of reference crude oil sample B near pipe wall, at multiple points near pipe end	105
Table 8.14 Numerical results for temperature distribution of reference crude oil sample A near pipe wall, at multiple points in inlet region	106
Table 8.15 Numerical results for temperature distribution of reference crude oil sample A near pipe wall, at multiple points near pipe end	107
Table 8.16 Comparison of numerical results for dimensionless temperature distribution of reference crude oils A and B between inner surface and centerline of pipe at multiple points in inlet region.....	109

Table 8.17 Comparison of numerical results for dimensionless temperature distribution of reference crude oils A and B from an area in the vicinity of inner surface to centerline at multiple points at pipe end.....	110
Table 9.1 Comparison of maximum dimensionless velocities of reference crude oils A and B on centerline between present study and those obtained from Skelland's study.....	114
Table 9.2 Comparison of dimensionless temperatures of reference crude oils A and B on centerline between present study and those obtained from Chhabra et al.'s study	115
Table 9.3 Comparison of dimensionless pressure drop of reference crude oil B in the vicinity of wall/plate inner surface between present study and those obtained from Etemad et al.'s study	116

LIST OF FIGURES

<u>Figure</u>	<u>Page</u>
Figure 1.1 Variation of cloud point in terms of pressure changes	4
Figure 1.2 Impact of cloud point on the viscosity of oil sample	10
Figure 1.3 Schematic view of shear flow in a fluid	11
Figure 1.4 Components of stress exerted on a fluid element	13
Figure 1.5 Flow curves of Newtonian and non-Newtonian fluids.....	16
Figure 1.6 Flow curves of non-Newtonian fluids.	16
Figure 2.1 f.Re for flow of Power-law fluid between parallel plates with flow behavior index n=1 (Etemad et al., 1994).	24
Figure 2.2 f.Re for flow of Power-law fluid between parallel plates with flow behavior index n=0.5 (Etemad <i>et al.</i> , 1994).	24
Figure 2.3 Dimensionless maximum velocity of Power-law fluid flow on centerline with flow behavior index n=1 (Etemad <i>et al.</i> , 1994).	25
Figure 2.4 Dimensionless maximum velocity of Power-law fluid flow on centerline with flow behavior index n=0.5 (Etemad <i>et al.</i> , 1994).	25
Figure 2.5 Flowchart for determination of distributions of velocity, pressure and temperature of flow of crude oil along a pipe.....	26
Figure 3.1 Anton Paar MCR 302 / Peltier temperature control, UV curing system and computer.	29
Figure 3.2 Anton Paar MCR 302 / Physical components	33
Figure 3.3 Schematic view of Peltier temperature control.....	34
Figure 3.4 Flow curve for reference crude oil B at 26 °C.....	35
Figure 3.5 Flow curve for reference crude oil A at 26 °C.....	35
Figure 3.6 Viscosity-shear rate curve for reference crude oils A and B at 26 °C	37
Figure 3.7 Flow curve for reference crude oil B at 22 °C	39

Figure 3.8 Flow curve for reference crude oil A at 22 °C.....	39
Figure 3.9 Viscosity-shear rate curve for reference crude oils A and B at 22 °C	41
Figure 4.1 Flucon GmbH measuring system /Electronic unit and sensor	47
Figure 4.2 Screw-on cup	47
Figure 4.3 Omega thermostat.....	48
Figure 5.1 Horizontal pipe with wall temperature T_w in which reference crude oil flows.....	55
Figure 5.2 Fluid element with differential volume $\Delta x \Delta y \Delta z$	56
Figure 5.3 Velocity, temperature, and pressure of fluid at pipe inlet / Velocity and temperature of fluid over inner surface of pipe	61
Figure 7.1 General three-dimensional CV and location of nodes neighboring general node .	72
Figure 7.2 Computational domain discretization	73
Figure 7.3 Collocated grid	80
Figure 7.4 CV in a collocated grid.....	80
Figure 7.5 Non-collocated grid and location of velocity and pressure CVs	82
Figure 7.6 Velocity CVs in a non-collocated grid	83
Figure 7.7 Flowchart for Solving Equations by SIMPLE and TDMA Algorithms	87
Figure 8.1 Velocity distribution of reference crude oil B on centerline from start to pipe end against number of CVs	91
Figure 8.2 Dimensionless velocity distribution near inlet from inner surface to centerline in reference crude oil B	93
Figure 8.3 Dimensionless velocity distribution near inlet from inner surface to centerline in reference crude oil A	94
Figure 8.4 Dimensionless velocity distribution at pipe end from inner surface to centerline in reference crude oil B	95
Figure 8.5 Dimensionless velocity distribution near pipe end from inner surface to centerline in reference crude oil A	96

Figure 8.6 Comparison of dimensionless velocity distribution of reference crude oils A and B in pipe inlet region, between pipe wall and centerline.....	97
Figure 8.7 Comparison of dimensionless velocity distribution of reference crude oils A and B near pipe end, between pipe wall and centerline	99
Figure 8.8 Dimensionless pressure distribution along pipe running reference crude oil B ..	100
Figure 8.9 Dimensionless pressure distribution along pipe running reference crude oil A ..	101
Figure 8.10 Comparison of dimensionless pressure in flow of reference crude oils A and B near wall and along pipe.....	102
Figure 8.11 Dimensionless temperature distribution for reference crude oil sample B in inlet region and near pipe wall	104
Figure 8.12 Temperature distribution for reference crude oil sample B in pipe end region and near inner surface	105
Figure 8.13 Temperature distribution for reference crude oil sample A in inlet region and near inner surface of pipe wall	106
Figure 8.14 Temperature distribution for reference crude oil sample A in pipe end region and near inner surface	108
Figure 8.15 Comparison of dimensionless temperature distribution of reference crude oils A and B in pipe inlet region, between pipe wall and centerline.....	109
Figure 8.16 Comparison of dimensionless temperature distribution in reference crude oils A and B near pipe end, between wall and centerline.....	111
Figure 9.1 Comparison of dimensionless pressure drop of reference crude oil sample B in the vicinity of inner surface of pipe wall from present study with dimensionless pressure drop in the vicinity of plate inner surface from Etemad <i>et al.</i> 's study.....	116

LIST OF VARIABLES

Surface area of parallel plates	A
Brinkman number	Br
Specific heat capacity	C_p
Fluid specific heat capacity at pipe inlet	$C_{p,in}$
Dimensionless specific heat capacity	C^*_p
Space between two plates	D_h
Fluid pressure drop	dP
Force exerted on upper plate	F
Gravitational acceleration on Earth in x-direction	g_x
Gravitational acceleration on Earth in y-direction	g_y
Gravitational acceleration on Earth in z-direction	g_z
Consistency index or Strength factor of fluid	K
Thermal conductivity	K
Fluid thermal conductivity at pipe inlet	K_{in}
Dimensionless thermal conductivity	K^*
Pipe length	ℓ

Distance traveled	L
Flow behavior index or Power-law index	N
Fluid pressure	P
Péclet number	Pe
Fluid pressure at pipe inlet	P_{in}
Prandtl number	Pr
Dimensionless fluid pressure	p^*
Speculative pressure	P_{spec}
Modified fluid pressure	\acute{P}
Pipe radius	R
Reynolds number	Re
Radial distance from centerline	R
Source	S
Fluid temperature	T
Fluid temperature at pipe inlet	T_{in}
Pipe wall temperature	T_w
Time	T
Fluid velocity in x-direction	u

Maximum velocity in x-direction	u_{\max}
Slip velocity on pipe wall in x-direction	u_{slip}
Dimensionless fluid velocity in x-direction	u^*
Speculative velocity in x-direction	u_{spec}
Modified velocity in x-direction	u'
Fluid velocity in y-direction	v
Fluid velocity at pipe inlet or entry velocity of fluid	v_{in}
Slip velocity on pipe wall in y-direction	v_{slip}
Dimensionless fluid velocity in y-direction	v^*
Speculative velocity in y-direction	v_{spec}
Modified velocity in y-direction	v'
Distance on longitudinal axis (horizontal)	x
Dimensionless distance on longitudinal axis (horizontal)	x^*
Distance on transverse axis (vertical)	y
Dimensionless distance on transverse axis (vertical)	y^*

GREEK SYMBOLS

Under-relaxation factor of pressure	α_p
Under-relaxation factor of velocity in x-direction	α_u
Under-relaxation factor of velocity in y-direction	α_v
Strain rate	γ
Shear rate	$\dot{\gamma}$
Thermal diffusivity	Γ
Kronecker delta	δ_{ij}
Dimensionless temperature	θ
Apparent viscosity	μ
Fluid viscosity at pipe inlet	μ_{in}
Dimensionless apparent viscosity	μ^*
Density	ρ
Fluid density at pipe inlet	ρ_{in}
Dimensionless density	ρ^*
Shear stress	τ
Yield stress	τ_o
Wall shear stress	τ_w

Dependent variables

φ

CHAPTER 1

Theoretical Background

1.1 Introduction

The scope of research in the field of crude oil is various when the fluid shows non-Newtonian behavior. This extended scope is due to the dependence of the fluid rheological behavior on important variables such as viscosity, shear stress, shear rate, environmental conditions, and temperature. Besides, the dependence of these variables with each other and their dependence on the physical or geometric characteristics of the problem has doubled the scope of the research.

Crude oil, with all its different forms and properties, is a mixture of light hydrocarbons (Benzene, Toluene, Xylene) as solvents and heavy hydrocarbons (Paraffins, Asphaltenes, Aromatics, Naphthenes, and Resins) as solutes.

The solubility of heavy hydrocarbons in crude oil depends very strongly on temperature. Under the temperature conditions in a reservoir (70–150 °C), the solubility of the heavy hydrocarbons is so high that it can be fully dissolved, thus forming a low-viscosity fluid. Among these, the solubility of paraffin and other solutes affecting their solubility in each step of production, storage, and transmission are essential for engineers and designers of processing equipment in the oil industries. In each of these processes, reducing the solubility of the hydrocarbon causes the change in the behavior of crude oil and may lead to the accumulation of the paraffin deposits at the wellbore, near the well, in ground-surface facilities, and the pipelines during transmission.

The temperature of the environment may be reduced during crude oil transfer from a reservoir to consumption centers and refineries or between processing units, especially during marine fluid transport. Consequently, the fluid temperature is also reduced due to heat transfer between the flowing crude oil and the pipeline wall. The kinetic energy of molecules is decreased as crude oil temperature is reduced, leading to a decrease in solubility of paraffin.

As crude oil temperature decreases to cloud point or lower temperatures, successive crystallization of paraffin will lead to bonds between paraffin crystals. In other words, the dissolved paraffin in crude oil is saturated; leading to an increase in the apparent viscosity of the fluid and a decrease in the velocity and pressure of the flow. This phenomenon in crude oils is more evident at high paraffin concentrations such as heavy oils.

Due to the increase in the apparent viscosity and the decrease in velocity and pressure, the crude oil transmission from the reservoir to consumption centers and refineries and between processing units is difficult.

It is necessary to boost the power of transmission equipment including pumps, pipeline networks, and heat exchangers (to improve the heat transfer efficiency) to compensate for the decrease in the velocity, and pressure of the crude oil flow. To achieve this, first, a realistic estimation of the flow velocity, pressure, and temperature at various sections of the flow path is required based on the correct description of the rheological behavior of the fluid (Adeyanju and Oyekunle, 2012).

1.2 Different Types of Crude Oil

Based on its content of each constituent, crude oil can be classified into paraffin, paraffin–naphthenic and aromatic groups.

- 1) Paraffinic crude oil
- 2) Paraffin–Naphthenic Crude Oil
- 3) Aromatic Crude Oil

1.3 Paraffins

Paraffins usually include the following groups (Lira-Galeana *et al.*, 1996):

- Normal paraffin
- Branched paraffin
- Cycloparaffins

Paraffin is a saturated hydrocarbon that has no tendency for addition reactions and has all its carbon atoms paired in single bonds. In other words, single bonds are characteristics of this hydrocarbon (Bishop *et al.*, 1995; Lira-Galeana *et al.*, 1996).

1.4 Key Temperatures

In general, three temperatures are of great significance, all of which depend on the composition of crude oil.

1.4.1 Cloud Point

The temperature at which, a paraffinic network forms due to paraffin crystallization. This paraffinic network is also known as wax. (Elsharkawy *et al.*, 1999). In other words, the nucleation of paraffin crystals begins at the temperature.

Fig. 1.1 illustrates the changes in the cloud point in an experiment, suggesting that large deviations in pressure incur small changes in the temperature.

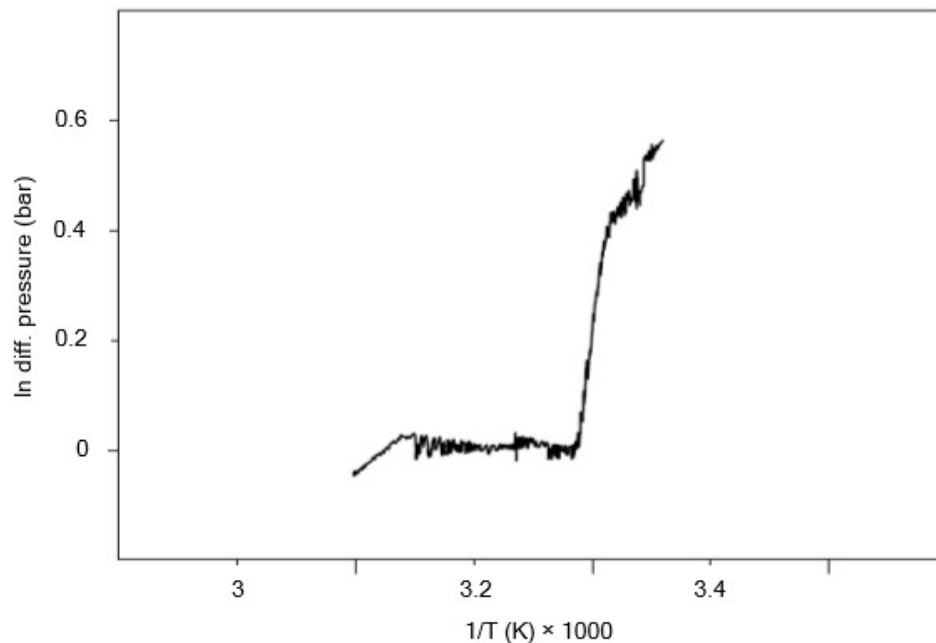


Figure 1.1 Variation of cloud point in terms of pressure changes (Pedersen *et al.*, 1991)

Fig. 1.1 illustrates the relation between pressure variations and a cloud point in a laboratory setting.

1.4.2 Gelation Temperature

As defined by Venkatesan *et al.* (2002), the gelation temperature is where the solid-like behavior of crude oil dominates over its liquid-like behavior. At this point, the viscosity and specific gravity of the liquid increase.

1.4.3 Pour Point

The temperature where the mixture, poured in a vessel, does not flow when kept horizontal. This point is of great industrial significance. The pour point of crude oil is the lowest temperature at which the fluid can flow under standard conditions. Credible international institutions for measuring this temperature proposed standard methods.

The ASTM D-97 standard procedure is employed to measure the pour point of crude oil. In this method, the sample is cooled down at a specific rate and is tested at 3 °C intervals to evaluate its behavior. The lowest point at which motions are found in the fluid is reported as a pour point (Zuo *et al.*, 2001). At pour point, crude oil is supersaturated with wax, which is manifested by a drastic increase in viscosity (Ajienka *et al.*, 1995).

1.4.4 Melting Point

The temperature at which a pure substance turns to liquid. For a pure substance, the cloud point and melting point are equal, but they are slightly different for a mix (Pedersen *et al.*, 2006).

1.5 Paraffin Crystallization

Crystallization generally is the separation of a solid (crystal) from a homogeneous solution.

The temperature can accelerate or hinder paraffin crystallization in crude oil.

1.5.1 Paraffin Crystallization Mechanism

Paraffin crystallization takes place in three steps as follows:

- Nucleation
- Crystal growth
- Clustering

1.5.1.1 Nucleation

Crystal nucleation is carried out through two-molecule reactions and, therefore, clustering of soluble monomers. After an optimal number of monomers are chained together, a critically sized cluster of them forms. Further attachment of monomers to the cluster results in nucleation and growth (Won, 1986).

In crude oil, paraffin dissolves in light hydrocarbon solvents. Molecular interactions of paraffin are affected by changes in temperature and increase by bringing the temperature down. In cases where intermolecular forces of paraffin become larger than paraffin–solvent interactions, paraffin molecules join and form a crystal nucleus.

1.5.1.2 Crystal Growth

Crystal growth takes place at sites where surface adhesion energy between the crystal and free paraffin is the highest. The phenomenon is often faster on lateral faces. At these points, paraffin crystals grow in both size and number with a three-dimensional structure expanding throughout the bulk of the oil. Paraffins can crystallize in various forms and regular structures. The structures can be composed of a single or multiple molecular layers. In multi-layer structures, molecular chains stack in parallel and a zigzag configuration (Won, 1986).

1.5.1.3 Clustering

In general, in deposition or crystallization, clustering is an important particle growth mechanism. Particle clustering proceeds in parallel to crystal growth. The nuclei, after formation, can grow by two mechanisms. Particles can grow and form the more massive clusters on their own or by collision. However, it is challenging to distinguish clustering from crystal growth. An analysis of the particle size distribution under static or dynamic conditions reveals a combination of both mechanisms (Won, 1986).

1.6 Flow Classification

In most industries handling fluids, including the oil and gas sector, the design of an extended range of models and estimations are contingent upon identifying the type of flow on which calculations and the type of the processes are based. Therefore, identifying flow types is essential and this chapter aims to discuss them briefly. The flow may be uniform, steady and laminar or else.

1.6.1 Uniform and Non-Uniform

The flow is uniform when, at any specific moment, the velocity is identical at all points throughout the fluid in terms of magnitude and direction. If velocity changes from one point to another, the flow is said to be non-uniform. In practice, when the fluid passes a solid boundary, there will be velocity differences in areas limited by the boundary. However, for a flow region of fixed size and shape, the flow is considered to be uniform.

1.6.2 Steady and Unsteady

The flow is said to be steady when the flow velocity, pressure, and region remain unchanged with time, although they can be different from point to point. The steady flow is also referred to as permanent flow. In other words, in the steady state, the kinetics of the problem is ignored. Now, if fluid states change with time at a specific point, the flow is said to be unsteady.

1.6.3 Steady and Uniform

In this type of flow, fluid states do not change with time and across the flow, and the velocity and flow cross-section remain unchanged in every region. For example, the flowing liquid travels at a fixed velocity in an overflowing, uniform pipe (with a uniform hole).

1.6.4 Steady and Non-Uniform

This flow is characterized by changing states from one point to another but not overtime. Flow velocity and cross-section can change from one region to another, but they remain unchanged

with time. An example would be the flow of a liquid at a fixed discharge rate in an overflowing, incrementally narrowing pipe.

1.6.5 Unsteady and Uniform

At any specific moment, all points are at equal velocity but one that changes with time. For example, the accelerating flow of a liquid passing a uniform, overflowing pipe. Similar to the situation where a pump starts.

1.6.6 Unsteady and Non-Uniform

Flow velocity changes from one region to another and changes with time. For example, waves passing through a pipe.

1.6.7 Laminar and Turbulent

Two distinct types of flow can be established based on Osborne Reynolds' observations of the discharge of water from a glass pipe draining a tank in 1883.

In case inertial forces are dominant in a moving fluid, the flow is most likely turbulent. In this case, fluid particles do not exhibit normal behavior but have different relative states. However, if viscous forces are dominant, the flow is laminar. Fluid particles in the laminar flow also referred to as viscous flow, have regular behavior and remain in similar relative states in consecutive regions.

1.6.8 Fully developed, Simultaneously Developing and Developing

In classical fluid dynamics, a flow is said to be fully developed when the velocity and temperature gradients remain unchanged. When none of the parameters is developed, the flow is said to be simultaneously developing. In the case of developed velocity and developing temperature, the flow is thermally developing (Hamilton and Crosser, 1962).

1.7 Rheology of Viscous Fluids

Rheology investigates the flow and deformation of fluids including gases and liquids, under external stress. Identifying rheological relations governing fluids helps change their behavior to comply with our requirements while identifying their properties.

In recent years, rheology has attracted much research focus. In some cases, the calculations of the flow of oil products require a knowledge of the fluid rheology (including the viscosity and exerted stress) and considering them.

1.7.1 Viscosity

Generally, viscosity is the resistance of a fluid against flowing and is a result of internal friction between molecules. The higher the viscosity, the higher the resistance of the fluid against flowing. From a rheological perspective, viscosity is a measure of fluidity for evaluating the resistance of a fluid to deformation.

For most liquids, temperature and pressure variations have a direct and reverse effect on viscosity, respectively. As a result, the temperature increase leads to a reduction in viscosity and an increase in pressure increases the viscosity. For gases, on the other hand, the temperature and pressure directly affect viscosity. The higher the viscosity of a fluid, the higher its resistance to flowing or being pumped. A solid can be assumed to be a fluid whose viscosity approaches infinity (Gilby, 1993).

1.7.1.1 Viscosity of Crude Oil

The viscosity of crude oil is of great significance as regards its movements in reservoirs, its production from reservoirs and designing transmission pipelines and refining processes. In this regard, the velocity, pressure and temperature distribution of the fluid are significant.

Under the temperature and pressure conditions of the reservoir, the solubility of potential heavy hydrocarbons is high enough to keep them entirely dissolved in crude oil, thus allowing it to behave similarly to a low-viscosity fluid. During extraction from the reservoir, pressure drops and the dissolved gases in oil leave the fluid. Thus resulting in a continuous change in the composition of the crude oil as the fluid becomes denser and more viscous (Beggs and Robinson, 1975).

During transmission through pipelines, as the temperature decreases to the cloud point, the crude oil is saturated with wax. At this point, viscosity increases. A further decrease in the temperature to pour point makes the crude oil supersaturated with wax, drastically increasing the fluid viscosity.

The figure below compares the measured viscosity of a crude oil sample with the specifications in **Table 1.1** with the results obtained from Bennison's equation (Bennison, 1998) to show the effect of the cloud point on the viscosity (Glaso, 1980).

Table 1.1 Specifications of a crude oil sample under viscosity measurement (Glaso, 1980)

API	Pour point	Cloud point
20.02	25	115

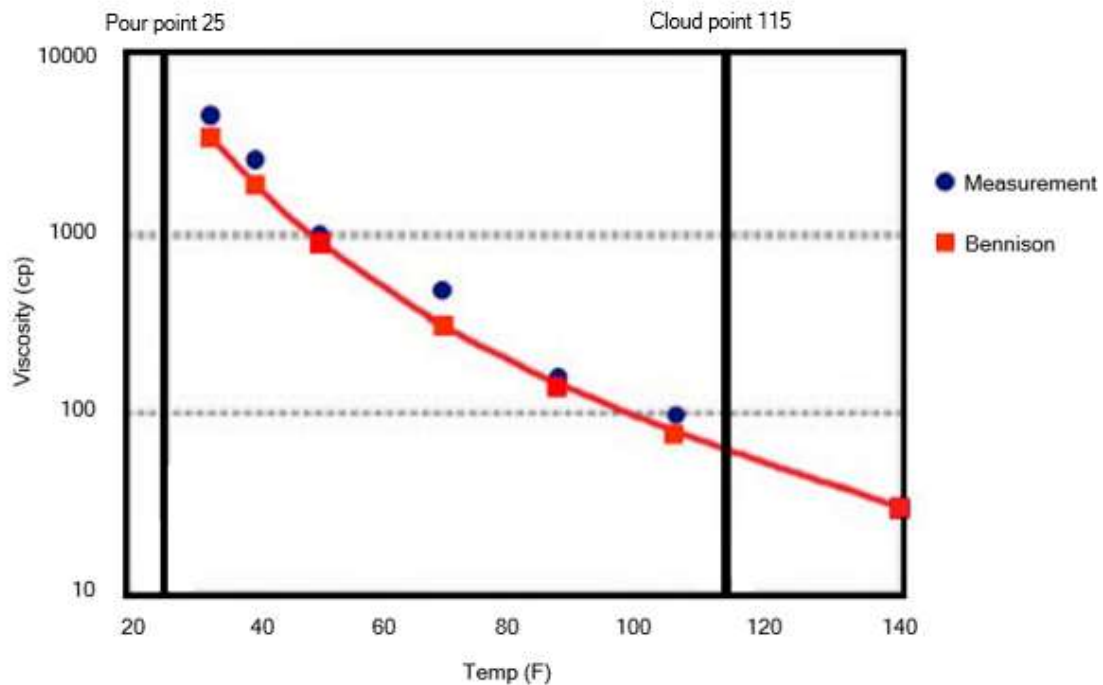


Figure 1.2 Impact of temperature on the viscosity of oil sample (**Table 1.1**) (Glaso, 1980)

1.7.2 Shear and Yield Stress, Strain and Shear Rate

Let us assume a fluid sandwiched between two parallel plates of area A that are spaced by dh under steady conditions (constant temperature and pressure) (Fig. 1.3).

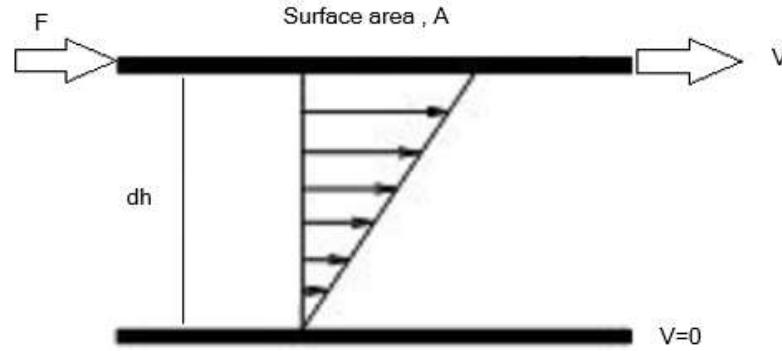


Figure 1.3 Schematic view of shear flow in a fluid (Barnes *et al.*, 1991)

The bottom plate is fixed, but the one on the top can move at a velocity of dv when the force F is exerted on it. Parallel plate viscometers can be named as an example of such a configuration. The top layer of the fluid moves at the velocity of plate (dv) but the underlying layers move at lower speeds. Each layer on top drags the layer beneath, thus resulting in a decreasing velocity profile from top to bottom. Furthermore, the layer adjacent to the bottom plate is stagnant ($dv=0$). Therefore, a velocity gradient (dv/dh) is established in the fluid. According to the definition of velocity, which is the distance traveled (L) in unit time, it can be written:

$$v = \frac{dL}{dt} \quad (1.1)$$

The force exerted on unit area of a body is referred to as stress and is measured in N/m^2 or Pa in SI units. Shear stress is the tangential stress exerted on a body (Barnes *et al.*, 1991):

$$\tau = \frac{F}{A} \quad (1.2)$$

Deformation in a fluid is the result of shear stresses. Accordingly, under shear stress, regardless of its magnitude, a fluid undergoes permanent deformation. In other words, when stagnant, the fluid is not subjected to any stress. In a stagnant fluid, shear stress develops when it begins to move. If fluid particles move as a result of having different relative speeds, the fluid changes states and deforms. Put differently, no shear stress develops if velocity is identical at all

points throughout the fluid and, therefore, fluid particles remain stationary relative to one another.

The stress that, when reduced, leads the fluid to exhibit a semi-solid behavior (discontinuous deformation) is the yield stress and is often represented by τ_o (Barnes, 1999). From a physical standpoint, the yield stress of a fluid is not a single scalar value, but a range of transition from solid to liquid (Aksel *et al.*, 2007).

The dimensional change made to a body relative to its original shape by an exerted stress is referred to as a strain. Often, the dimensionless strain resulting from shear stress is denoted by γ (Barnes *et al.*, 1991).

Exhibiting large strain with instantaneous variation under an exerted stress is known as flow behavior. It must be noted that under flow behavior, the material does not return to its initial state after the stress is removed. Flow behavior deals with instantaneous strain. The instantaneous strain is strain rate which by definition, is the time derivative of strain and is measured in s^{-1} . In most types of flow behavior, shear stress results in strain rate.

Most engineering references traditionally refer to the strain rate as the shear rate (Barnes *et al.*, 1991), which is adopted in this study:

$$\dot{\gamma} = \frac{d\gamma}{dt} \quad (1.3)$$

To understand the relation between shear rate and shear stress, consider **Fig. 1.3**. Based on Eqs. (1.1) and (1.2), the following equation is written (Barnes *et al.*, 1991):

$$\dot{\gamma} = \frac{d\gamma}{dt} = \frac{dL}{h \cdot dt} = \frac{v}{h} \quad (1.4)$$

1.7.2.1 Stress Components

The force exerted on any point in the fluid is a vector that can be broken into three components coordinate axes. Accordingly, the stress exerted on each side of the fluid element can be expressed by three components. Each stress component is written with two subscripts. The first subscript refers to the side on which stress is exerted and the second is the direction in which the stress is exerted.

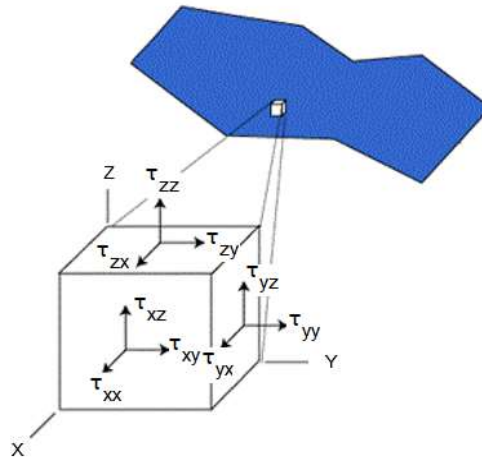


Figure 1.4 Components of stress exerted on a fluid element

The stress components can be classified into two groups. One group encompasses tangential components such as τ_{xy} , τ_{yx} , and τ_{yz} that create shear. These components can be identified as shear stress. The other group includes τ_{xx} , τ_{yy} , and τ_{zz} components that are normal to the side of the element. These components are referred to as vertical stress components or, in short, vertical stresses.

1.7.3 Viscous Fluids

From a rheological point of view, a viscous fluid is one in which the exerted stress creates irreversible flow or deformation. Based on their rheological properties, viscous fluids can be generally classified into Newtonian and non-Newtonian (Abulencia and Theodore, 2009) that exhibit different behaviors depending on the stress they withstand.

1.7.3.1 Newtonian Fluid

A Newtonian fluid is one that, generally, exhibits no elasticity and follows Newton's law of viscosity. Although, it must be noted that a perfect Newtonian fluid does not exist. According to **Fig. 1.3**, should the fluid be subjected to simple shear under steady conditions (constant

temperature and pressure) by the exertion of the force F an equal frictional force develops in the opposite direction.

The shear stress in an incompressible, Newtonian fluid in laminar flow conditions is equal to the product of fluid viscosity and shear rate (Barnes *et al.*, 1991). In other words:

$$\frac{F}{A} = \tau = \mu \left(-\frac{dv}{dh} \right) = \mu \dot{\gamma} \quad (1.5)$$

The negative sign in the above equation indicates resistance against the flow. For an incompressible fluid with a density (ρ), the following relation is written (Barnes *et al.*, 1991):

$$\tau = -\frac{\mu}{\rho} \frac{d(\rho v)}{dh} \quad (1.6)$$

The product ρv is linear momentum in a unit of the fluid. The proportionality constant μ or the ratio of shear stress to shear rate is the viscosity of the fluid, which depends only on the fluid, temperature, and pressure. Therefore, the curve plotting shear stress against shear rate, which is known as the flow curve or rheogram, is a straight line with the constant slope μ for the Newtonian fluid. In other words, the Newtonian fluid has constant viscosity at all stresses and shear rates. Viscosity, in its own right, can describe the behavior of a Newtonian fluid at constant temperature and pressure.

In brief, the shear stress can be said to have a linear relation with the velocity slope in Newtonian fluids. Most common fluids fall into this category.

1.7.3.2 Non-Newtonian Fluid

Non-Newtonian fluids have a wide range of reactions in nature and technology and usually exhibit a large resistance against flow given their high viscosity. Non-Newtonian fluids usually differ with Newtonian fluids in terms of flow characteristics.

The shear stress in a Newtonian fluid is linearly related to the shear rate. The shear stress-shear rate relation in a non-Newtonian fluid, however, is non-linear. In other words, the flow curve for a non-Newtonian fluid is non-linear.

A non-Newtonian fluid is not governed by the Newtonian fluid equation. In other words,

viscosity measurements are not adequate to determine all rheological characteristics of a non-Newtonian fluid. When a non-Newtonian fluid is exposed to a continuous simple shear, its viscosity does not remain constant but changes with the shear rate. Unlike Newtonian fluids, the viscosity of a non-Newtonian fluid is, in fact, a function of shear rate. Therefore, the use of the simple term “viscosity” for non-Newtonian fluids is meaningless unless it is assigned to a specific shear rate, in which case it is known as apparent viscosity. A non-Newtonian fluid may be classified in one of the following categories:

- **Plastic:** In these materials, shear stress must reach a minimum level before the fluid begins to flow and then shear stress increases depending on the shear rate.
- **Pseudoplastic:** In this rheological behavior, the apparent viscosity of the fluid decreases by increasing the shear rate.
- **Dilatant:** The apparent viscosity increases in a dilatant substance by raising the shear rate.
- **Bingham Plastic:** Apparent viscosity in these substances can be dependent on any parameter except time. By definition, Bingham plastics are Newtonian elastic fluids. The reason being that these fluids behave similarly to a rigid body up to the yield stress beyond which they flow similar to a Newtonian fluid with fixed viscosity. There is no perfect example of Bingham fluids. However, such substances as the drilling fluid and toothpaste are assumed to be Bingham fluids to facilitate their calculation and modeling.
- **Viscoelastic:** These substances behave similarly to Newtonian fluids under steady state conditions, but exhibit Pseudoplastic behavior under abrupt changes in shear stress.
- **Thixotropic:** In these materials, apparent viscosity declines with time under a fixed shear force.
- **Rheoplectic:** In these materials, apparent viscosity increases with time under a fixed shear force.

Given that the apparent viscosity of non-Newtonian fluids changes with the shear rate, the flow curves for this type of fluid should be first determined. Although the apparent viscosity of thixotropic and rheoplectic fluids changes with the shear rate, viscosity can be properly measured in the case of slow variations. To improve readability, the term “viscosity” is used instead of

“apparent viscosity” of non-Newtonian fluids throughout the manuscript.

The flow curves of non-Newtonian fluids are illustrated qualitatively in **Figs. 1.5-6**:

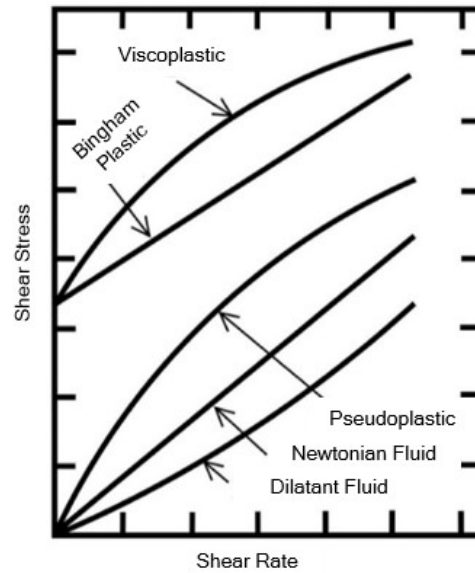


Figure 1.5 Flow curves of Newtonian and non-Newtonian fluids
(Chhabra and Richardson, 2008)

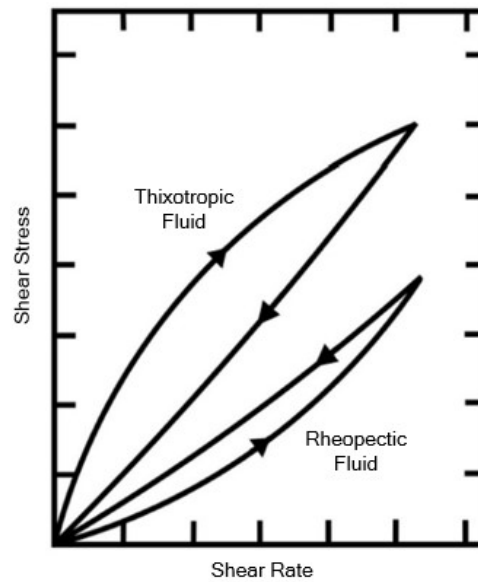


Figure 1.6 Flow curves of non-Newtonian fluids (Chhabra and Richardson, 2008)

In conclusion, non-Newtonian behavior is more difficult to predict than the Newtonian, while the behavior of a Newtonian fluid can easily and accurately be obtained by using empirical relation in terms of the function of measurable physical quantities, such as viscosity (Ely and Hanley, 1981; Johnson *et al.*, 1987; Beggs and Robinson, 1975).

The temperature dependence of the rheological properties of non-Newtonian fluids results in the complexity of continuity, momentum and energy equations (Naderi and Shokoohi, 2014). Therefore, in most cases, the use of numerical methods is inevitable to obtain an answer, even after simplifying it under the conditions of the problem.

1.7.4 Non-Newtonian Crude Oil

As mentioned earlier, when the temperature of the crude oil flowing through pipelines, decreases to cloud point or lower, a strong paraffinic structure forms due to paraffin crystallization, which exhibits resistance against the exerted stresses. These conditions, in the first place, have a tangible impact on viscosity (as a rheological property of oil) and increase it which, in turn, changes the fluid behavior to non-Newtonian. Under such circumstances, the flow curves of crude oil become non-linear in an extended range of shear rates (El-Gamal and Gad, 1998; Kirsanov and Remizov, 1999). The change in the behavior is more pronounced in crude oils with a high content of paraffin, such as the heavy crude oil. Heavy crude oil, drilling fluid, and several other oil products fall in the non-Newtonian category as they separate from a Newtonian behavior (Ajienka and Ikoku, 1991; Fernandez and Rodriguez, 1984; Agrawal and Joshi, 1994; Khan *et al.*, 1998; Ronningsen *et al.*, 1991; Kandwal, 2000).

In the case of non-linear flow curves, well-known relations including the Power-law, Herschel–Bulkley and Bingham plastic are employed to approximate flow curves and compare them with experimental results. Furthermore, in some cases, different models that draw on the concept of shear stress are used to describe different parts of a flow curve (Wardhaugh and Boger, 1991; Chang *et al.*, 1998; Kané *et al.*, 2004).

Overall, working with non-Newtonian crude oil in the oil sector is challenging because the transmission of fluid from hydrocarbon reservoirs to consumers and refineries may face considerable pressure drop (Zhang and Liu, 2008). The optimal design of equipment, including

pumps and heat exchangers, can play an essential role in helping save energy in the industry.

1.7.5 Power-law Model

The flow curve of a fluid can be approximated in a specific range of shear rate by the Power-law equation also known as the Ostwald de Waele equation:

$$\tau = k(\dot{\gamma})^n \quad (1.7)$$

Alternatively:

$$\ln \tau = \ln k + n \ln(\dot{\gamma}) \quad (1.8)$$

Where k denotes the consistency index or the strength factor of fluid, which is equal to shear stress at a shear rate 1s^{-1} . Furthermore, n represents the flow behavior index or the Power-law index. Both parameters are determined experimentally for a specific fluid and are dependent on a range of selected shear rates and a specific temperature (Chhabra and Richardson, 2008).

The flow behavior index is variable from 0 to 1 for Pseudoplastics. In other words, the Power-law model applies to Pseudoplastics when $n < 1$. The smaller n , the more dominant the Pseudoplastic behavior. When n is greater than one, it represents a dilatant fluid, whereas when $n=1$, the fluid exhibits Newtonian behavior. Overall, any deviation from $n=1$ is suggestive of a non-Newtonian fluid.

The Power-law model generally applies to average shear rates but not too extremely small (almost zero) or extremely large ones. However, practice suggests such rates cannot be found in real fluids.

The Herschel–Bulkley equation that adds a yield stress term to the Power-law equation is a more general relation that describes plastic behavior in addition to Newtonian, Pseudoplastic and dilatant. Given that yield stress is 0 for Pseudoplastic and dilatant fluids, the Herschel–Bulkley model is simplified to the Power-law for these fluids:

$$\tau = k(\dot{\gamma})^n + \tau_o \quad (1.9)$$

Previous studies have compared the Power-law, Herschel–Bulkley, and Bingham plastic models by fitting the experimental results¹ at different temperatures. However, generally speaking, the Power-law and Bingham plastic models are better fits for modeling as far as design and engineering calculations are concerned (Wardhaugh and Boger, 1991; Chang *et al.*, 1998; Kané *et al.*, 2004).

¹ Statistical parameters, including the coefficient of determination (R^2), Mean Percentage Error (MPE), the Mean Bias Error (MBE), and the Root Mean Squared Error (RMSE), are employed to identify the relation or model that is the best match to experimental data. In a multivariable fitting, higher R^2 and lower absolute MBE, MPE, and RMSE for a model are suggestive of its capability for fitting experimental data (Togrul and Arslan, 2004).

CHAPTER 2

Literature Review

2.1 Introduction

From a rheological point of view, fluids behave differently based on the stresses in which they resist. Hence, they are classified into two groups of Newtonian and non-Newtonian fluids. The exerted stresses can be due to heat transfer. To describe the fluid rheological behavior, the equation of Power-law is suitable for modeling in the engineering calculations.

Many industries such as oil and gas industries, because of the heat transfer phenomenon, are faced with the deviation of the fluid behavior from Newtonian to non-Newtonian.

2.2 Studies on Flow Variables

The study of flow variables including velocity, pressure, and temperature based on a correct description of fluid rheological behavior has received considerable attention from many researchers in this field.

Many of these researchers used the structural equation of Power-law in describing fluid rheological behavior. In these studies, in addition to the geometrical variety of flow path (channel, pipe and parallel plates), the variety of initial and boundary conditions and environmental or laboratory conditions are observed. In this regard, considering the Power-law model for predicting the behavior of non-Newtonian fluids, laminar flow and heat transfer in square channels were studied (Hartenett and Kostic, 1989). Also, ignoring heat loss and viscosity changes with temperature, the rheological behavior and heat transfer in non-Newtonian fluids in a channel were analytically studied (Flores, 1991). The mixed flow of a constant-temperature Power-law fluid with a parabolic inlet velocity gradient in a vertical channel was studied by taking into account linear temperature variations (Bejan and Sciubba, 1992). The effect of temperature on viscosity and the effect of buoyancy flow on the water as a Newtonian fluid and a non-Newtonian fluid were studied in a horizontal square channel (Chang *et al.*, 1998).

Since in the present study, the two-dimensional flow of power-law fluid in a pipe is studied, therefore, the above studies on the channels are not discussed, and merely, studies on the flow variables of the Power-law fluid in a pipe or between the parallel plates are discussed. The models presented in these studies suffer from serious common weaknesses as follows. It is worth

noting that studies of the flow of Power-law fluid between parallel plates somehow focus on the two-dimensional flow of fluid in a pipe.

- Mass transfer and heat transfer are considered as separate phenomena
- Heat loss is ignored
- Merely the study of fluid flow in a fully developed state is discussed

Therefore, the proposed models do not have the integrated capabilities to calculate all three variables of velocity, pressure, and temperature of the fluid flow.

Skelland (1967) studied the heat transfer in a fully developed flow of Power-law fluids ignoring the heat loss and the viscosity variation caused by temperature changes, to provide a relation for the maximum dimensionless velocity at the cross-section of x on the centerline:

$$u_{\max} = \frac{(2n+1) \left(1 - \left| x - 0.25 \right|^{\frac{n+1}{n}} \right)}{(n+1)} \quad (2.1)$$

Where n is the flow behavior index.

Chhabra *et al.* (2008), by ignoring heat loss, studied the heat transfer in a fully developed flow of a Power-law fluid in a pipe. The relation proposed for the linear distribution of shear stress on the pipe cross-section indicated a zero shear stress on the pipe centerline. Besides a no-slip condition on the pipe wall was also considered. According to their results, the velocity u and temperature T are the functions of x and r .

Eq. (2.2) shows the relation between thermal conductivity C_p , specific heat capacity K , temperature T , and velocity u at each (x, r) .

$$C_p u \frac{\partial T}{\partial x} = K \frac{\partial^2 T}{\partial x^2} + \frac{K}{r} \frac{\partial}{\partial r} \left(r \frac{\partial T}{\partial r} \right) \quad (2.2)$$

On the other hand, the thermal conductivity along the x -axis can be ignored compared with convective heat transfer (Dutta and Mashelkar, 1987) and thus the term $\frac{\partial^2 T}{\partial x^2}$ can be deleted:

$$C_p u \frac{\partial T}{\partial x} = \frac{K}{r} \frac{\partial}{\partial r} \left(r \frac{\partial T}{\partial r} \right) \quad (2.3)$$

Now, the dimensionless temperature θ is defined as below:

$$\theta = \frac{T - T_w}{T_{in} - T_w} \quad (2.4)$$

Where, T , T_{in} and T_w are, respectively, the fluid temperature along the pipe, the fluid temperature at the pipe inlet and the wall temperature. Using Eq. (2.4) and substituting θ in Eq. (2.3):

$$u \frac{\partial \theta}{\partial x} = \frac{K}{r C_p} \frac{\partial}{\partial r} \left(r \frac{\partial \theta}{\partial r} \right) \quad (2.5)$$

Bird *et al.* (1987) solved Eq. (2.5) by separation of variables for given values in the range of $0 \leq n \leq 1$.

The rheological behavior and heat transfer of Power-law fluid between parallel plates were also studied. In this regard, the fully developed flow of Power-law fluid between two parallel plates was studied in a certain range of flow behavior index ($n=1$ and $n=0.5$) (Etemad *et al.*, 1994).

Etemad *et al.* used the relationship between the Fanning friction factor (f) (Edwin *et al.*, 2007) and Reynolds number (Re) to estimate the pressure drop of the flow of Power-law fluid. Dimensionless results estimated by Etemad *et al.* for two Power-law fluids with different flow behavior indices are shown in **Figs. 2.1-4**.

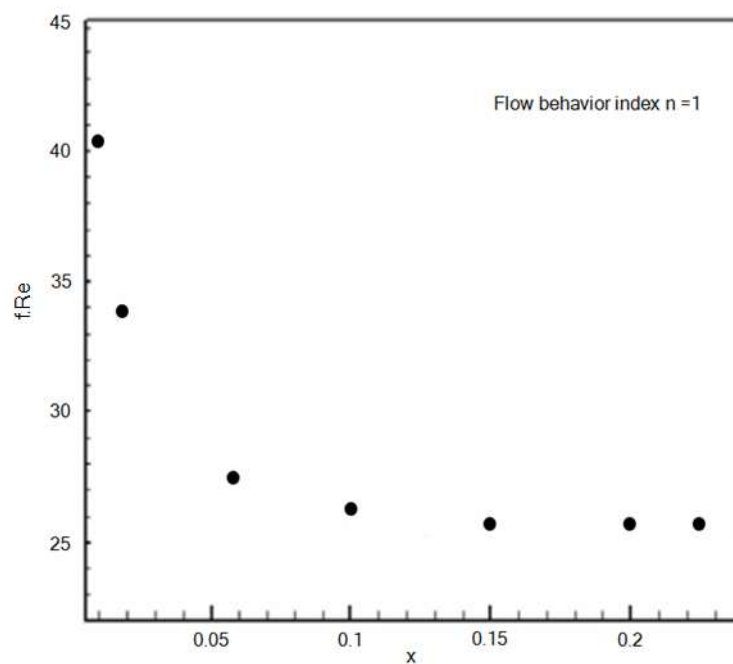


Figure 2.1 fRe for flow of Power-law fluid between parallel plates with flow behavior index $n=1$
(Etemad *et al.*, 1994)

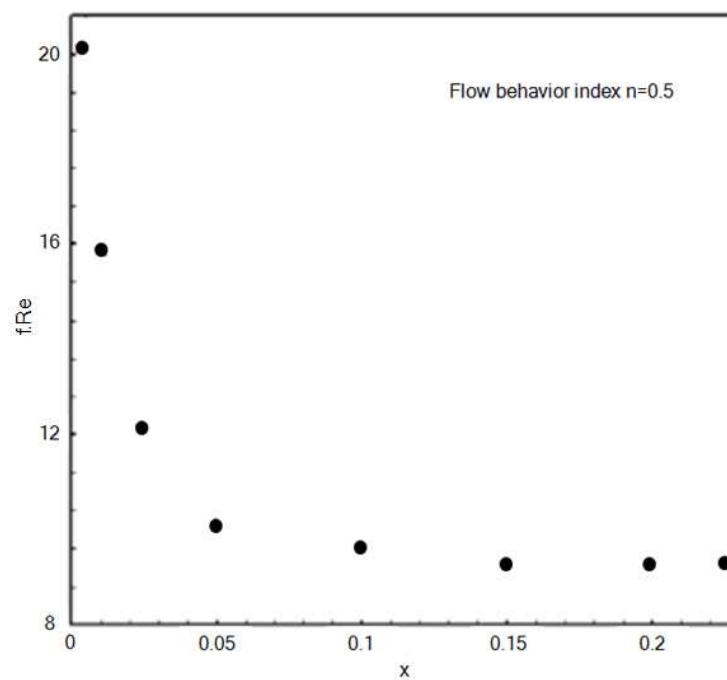


Figure 2.2 fRe for flow of Power-law fluid between parallel plates with flow behavior index $n=0.5$ (Etemad *et al.*, 1994)

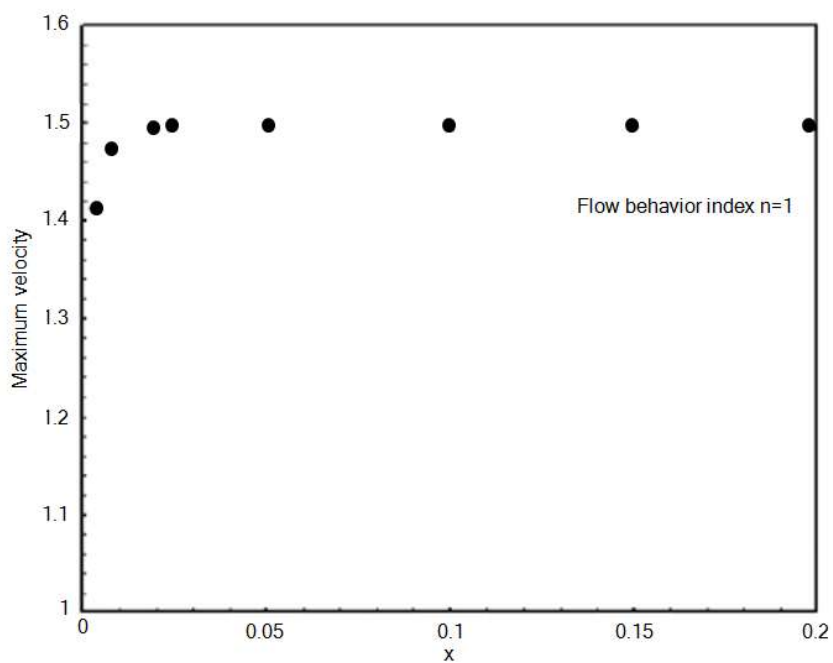


Figure 2.3 Dimensionless maximum velocity of Power-law fluid flow on centerline with flow behavior index $n=1$ (Etemad *et al.*, 1994)

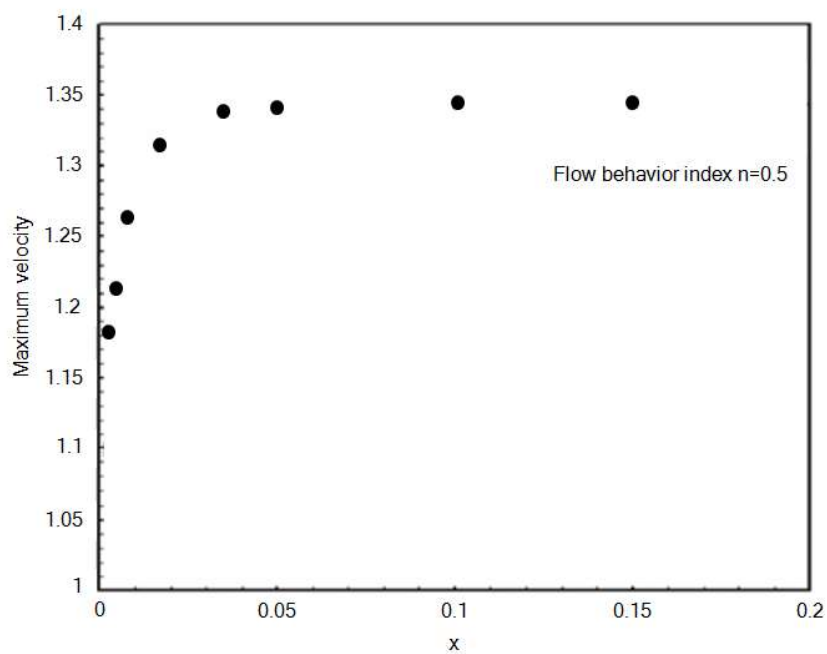


Figure 2.4 Dimensionless maximum velocity of Power-law fluid flow on centerline with flow behavior index $n=0.5$ (Etemad *et al.*, 1994)

2.3 Procedure of simultaneous determination of distributions of velocity, pressure and temperature of flow of crude oil along a pipe

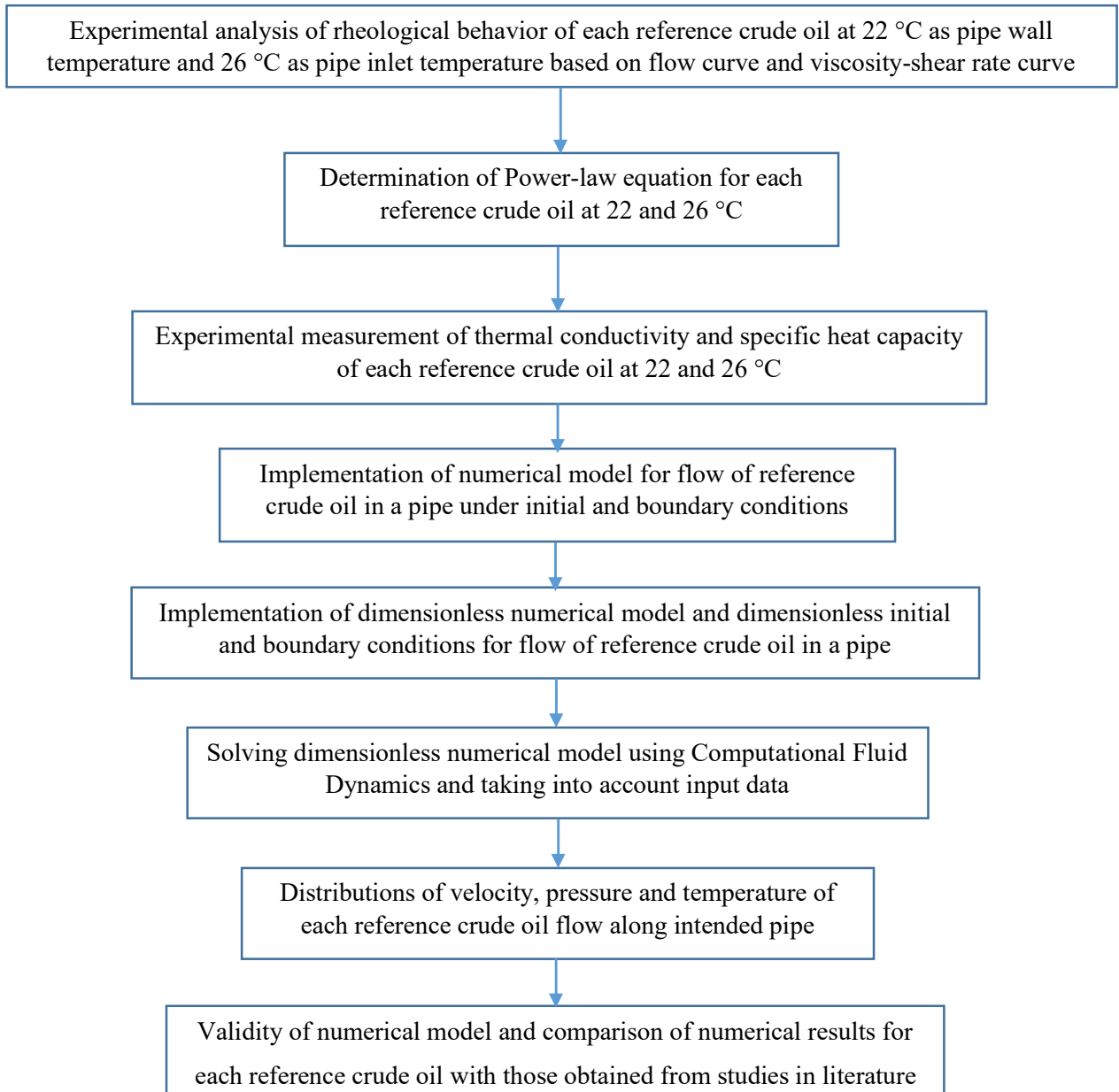


Figure 2.5 Flowchart for determination of distribution of velocity, pressure and temperature of flow of crude oil along a pipe

CHAPTER 3

Flow Curve and Viscosity-Shear Rate Curve

3.1 Introduction

Modern transmission processes delivering crude oil from the reservoir to refineries and between processing units is contingent upon the correct prediction of the rheological behavior of crude oil (Newtonian or non-Newtonian). The rheological behavior of crude oil is highly dependent on important factors such as paraffin content, shear stress, shear rate, and temperature. Based on the available samples, to study the impact of paraffin content on the rheology, two types of paraffinic crude oils with different paraffin contents (7 and 25 wt.%) (Referred to as reference crude oils samples) are considered.

The desired temperatures are 22 °C and 26 °C and it is required to plot flow curve (shear stress-shear rate curve) and viscosity-shear rate curve for each of the given crude oils at these temperatures. To this end, various rheometers can be used, each with a specific range of shear rates according to the predefined research conditions. Generally, a rheometer is a laboratory device that is used to measure how a liquid or suspension flows in response to applied forces. The rheometer used in this study is Anton Paar MCR 302, by which shear-rotary rheometric tests are conducted.

3.2 Rheological Properties of Crude Oil

The study of rheological properties of crude oil began about three decades ago. The collective agreement in all studies carried out by shear-rotary rheometry tests indicates that crude oil is non-Newtonian at cloud point or lowers (El-Gamal *et al.*, 1998; El-Gamal, 1998; Lorge *et al.*, 1997; Alboudwarej *et al.*, 2006; Agarwal *et al.*, 1989; Chandaa *et al.*, 1998).

Several studies indicate that a decrease in temperature and increase of paraffin content increases non-Newtonian behavior of crude oil (Van Der Geest *et al.*, 2015; Guo *et al.*, 2015; Jaafar *et al.*, 2014).

Many researchers have tried to provide models for predicting the rheological behavior of crude oil in recent years. Accordingly, to present relation between rheological properties of crude oil, some empirical rheological models have been provided (Al-Zahrani and Al-Fariss, 1998; Al-Fariss *et al.*, 1993). Meanwhile, indices of these models have been determined using several experimental data (Iktisanov and Sakhabutdinov, 1999).

In another study, a rheological binomial equation is proposed to consider the dependence of rheological parameters of paraffinic crude oil on temperature (Iktisanov and Sakhabutdinov, 1999).

A model has been proposed to predict yield stress in terms of the difference between desired temperature and formation temperature of gel and density of oil sample, which is consistent with experimental data (Li *et al.*, 2015).

3.3 Anton Paar MCR 302

Anton Paar MCR 302 (Anton Paar Co., Austria) is primarily utilized to perform a variety of rheological tests, such as rotational tests, oscillatory tests and a combination of them. MCR 302 can be used to determine the rheological behavior of materials, such as fluids, gels, and solids.

It is equipped with a parallel-plate measuring system, Peltier temperature control for heating/cooling and a UV curing system for photosensitive samples (**Fig. 3.1**). Peltier temperature system (P-PTD 200) allows temperature sweep experiments in the range of -40°C up to 200°C with high heating and cooling rates. The UV curing system (Delolux 80) allows the investigation of UV-initiated curing reactions, following materials development from their original to their fully cured state (**Table 3.1**).



Figure 3.1 Anton Paar MCR 302/ Peltier temperature control (middle), UV curing system (left) and computer (right)

Table 3.1 Anton Paar MCR 302 specifications

Technical data	Rheometer MCR 302
Parallel-plate geometry	20 and 40 mm
Peltier temperature rang	-20...200 °C
UV curing system (356 nm)	0...>1000 mW/cm ²
Maximum torque	200 nNm
Min. torque, rotation	10 nNm
Min. torque, oscillation	2 nNm
Torque resolution	0.1 nNm
Angular velocity	10-9...314 rad/s
Normal force range	0.005...50 N
Normal force resolution	0.50 N

MCR 302 can be used for:

- Drawing flow curves and studying melt-flow behavior and solubility of materials
- Drawing scan curve of the frequency of saving module, loss module, complex module, and complex viscosity, dissipating viscosity and other linear viscoelastic properties as a function of frequency
- Drawing temperature scan curve
- Drawing time scan curve
- Drawing strain scan curve
- Drawing creep curve and stress depletion
- Drawing relaxation time distribution function curve
- Drawing a hysteresis curve
- Checking temperature and time of gelation

3.4 Reference Crude Oils

Crude oils with 7 wt.% and 25 wt.% paraffin contents are considered to be reference crude oils. The physicochemical properties of the reference material are presented in **Table 3.2**. Any kind of crude oil with at least 5 wt.% paraffin content is referred to as paraffinic oil (Zhang and Liu, 2008).

The reference crude oils have the potential for the formation of paraffin crystals. The formation of paraffin crystals and their bonding together lead to non-Newtonian fluid behavior (Zhang and Liu, 2008). The reference crude oils vary in color from black to light brown, and density from 0.872 to 0.896 g/cm³ at 26 °C. The pour points vary between 10 and 12 °C. The water content in all the reference crude oils is insignificant (less than 0.05 vol.%). The API gravity ranges from 22.30 to 38.50.

Table 3.2 Physicochemical properties of reference crude oils

Reference crude oils	A	B
Density @ 26 °C (g/cm ³)	0.872	0.896
API Gravity	38.50	22.30
Paraffin content (wt.%)	7	25
Sulfur Content (wt.%)	0.41	4.25
Water content (vol.%)	<0.025	<0.05
Pour point (°C)	12	10
Nitrogen content (wt.%)	0.08	0.12

According to this table, the difference between the pour points of reference crude oils and desired temperatures completely supports the assumption of no appearance of a solid phase at these temperatures.

3.5 Experimental Procedure

MCR 302 is a rheometer that utilizes an EC motor technique, low friction bearing, and an optimized normal force sensor to optimize its performance. EC (Electronically Commuted, or

Electronically Controlled) motors are electric motors which have permanent magnets on the rotor and use electronics to control the voltage and current applied to the motor. The modularity of the system allows for the integration of a broad range of temperature devices and application-specific accessories (**Table 3.3**). Anton Paar Rheo Compass software is used for system control and report generation. This software is certified by Anton Paar Company.

Table 3.3 Specifications of Anton Paar MCR

Torque Range (nNm)	Technology / Test Method	Display & Special Features	Industry / Application
1.00E-5 to 200	Controlled Strain	Benchtop or Laboratory; PC Interface / Networkable; SPC or Application Software; Temperature Measurement; Video	Biotechnology; Cosmetics; Chemical Processing; Food and Beverage; Oil; Pharmaceutical; Education and Research

After reaching the compressed air with the pressure (at least) 90 psi, the Anton Paar Rheo Compass software is utilized. The measurement tool is connected to quick-connector coupling (**Fig. 3.2**). Then, samples are loaded onto the mount. If there is too much [load] on the samples, they are needed to be trimmed with a spatula; Besides, if the samples stick to the measuring plate, unscrew the Base Mount and insert the Disposable Metal Pan + Fixture (**Fig. 3.2**).

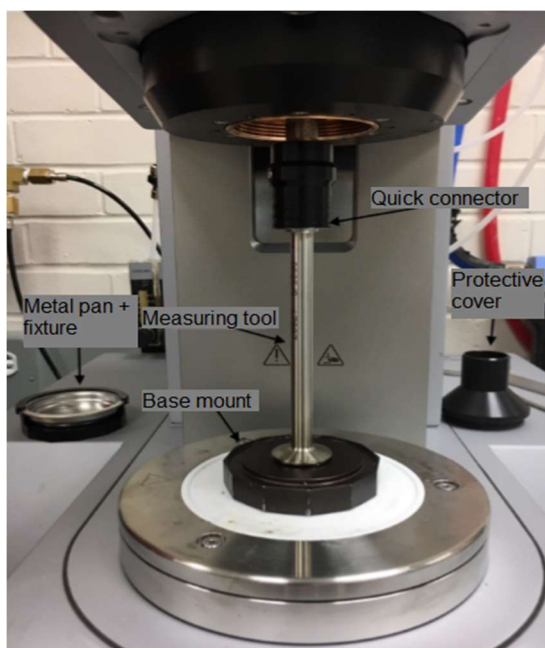


Figure 3.2 Anton Paar MCR 302 / Physical components

MCR 302 provides two measuring methods, namely shear-rotary test, and oscillatory test. The shear-rotary test is used for data collection, in which the measuring device turns in only one direction (**Fig. 3.3**). The shear rate profile, made up of different rotational speeds, is set to determine the shear rate. Using this profile, the rheometer can determine required shear stress according to the Viscosity Law. Viscosity Law states that the stress on fluid layers is directly proportional to the shear rate. For each reference crude oil sample, a shear-rotary test is applied. To conduct a test, the following settings are performed on MCR 302:

Table 3.4 Settings for conducting a shear-rotary test

1	Parallel-plate diameter	30 mm
2	Distance between Parallel plate and Base mount	0.05 mm
3	Rotation torque	100 nNm
4	Shear rate range	100-600 s ⁻¹
5	heating/cooling temperature	26 °C

Then, the Rheo Compass software is employed to collect data and generate a report. After collecting data and generating a report at 26 °C, the heating/cooling temperature is set at 22 °C, and the settings 1 to 4 of **Table 3.4** are again performed on MCR 302 and another test is run.

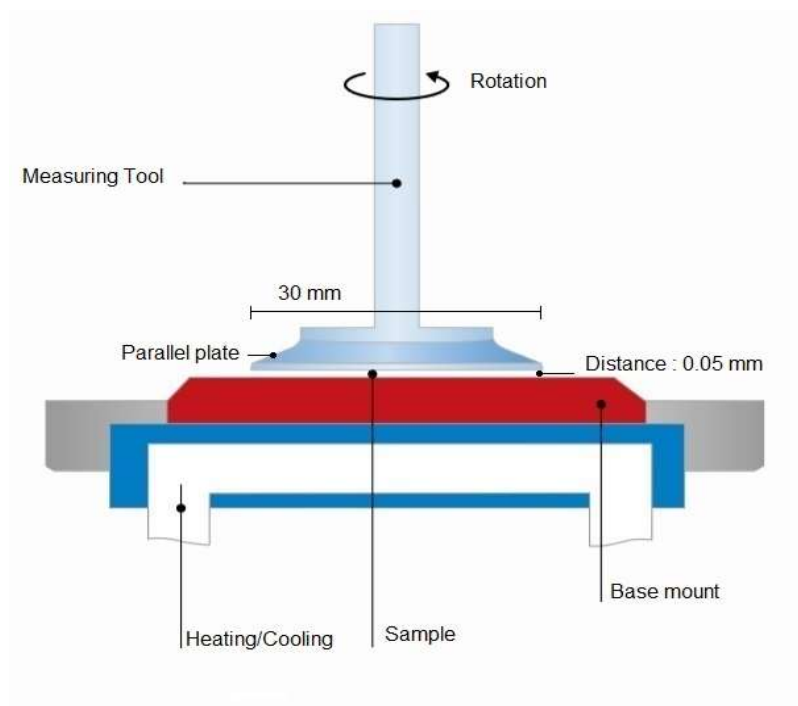


Figure 3.3 Schematic view of Peltier temperature control

3.5.1 Experimental Outputs

According to the specifications of reference crude oils, the rheological measurements may produce different results. The flow curves and viscosity-shear rate curves have been generated with Rheo Compass.

3.5.1.1 Flow Curve and Viscosity-Shear Rate Curve at 26 °C

As shown in **Figs. 3.4-5**, by increasing the paraffin content, the flow curve moves to higher shear stress levels, indicating an increase in the strength of the paraffinic network structure of the fluid, which is responsible for changing the rheological behavior of the fluid.

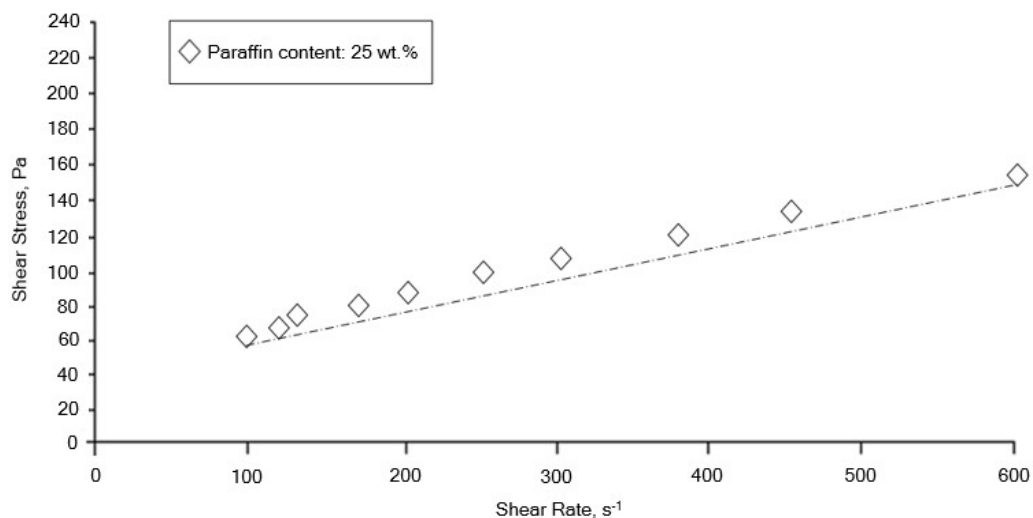


Figure 3.4 Flow curve for reference crude oil B at 26 °C

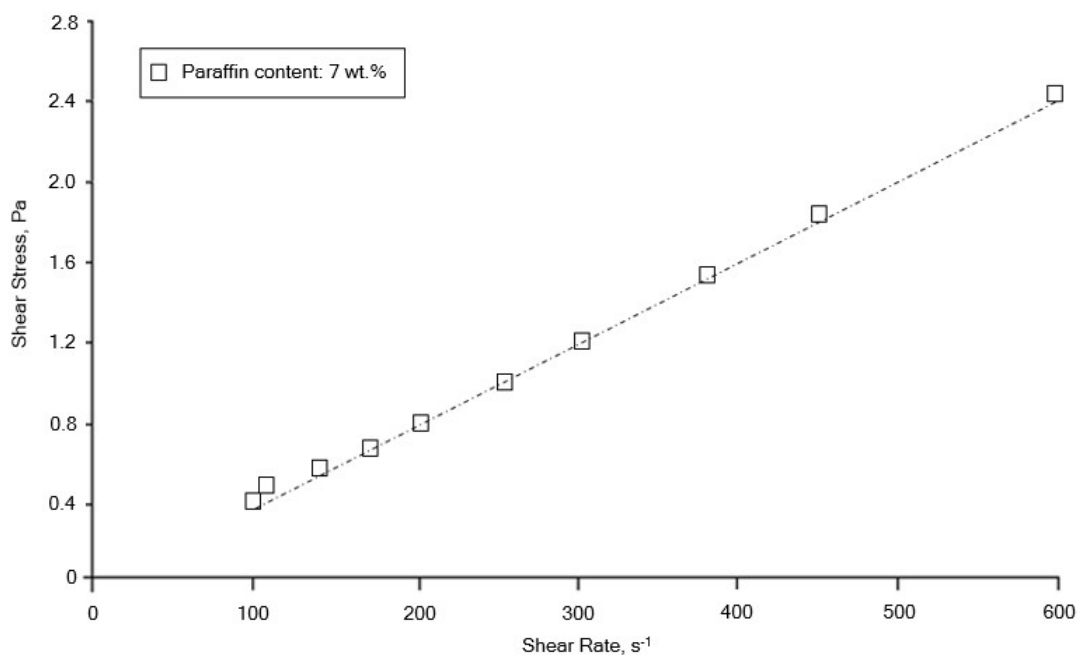


Figure 3.5 Flow curve for reference crude oil A at 26 °C

At 26 °C, as the paraffin content of reference crude oil decreases, its non-linear flow curve tends into a diagonal line. In other words, the reduction of paraffin content leads to a relatively linear relation between the shear stress and shear rate and the rheological profile of reference crude oil approaches a Newtonian profile.

At 26 °C, changes in the paraffin content of the reference crude oils have a significant effect on their rheological behavior.

Table 3.5 Experimental flow curves data for reference crude oils A and B at 26 °C

Shear rate (s^{-1})	Shear stress (Pa)	
	7 wt. %	25 wt. %
100	0.411	63.214
120	0.492	69.386
140	0.574	75.071
170	0.696	82.90
200	0.819	90.077
250	1.023	100.954
300	1.226	110.81
380	1.552	125.034
450	1.836	136.315
600	2.445	157.897

Concerning **Table 3.5**, the shear stress of reference crude oil A changes from 0.411 to 2.445 Pa, while the shear stress of reference crude oil B changes from 63.214 to 157.897 Pa. In other words, the lower paraffin content results in a smaller shear stress range in terms of the shear rate from 100 to 600 s^{-1} .

By fitting the flow curves to the Power-law equation, the flow equation indices can be obtained for each of the reference crude oils. **Table 3.6** shows the resulting indices. As seen, the flow behavior index of reference crude oil B is close to 0.50 indicating Pseudoplastic profile for this fluid at 26 °C.

Table 3.6 Power-law indices for reference crude oils A and B at 26 °C

Paraffin (wt.%)	n	k	R ²
7	0.9953	0.0042	0.9995
25	0.5109	6.012	0.9748

Table 3.7 shows the Power-law equations to describe the rheological behavior of reference crude oils A and B in the shear rate range of 100-600 s⁻¹ at 26 °C.

Table 3.7 Power-law equations for reference crude oils A and B at 26 °C

Paraffin (wt.%)	Power-law equation
7	$\tau = 0.0042(\dot{\gamma})^{0.9953}$
25	$\tau = 6.012(\dot{\gamma})^{0.5109}$

As **Fig. 3.6** shows, by increasing the shear rate, the viscosity of reference crude oil B decreases and the shear rate changes do not have a significant effect on the viscosity of crude oil A at 26 °C.

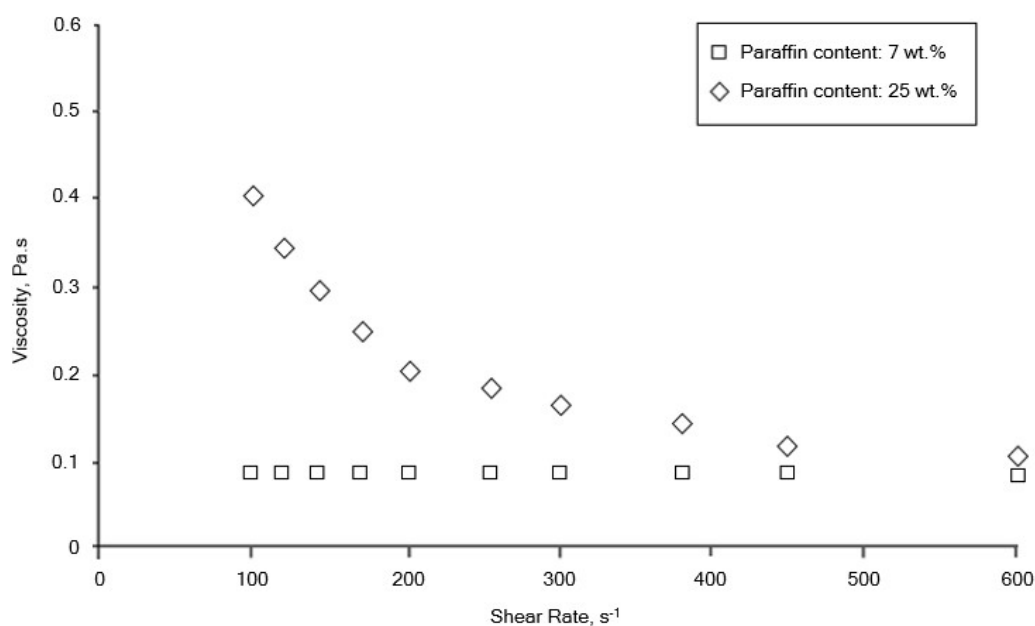


Figure 3.6 Viscosity-shear rate curve for reference crude oils A and B at 26 °C

As **Table 3.8** shows, at 26 °C, the viscosity of reference crude oil B changes from 0.410 to 0.123 Pa.s with changing the shear rate, while the viscosity of reference crude oil A is approximately remained unchanged at 0.091 Pa.s.

In other words, the viscosity of reference crude oil A is independent of the shear rate and thus the rheological behavior of fluid does not depend on the shear rate.

Table 3.8 Experimental viscosity-shear rate curve data for reference crude oils A and B
at 26 °C

Shear rate (s ⁻¹)	Viscosity (Pa.s)	
	7 wt. %	25 wt. %
100	0.091	0.410
120	0.091	0.343
140	0.091	0.292
170	0.091	0.257
200	0.091	0.228
250	0.091	0.202
300	0.091	0.182
380	0.091	0.160
450	0.091	0.141
600	0.091	0.123

3.5.1.2 Flow Curve and Viscosity-Shear Rate Curve at 22 °C

By performing a similarly experimental process and using Anton Paar MCR 302, the shear stress and viscosity changes of reference crude oils A and B are studied in the shear rate range of 100-600 s⁻¹ at 22 °C.

As shown in **Figs. 3.7-8**, at 22 °C, by increasing the paraffin content, the flow curve moves to higher shear stress levels, indicating an increase in the strength of the paraffinic structure of the fluid. At this temperature, the reference crude oil A has a non-linear flow curve with very low curvature.

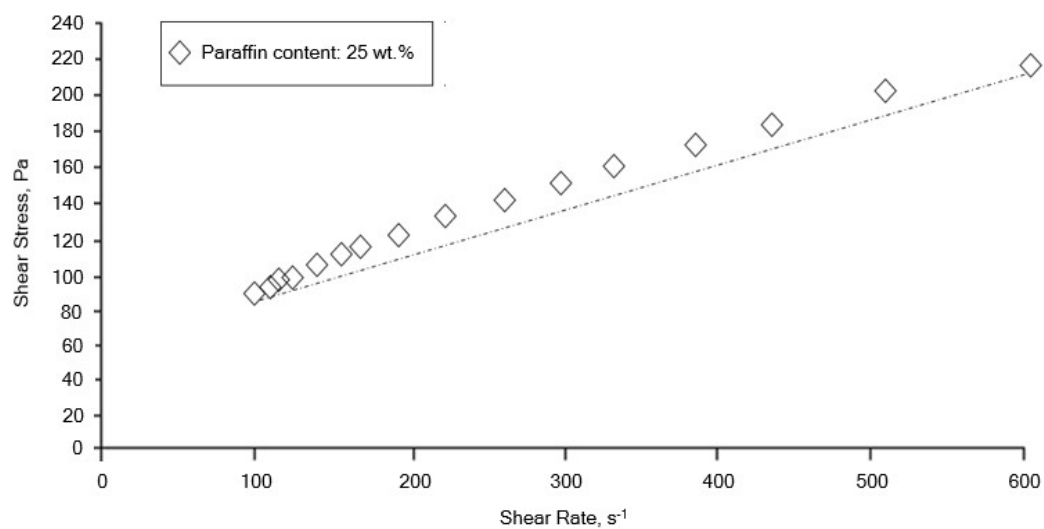


Figure 3.7 Flow curve for reference crude oil B at 22 °C

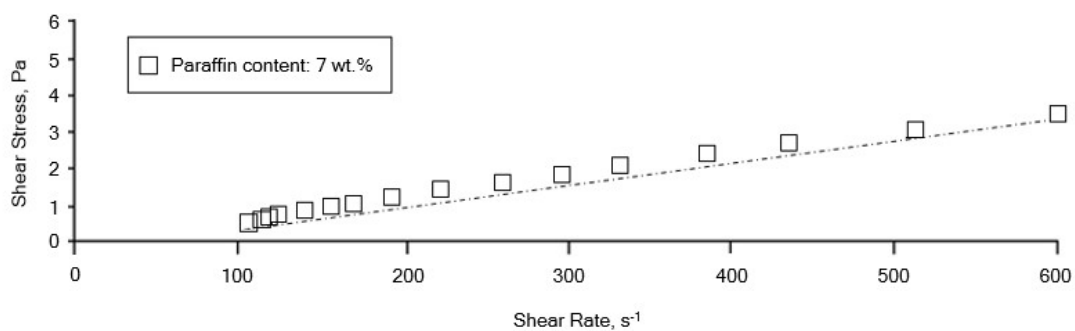


Figure 3.8 Flow curve for reference crude oil A at 22 °C

As shown in **Table 3.9**, the shear stress of reference crude oil A changes from 0.643 to 3.772 Pa; whereas, the shear stress of reference crude oil B varies from 89.132 to 218.450 Pa. In other words, the lower content of paraffin results in a smaller range of shear stress in the shear rate range of 100-600 s^{-1} .

Table 3.9 Experimental flow curves data for reference crude oils A and B at 22 °C

Shear rate (s ⁻¹)	Shear stress (Pa)	
	7%	25%
100	0.643	89.132
110	0.701	93.481
118	0.752	96.834
125	0.790	99.660
140	0.891	105.471
155	0.983	110.983
168	1.074	115.551
189	1.201	122.560
220	1.395	132.231
260	1.642	143.762
295	1.860	153.143
330	2.081	161.970
385	2.432	174.962
435	2.740	185.981
510	3.214	201.393
600	3.772	218.450

By fitting the flow curves to the Power-law equation, the indices of flow equation can be obtained for each of the reference crude oils samples. As **Table 3.10** shows, the flow behavior index approaches 0.50 by increasing the paraffin content, indicating an increase in the Pseudoplastic profile. In addition, by comparing the values of R^2 for each reference crude oil at 22 °C, it can be concluded that the Power-law model for the reference crude oil A is the best fit to the experimental data.

Table 3.10 Power-law indices for reference crude oils A and B at 22 °C

Paraffin (wt.%)	n	K	R ²
7	0.9902	0.0067	0.9825
25	0.5003	8.9012	0.9639

Table 3.11 shows the Power-law equations to describe the rheological behavior of reference crude oils samples in the shear rate range of 100-600 s⁻¹ at 22 °C.

Table 3.11 Power-law equations for reference crude oils A and B at 22 °C

Paraffin (wt.%)	Power-law equation
7	$\tau=0.0067(\dot{\gamma})^{0.9902}$
25	$\tau=8.9012(\dot{\gamma})^{0.5003}$

Regarding **Fig. 3.9**, the reference crude oil with the higher paraffin content has a higher viscosity at 22 °C. The viscosity is directly related to the amount of paraffin crystallized at this temperature. Meanwhile, the slope curve becomes upward; therefore, the viscosity reduces sharply and tends to a constant value by increasing the shear rate. In other words, as the shear rate increases, the forces applied to the paraffin crystal bonds also increase, and eventually lead to the breaking of these bonds.

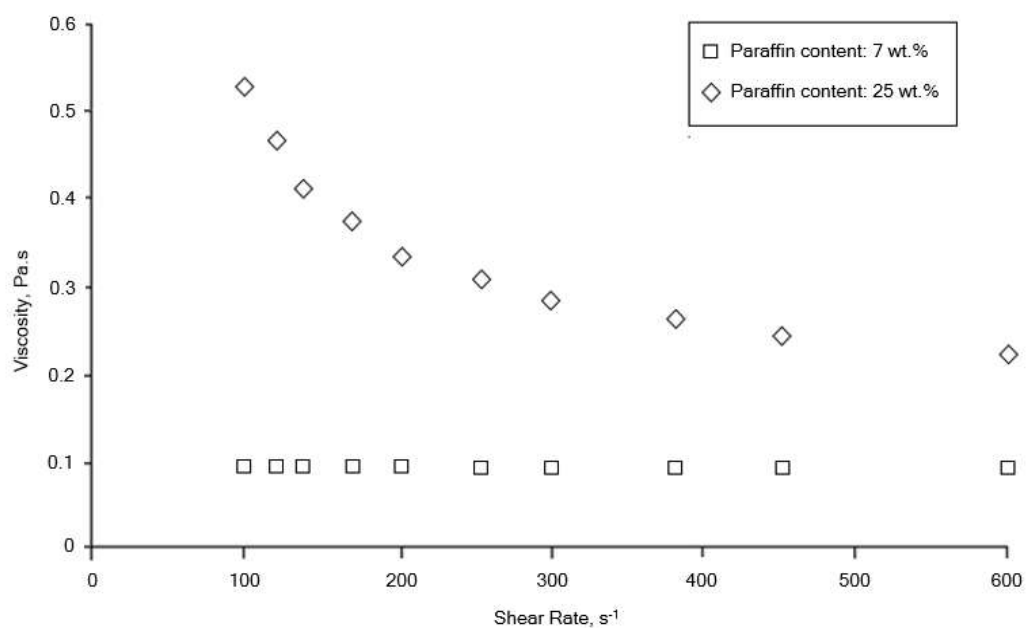


Figure 3.9 Viscosity-shear rate curve for reference crude oils A and B at 22 °C

It is observed that by decreasing the paraffin content, the slope of the curve falls so that for the reference crude oil A, changes in the curve are close to 0 and the curve is almost a horizontal line. In other words, changes in the shear rate at 22 °C do not have much effect on the viscosity of this fluid and thus the rheological behavior of the fluid does not depend on the shear rate.

Table 3.12 Experimental viscosity-shear rate curves data for reference crude oils A and B
at 22 °C

Shear rate (s ⁻¹)	Viscosity (Pa.s)	
	7%	25%
100	0.098	0.525
120	0.098	0.462
140	0.098	0.401
170	0.098	0.342
200	0.098	0.291
250	0.098	0.246
300	0.098	0.201
380	0.098	0.168
450	0.098	0.149
600	0.098	0.127

Regarding the obtained results:

- The flow curves for each reference crude oil at 26 and 22 °C indicate the existence of a paraffinic network. The existence of this network at both temperatures indicates that the cloud point of each reference crude oil can be estimated at least 26 °C ($26\text{ °C} \leq \text{Cloud point}$). As temperature decreases from 26 to 22 °C, the strength of this network increases (especially in the reference crude oil B) and results in a more viscosity.
- As the temperature reduces from 26 to 22 °C, the maximum viscosity of crude oils samples B and A, respectively, increases from 0.410 to 0.525 Pa.s and from 0.091 to 0.098 Pa.s. The increase in the viscosity of reference crude oil B in comparison with the reference crude oil A, is because of the formation of more paraffin crystals.

CHAPTER 4
Thermal Conductivity and Specific Heat Capacity

4.1 Introduction

In general, the study of non-Newtonian fluids is very extensive and consists of a variety of variables. In addition to variables such as stresses, viscosity, consistency index and flow behavior index mentioned in the previous chapter, thermal conductivity, and specific heat capacity are other significant variables in non-Newtonian fluid calculations. Dependence of thermal conductivity and specific heat capacity on one or more variables, their impact on each other and their compliance with the temperature have resulted in a much broader scope.

4.2 Thermal Conductivity and Specific Heat Capacity

Thermal conductivity and specific heat capacity values as important thermal properties of the materials are necessary whenever a heat transfer problem occurs. For both liquids and gases, these two parameters highly depend on the temperature, whereas their pressure dependence is comparatively low.

The thermal conductivity of a material is a measure of its ability to conduct heat. The higher the thermal conductivity of the material, the more conductive the material will be resulting in a greater heat transfer. The thermal conductivity is measured in Watts per Meter-Centigrade ($\text{W/m}^\circ\text{C}$).

Specific heat capacity is the ratio of the heat added to (or removed from) an object to the temperature change. Specific heat capacity is measured in Joule per Gram- Centigrade ($\text{J/gr}^\circ\text{C}$).

Thermal conductivity and specific heat capacity of some pure, low molecular weight liquid hydrocarbons can be found in (Touloukian, 1970). It is worth noting that crude oil is a mixture of light and heavy hydrocarbons, so it is difficult to determine thermal conductivity and specific heat capacity.

Thermal conductivity and specific heat capacity values of crude oil are generally not available and there is no accepted theory for estimating the thermal properties of hydrocarbon mixtures (Reid *et al.*, 1977).

This study presents results from measurements of thermal conductivity and specific heat capacity for the reference crude oils using the Flucon GmbH measuring system, based on hot-wire technology (Healy *et al.*, 1976).

4.3 Flucon GmbH Measuring System

Accurate measurements of thermal conductivity and specific heat capacity are challenging. Methods and geometries for each system have their specific adherents and inherent drawbacks (Yu *et al.*, 2008; Zeller *et al.*, 1971).

The steady state hot-wire experiment is one of the older, well-established methods. The evolution of the modern hot-wires experiment for thermal conductivity can be traced back to the experiments carried out by Pittman (1968), Haarman (1969) and Mani (1971). However, the major exposition of the aforementioned researchers' theories and application of them for the gas phase were provided during the last decade (De Groot *et al.*, 1974; Healy *et al.*, 1976; De Groot *et al.*, 1978; Kestin *et al.*, 1980; Kestin *et al.*, 1978; Clifford *et al.*, 1980). Similar instruments were also used for both gas and liquid measurements (Assael *et al.*, 1981; Menashe *et al.*, 2010). Besides, De Castro *et al.* (1976) have used similar instruments for liquid measurements.

The hot wire method, however, has been developed owing to recent advances in digital electronics, such as the Flucon GmbH measuring system. This hot-wire technology is both precise and easy to handle and allows us to determine the temperature-dependent thermal conductivity and specific heat capacity of the reference crude oils samples.

4.3.1 Measuring System Components

The Flucon GmbH measuring system facilitates the fast determination of thermal conductivity and specific heat capacity in the temperature range of -50 °C to 300 °C using the hot-wire method according to ASTM D7896-14. This system is suitable for fluid analysis in the laboratory and consists of three components:

- Electronic unit
- Robust stainless steel sensor
- Omega thermostat for sample temperature control

The Flucon GmbH measuring system can operate in the stand-alone mode or by Windows-based computer via digital interface RS-232 or USB.

4.4 Experimental Procedure

To measure the thermal conductivity and specific heat capacity of the reference crude oils samples, the following steps are taken by using the Flucon GmbH measurement system, according to technical data shown in **Table 4.1**:

- Switching on the electronic unit

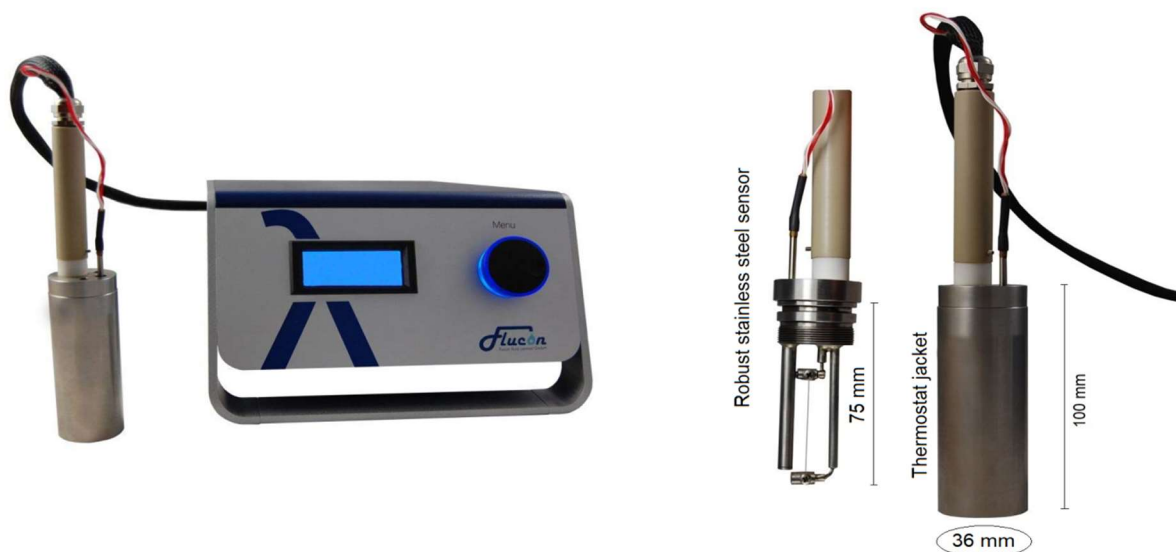


Figure 4.1 Flucon GmbH measurement system /Electronic unit and sensor
(With thermostat jacket)

- Pouring 35 ml of the reference crude oil in the screw-on cup



Figure 4.2 Screw-on cup

- Placing the Robust stainless steel sensor inside the screw-on cup. The sensor is immersed in measuring oil
- Placing the sensor and screw-on cup assembly, inside the thermostat jacket
- Placing the sensor with a jacket in the thermostat
- Setting the thermostat temperature at 26 °C

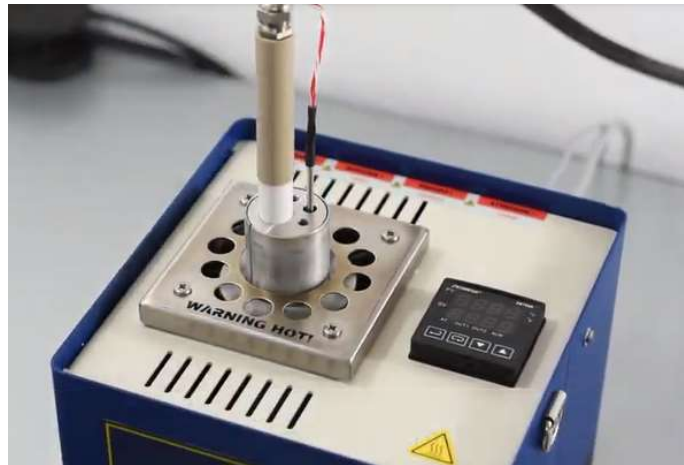


Figure 4.3 Omega thermostat

- With the intervals about 60 seconds, the system determines the thermal conductivity as well as the specific heat capacity of the fluid
- The values of the thermal conductivity and specific heat capacity are shown in the electronic unit displayer. Besides, via digital interface RS-232 or USB, the results can be displayed on a PC monitor

Table 4.1 Technical data used in experimental procedure
(Using Flucon GmbH measurement system)

Sample quantity	approx. 35 ml
Temperature range	-50 °C - 300 °C
Temperature accuracy	$\pm 0,1$ °C
Temperature measurement	PT100
Pressure range	0-35 bar
Measuring time	approx. 60 s
Response time	ca. 60 s
Outer dimensions measuring vessel (Screw-on cup)	D = 36 mm (equals inner diameter of thermostat jacket); L = 100 mm (equals immersion depth into thermostat)

After collecting data at 26 °C, the steps above repeated at 22 °C.

4.4.1 Experimental Results

As can be seen in **Table 4.2**, when the temperature changes from 26 °C to 22 °C, the thermal conductivity and specific heat capacity of each reference crude oil, respectively, have changes about 0.001 and 0.01. These parameters have no significant sensitivity to the temperature changes from 26 °C to 22 °C.

Table 4.2 Thermal conductivity and specific heat capacity measured at temperatures 26 °C and 22 °C for reference crude oils

Reference crude oil	T (°C)	C _P (J/g °C)	K (W/m °C)
A	26	1.831	0.138
	22	1.829	0.139
B	26	1.901	0.144
	22	1.898	0.145

The obtained values for the thermal conductivity and specific heat capacity of each reference crude oil sample are used in the next chapters.

CHAPTER 5

Numerical Model, Initial and Boundary Conditions

5.1 Introduction

The experimental results presented for shear stress, viscosity and the Power-law model at 22 and 26 °C (Chapter 3) in the shear rate range of 100-600 s⁻¹ revealed a considerable behavioral difference between the two crude oils samples (A and B). Accordingly, in the following, it appears that the two fluids are excellent choices for calculating and comparing the distribution of velocity, pressure, and temperature in the Power-law crude oil flow that exhibits two different behaviors against reduced pipeline wall temperature as a result of the decrease in ambient temperature.

5.2 Fluid Flow Mechanism

In most studies, Reynolds number is used to express the impact of viscosity on the flow mechanism, hence the generated role of the parameter in the calculations. The Reynolds number indicates the ratio of the inertial force to the viscous (shear) force due to fluid motion. Considering that these forces determine the flow regime (turbulent or laminar), the flow mechanism can be found based on the Reynolds number.

Depending on the model employed to describe the behavior of the fluid, different theories are proposed for Reynolds number calculation.

For Power-law fluids, the value of the Reynolds number is a function of the type and extent of their behavior. In other words, the Power-law behavior index has a substantial role in determining the Reynolds number in such fluids.

Assuming a shear rate range of 100-600 s⁻¹ and an input temperature 26 °C (at the pipe inlet) and a wall temperature 22 °C, the flow behavior index is estimated for each reference crude oil sample (**Tables 5.5 and 5.9**). Given that, the fluid temperature varies between 22 and 26 °C, the behavior indices of reference crude oils samples A and B, respectively, fall in $0.9902 \leq n \leq 0.9953$ and $0.5003 \leq n \leq 0.5109$ ranges.

On the one hand, the criterion proposed by Ryan (1959) can be used to calculate the Reynolds number for a Power-law fluid:

$$Re = \frac{6464n}{(3n+1)^2} (2+n)^{\left(\frac{2+n}{1+n}\right)} \quad (5.1)$$

Furthermore, Mishra *et al.* (1971) proposed the following relation for the Reynolds number of Power-law fluids:

$$Re = \frac{2100(4n+2)(5n+3)}{3(3n+1)^2} \quad (5.2)$$

Both above equations calculate the Reynolds number at 2100 for Newtonian fluids ($n=1$) which is regarded as a general criterion for Newtonian fluids.

The Reynolds number limits estimated by Ryan's equation for Power-law fluids increase as the behavior index decreases, reaching a maximum of 2400 at $n=0.4$ and dropping down to 1600 again at $n=0.1$.

According to Eq. (5.2), the Reynolds number increases for the Power-law fluid as the flow behavior index decreases reaching 4200 when $n=0$. Given the complex dependence of Reynolds number on flow behavior index, a laminar flow is not established for Reynolds number greater than $Re < 2500$ (Ryan, 1959; Mishra and Tripathi, 1971).

Accordingly, the Reynolds number is calculated for reference crude oils samples A and B using both Ryan's and Mishra's equations. Based on the estimated range for flow behavior index, the Reynolds number calculated for each reference crude oil sample, respectively, falls in $2101 < Re_{\text{Crude oil A}} < 2104$ and $2154 < Re_{\text{Crude oil B}} < 2377$ ranges. Considering the range defined for laminar flow, a laminar flow is expected for both reference crude oils samples A and B in the pipe.

5.3 Assumptions for Measured Parameters

Given that the flow behavior index, viscosity, thermal conductivity, and specific heat capacity of reference crude oils are functions of temperature, in cases where the difference between input and output temperatures is considerable, the parameters above are required to be calculated at each point of the computational domain separately, which is too complicated and even impossible. The fluid temperature along with its velocity and pressure are the unknowns in the

computational domain and must be determined. If the temperature of the fluid is known all across the computational domain, then the fewer unknowns will remain at hand, and the parameters above can be calculated at any point in the computational domain (although with some difficulty).

The flow behavior indices in **Tables 3.6** and **3.10** are considered to be precise to two decimal places. In this case, when the temperature decreases from 26 to 22 °C, the flow behavior index doesn't change significantly for each of the reference crude oils A and B and respectively remains at 0.99 and 0.50. Furthermore, the results shown in **Tables 3.7, 3.11** and **4.2** are considered with precision to 2 decimal places. In these cases, the following results obtained:

- The viscosity of reference crude oil A in the range of 100-600 s⁻¹ can be considered 0.09.
- The viscosity of reference crude oil B is increased as the temperature decreases from 26 to 22 °C, but at both temperatures, the viscosity of the fluid is reduced as the shear rate rises. The viscosity of reference crude oil B can be considered 0.20 with the mentioned precision.
- By the given precision, the thermal conductivity and specific heat capacity measured for the reference crude oils A and B (**Table 4.2**), do not change with temperature variations, and respectively remain for the reference crude oil A at 0.13 and 1.83, and for the reference crude oil B at 0.14 and 1.90.

5.4 Numerical Model

To present a convenient mathematical model for comparing the numerical results with those obtained from other studies, it is assumed that the flow of Power-law crude oil enters a horizontal pipe with length ℓ , diameter $2R$ and wall temperature T_w at uniform velocity v_{in} , pressure P_{in} and temperature T_{in} (**Fig. 5.1**) also $T_w < T_{in}$. Moreover, viscosity, thermal conductivity and specific heat capacity of the fluid are, respectively, μ , K and C_p along the pipe at temperature T . The flow is simultaneously developing from the standpoint of fluid dynamics. Put differently, the velocity and temperature gradients are changing along the pipe. It must be noted that the assumptions made in the previous section for μ , K and C_p are taken into account in

every step of presenting the mathematical model.

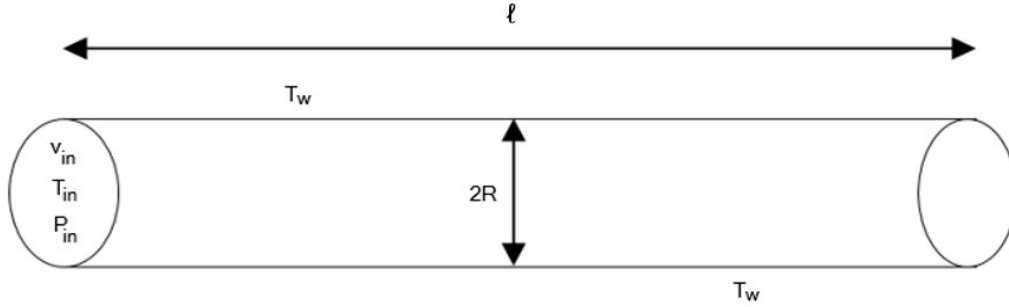


Figure 5.1 Horizontal pipe with wall temperature T_w in which reference crude oil flows

In this study, the governing equations are discretized and the resulting system of algebraic equations is solved after establishing the basic equations governing the flow. The problem is governed by Navier–Stokes equations that include continuity and momentum equations besides the energy equation. The numerical solution is compared with available results to ensure its reliability.

5.4.1 Governing Equations

Assuming a Power-law crude oil element with the differential volume $\Delta x \Delta y \Delta z$ according to **Fig. 5.2**, the continuity equation is obtained by writing a mass balance over the volume. The mass balance can be written as follows:

$$\text{Rate of accumulation} + \text{Rate of mass out} - \text{Rate of mass in} = 0$$

In other words:

$$\Delta x \Delta y \Delta z \frac{\partial \rho}{\partial t} = \Delta y \Delta z \left((\rho v_x)|_x - (\rho v_x)|_{x+\Delta x} \right) + \Delta x \Delta z \left((\rho v_y)|_y - (\rho v_y)|_{y+\Delta y} \right) + \Delta x \Delta y \left((\rho v_z)|_z - (\rho v_z)|_{z+\Delta z} \right) \quad (5.3)$$

Through a division of both sides by $\Delta x \Delta y \Delta z$, provided $\Delta x \rightarrow 0$, $\Delta y \rightarrow 0$ and $\Delta z \rightarrow 0$, the above equation is transformed into the following which is the continuity equation:

$$\frac{\partial \rho}{\partial t} = - \left(\frac{\partial}{\partial x} \rho v_x + \frac{\partial}{\partial y} \rho v_y + \frac{\partial}{\partial z} \rho v_z \right) \quad (5.4)$$

the above equation can be modified to:

$$\frac{\partial \rho}{\partial t} + v_x \frac{\partial \rho}{\partial x} + v_y \frac{\partial \rho}{\partial y} + v_z \frac{\partial \rho}{\partial z} = -\rho \left(\frac{\partial v_x}{\partial x} + \frac{\partial v_y}{\partial y} + \frac{\partial v_z}{\partial z} \right) \quad (5.5)$$

which can be rewritten:

$$\frac{1}{\rho} \frac{D\rho}{Dt} = \frac{\partial v_x}{\partial x} + \frac{\partial v_y}{\partial y} + \frac{\partial v_z}{\partial z} \quad (5.6)$$

Where $\frac{D\rho}{Dt}$ indicates the magnitude of change in ρ that is the substantive derivative of density.

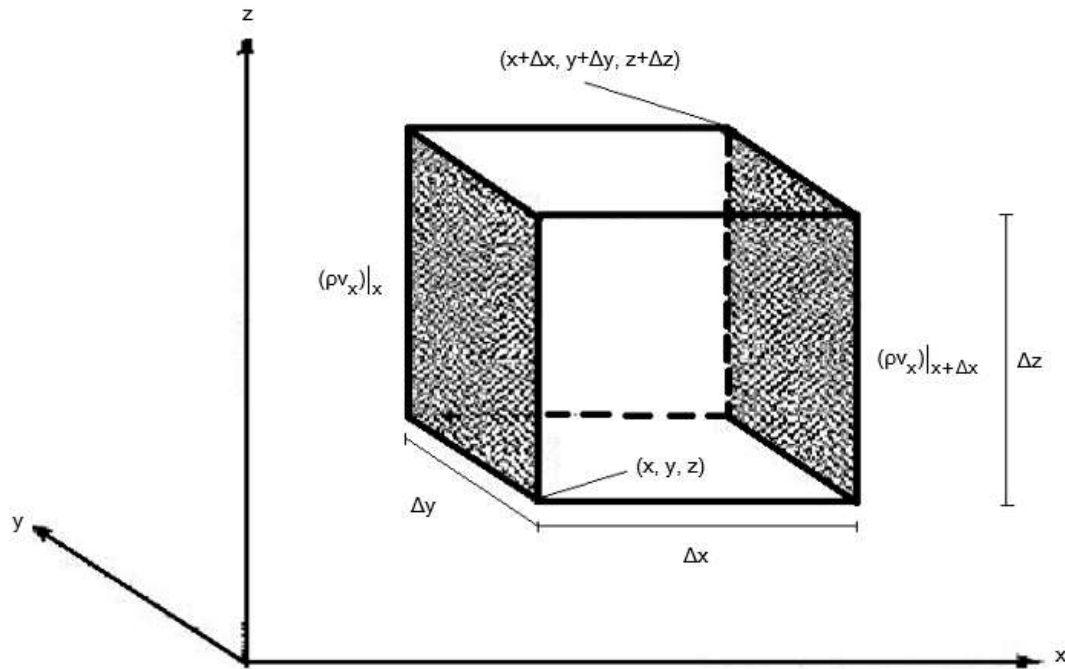


Figure 5.2 Fluid element with differential volume $\Delta x \Delta y \Delta z$

A momentum balance is written over the differential volume Fluid element with differential volume $\Delta x \Delta y \Delta z$ as follows to obtain the momentum equation:

Rate of momentum accumulation = Rate of momentum in - Rate of momentum out + Sum of forces acting on the system

One must note that the above equation has components in all three directions x, y, and z. The x component of each term of the equation is obtained as follows. The components y and z can be obtained similarly. Momentum flows enter the differential volume $\Delta x \Delta y \Delta z$ and leave it by two mechanisms:

- By convection (property of the fluid mass)
- By molecular transmission (property of velocity gradient)

The rate of momentum entering the x face of the element by convection along the x component is $\tau_{xx}|_x \Delta y \Delta x$ and the rate of momentum along the x component that leaves from the $x+\Delta x$ face is, $\tau_{xx}|_{x+\Delta x} \Delta y \Delta x$ where τ_{xx} represents vertical stress over the x face.

Assuming τ_{yx} to be shear stress along the x component developed by the viscous force on the y face of the element, the input and output momentum rates along the x component through y and $y+\Delta y$ faces are, respectively, $\tau_{yx}|_y \Delta z \Delta x$ and $\tau_{yx}|_{y+\Delta y} \Delta z \Delta x$. Similarly, the phrase can be rewritten for the other three faces. Thus, it is clear that convective momentum exists on all six faces of the element along the x component.

Accordingly, the momentum rate along the x component entering through the x face by the molecular mechanism is $\tau_{xx}|_x \Delta y \Delta z$ and the momentum rate along the x component leaving through $x+\Delta x$ face is $\tau_{xx}|_{x+\Delta x} \Delta y \Delta z$. The rate of momentum input along the x component through the y face is $\tau_{yx}|_x \Delta x \Delta z$, similarly, the input flow rate can be written for the other faces.

The sum of contributions of the six faces is:

$$\Delta y \Delta z (\tau_{xx}|_x - \tau_{xx}|_{x+\Delta x}) + \Delta x \Delta z (\tau_{yz}|_y - \tau_{yz}|_{y+\Delta y}) + \Delta x \Delta y (\tau_{zx}|_z - \tau_{zx}|_{z+\Delta z}) \quad (5.7)$$

The net of the flow pressure force (P) and gravity per unit mass (g) along the x-direction is:

$$\Delta y \Delta z (P|_z - P|_{z+\Delta z}) + \rho g_x \Delta x \Delta y \Delta z \quad (5.8)$$

Finally, the momentum accumulation rate in the x-direction is $\Delta x \Delta y \Delta z \frac{\partial}{\partial t} \rho v_x$. Replacing the above results in Eq. (5.7) and dividing both sides by $\Delta x \Delta y \Delta z$ if $\Delta x \rightarrow 0$, $\Delta y \rightarrow 0$ and $\Delta z \rightarrow 0$ the equation of motion is obtained along the x component as follows:

$$\frac{\partial}{\partial t} \rho v_x = - \left(\frac{\partial}{\partial x} \rho v_x v_x + \frac{\partial}{\partial y} \rho v_y v_x + \frac{\partial}{\partial z} \rho v_z v_x \right) + \left(\frac{\partial}{\partial x} \tau_{xx} + \frac{\partial}{\partial y} \tau_{yx} + \frac{\partial}{\partial z} \tau_{zx} \right) - \frac{\partial P}{\partial x} + \rho g_x \quad (5.9)$$

Accordingly, the equation of motion along directions of y and z is as follows:

$$\frac{\partial}{\partial t} \rho v_y = - \left(\frac{\partial}{\partial x} \rho v_x v_y + \frac{\partial}{\partial y} \rho v_y v_y + \frac{\partial}{\partial z} \rho v_z v_y \right) + \left(\frac{\partial}{\partial x} \tau_{xy} + \frac{\partial}{\partial y} \tau_{yy} + \frac{\partial}{\partial z} \tau_{zy} \right) - \frac{\partial P}{\partial y} + \rho g_y \quad (5.10)$$

$$\frac{\partial}{\partial t} \rho v_z = - \left(\frac{\partial}{\partial x} \rho v_x v_z + \frac{\partial}{\partial y} \rho v_y v_z + \frac{\partial}{\partial z} \rho v_z v_z \right) + \left(\frac{\partial}{\partial x} \tau_{xz} + \frac{\partial}{\partial y} \tau_{yz} + \frac{\partial}{\partial z} \tau_{zz} \right) - \frac{\partial P}{\partial z} + \rho g_z \quad (5.11)$$

Where ρv_x , ρv_y and ρv_z are the components of the mass velocity vector ρv , whereas g_x , g_y and g_z are the components of gravitational acceleration g .

The complexity of Eqs. (5.9), (5.10) and (5.11) prompts us to rewrite them as follows considering a two-dimensional configuration:

$$\frac{\partial}{\partial t} \rho v_x = - \left(\frac{\partial}{\partial x} \rho v_x v_x + \frac{\partial}{\partial y} \rho v_y v_x \right) + \left(\frac{\partial}{\partial x} \tau_{xx} + \frac{\partial}{\partial y} \tau_{yx} \right) - \frac{\partial P}{\partial x} + \rho g_x \quad (5.12)$$

$$\frac{\partial}{\partial t} \rho v_y = - \left(\frac{\partial}{\partial x} \rho v_x v_y + \frac{\partial}{\partial y} \rho v_y v_y \right) + \left(\frac{\partial}{\partial x} \tau_{xy} + \frac{\partial}{\partial y} \tau_{yy} \right) - \frac{\partial P}{\partial y} + \rho g_y \quad (5.13)$$

Where v_x and v_y are components of flow velocity along x and y axes and are, respectively, represented by u and v .

As mentioned in the previous section, laminar flow is expected from both reference crude oils samples in the pipe. Accordingly, the fluid density can be assumed to remain fixed. This assumption often results in a negligible error in engineering practices. Therefore, Eq. (5.6) and Eqs. (5.12) and (5.13) can be written as follows:

$$\frac{\partial u}{\partial x} + \frac{\partial v}{\partial y} = 0 \quad (5.14)$$

$$\rho \frac{\partial u}{\partial t} = - \rho \left(\frac{\partial}{\partial x} u \cdot u + \frac{\partial}{\partial y} v \cdot u \right) + \left(\frac{\partial}{\partial x} \tau_{xx} + \frac{\partial}{\partial y} \tau_{yx} \right) - \frac{\partial P}{\partial x} + \rho g_x \quad (5.15)$$

$$\rho \frac{\partial v}{\partial t} = - \rho \left(\frac{\partial}{\partial x} u \cdot v + \frac{\partial}{\partial y} v \cdot v \right) + \left(\frac{\partial}{\partial x} \tau_{xy} + \frac{\partial}{\partial y} \tau_{yy} \right) - \frac{\partial P}{\partial y} + \rho g_y \quad (5.16)$$

It is therefore best to break down the stress component τ_{ij} as follows:

$$\tau_{ij} = P\delta_{ij} + \sigma_{ij} \quad i, j = x, y \quad (5.17)$$

Where δ_{ij} denotes Kronecker delta with the following properties:

$$\delta_{ij} = \begin{cases} 1 & \text{if } i = j \\ 0 & \text{if } i \neq j \end{cases} \quad (5.18)$$

Each σ_{ij} is considered a deviation stress component. According to Eq. (5.18), the stress components τ_{xx} and τ_{yx} are related to deviation stress components as follows:

$$\begin{cases} \tau_{xx} = P + \sigma_{xx} \\ \tau_{yx} = \sigma_{yx} \end{cases} \quad (5.19)$$

Overall, for an incompressible viscous fluid, one can write:

$$\begin{cases} \sigma_{xx} = -2\mu \frac{\partial u}{\partial x} \\ \sigma_{yx} = -\mu \left(\frac{\partial u}{\partial y} + \frac{\partial v}{\partial x} \right) \end{cases} \quad (5.20)$$

By using Eqs. (5.19), (5.20) and (5.14), Eq. (5.15) can be written as below:

$$\rho \left(\frac{\partial u}{\partial t} + u \frac{\partial u}{\partial x} + v \frac{\partial u}{\partial y} \right) = \rho g_x - \frac{\partial P}{\partial x} + \mu \left(\frac{\partial^2 u}{\partial x^2} + \frac{\partial^2 v}{\partial y^2} \right) \quad (5.21)$$

Similarly, Eq. (5.16) can be written as:

$$\rho \left(\frac{\partial v}{\partial t} + v \frac{\partial v}{\partial y} + u \frac{\partial v}{\partial x} \right) = \rho g_y - \frac{\partial P}{\partial y} + \mu \left(\frac{\partial^2 u}{\partial x^2} + \frac{\partial^2 v}{\partial y^2} \right) \quad (5.22)$$

Eqs. (5.21) and (5.22) can be written as:

$$\rho \left(\frac{\partial u}{\partial t} + \frac{\partial u^2}{\partial x} + \frac{\partial uv}{\partial y} \right) = \rho g_x - \frac{\partial P}{\partial x} + \mu \left(\frac{\partial^2 u}{\partial x^2} + \frac{\partial^2 v}{\partial y^2} \right) \quad (5.23)$$

$$\rho \left(\frac{\partial v}{\partial t} + \frac{\partial v^2}{\partial y} + \frac{\partial vu}{\partial x} \right) = \rho g_y - \frac{\partial P}{\partial y} + \mu \left(\frac{\partial^2 u}{\partial x^2} + \frac{\partial^2 v}{\partial y^2} \right) \quad (5.24)$$

The above equations are momentum equations in directions of x and y . The energy balance for the said element is the first law of thermodynamics for an open system and is composed as follows:

$$\rho C_P \left(\frac{\partial T}{\partial t} + \frac{\partial(vT)}{\partial y} \right) = K \frac{\partial}{\partial x} \left(\frac{\partial T}{\partial y} \right) + \tau_{xy} \frac{\partial u}{\partial y} \quad (5.25)$$

The energy equation is written as follows:

$$\rho C_P \left(\frac{\partial}{\partial t} T + \frac{\partial}{\partial x} (uT) + \frac{\partial}{\partial y} (vT) \right) = K \left(\frac{\partial^2 T}{\partial x^2} + \frac{\partial^2 T}{\partial y^2} \right) + \left(\tau_{xx} \frac{\partial u}{\partial x} + \tau_{xy} \frac{\partial u}{\partial y} + \tau_{yx} \frac{\partial v}{\partial x} + \tau_{yy} \frac{\partial v}{\partial y} \right) \quad (5.26)$$

As it is evident, the temperature of the fluid along the pipe appears in the equation. In this equation, the last term on the right side is a function of the velocity gradients and stresses exerted on the fluid.

Heat loss can take place in the flow of a viscous fluid in a pipe for either of the following reasons:

- Friction between the fluid and the inner surface of the pipe
- Friction between layers of fluid

The force resulting from the friction exerts shear stress on the fluid; therefore, the higher the friction, the larger the resulting stress and heat generation that promotes heat loss.

The last term on the right side of the energy equation can be simplified as follows:

$$\left\{ \begin{array}{l} \tau_{xx} \frac{\partial u}{\partial x} = -2\mu \left(\frac{\partial u}{\partial x} \right)^2 \\ \tau_{xy} \frac{\partial u}{\partial y} = -\mu \left(\left(\frac{\partial u}{\partial y} \right)^2 + \left(\frac{\partial v}{\partial x} \right) \left(\frac{\partial u}{\partial y} \right) \right) \\ \tau_{yx} \frac{\partial v}{\partial x} = -\mu \left(\left(\frac{\partial v}{\partial x} \right)^2 + \left(\frac{\partial v}{\partial x} \right) \left(\frac{\partial u}{\partial y} \right) \right) \\ \tau_{yy} \frac{\partial v}{\partial y} = -2\mu \left(\frac{\partial v}{\partial y} \right)^2 \end{array} \right. \quad (5.27)$$

In the end, the energy equation for this fluid changes to the following form:

$$\frac{\partial T}{\partial t} + \frac{\partial(uT)}{\partial x} + \frac{\partial(vT)}{\partial y} = \frac{K}{\rho C_P} \left(\frac{\partial^2 T}{\partial x^2} + \frac{\partial^2 T}{\partial y^2} \right) - \mu \left(2 \left(\frac{\partial u}{\partial x} \right)^2 + 2 \left(\frac{\partial v}{\partial y} \right)^2 + \left(\frac{\partial u}{\partial y} + \frac{\partial v}{\partial x} \right)^2 \right) \quad (5.28)$$

Where $\frac{K}{\rho C_P}$ denotes thermal diffusivity [84].

5.4.2. Initial and Boundary Conditions

When $T > T_w$, because of the heat transfer between the fluid and the pipe wall, the temperature of the fluid adjacent to the inner surface of the pipe remains close to that of the wall.

Considering the increased viscosity of the fluid near the internal surface of the pipe, the no-slip assumption applies and the velocity of the fluid can be assumed negligible over the pipe wall.

$$\begin{cases} x = 0 & \begin{cases} u = v_{in} \\ v = 0 \end{cases}, \quad P = P_{in} \quad \text{and} \quad T = T_{in} \\ \begin{cases} y = 0 \\ y = 2R \end{cases} & u_{slip} = 0 \quad \text{and} \quad v_{slip} = 0 \end{cases} \quad (5.29)$$

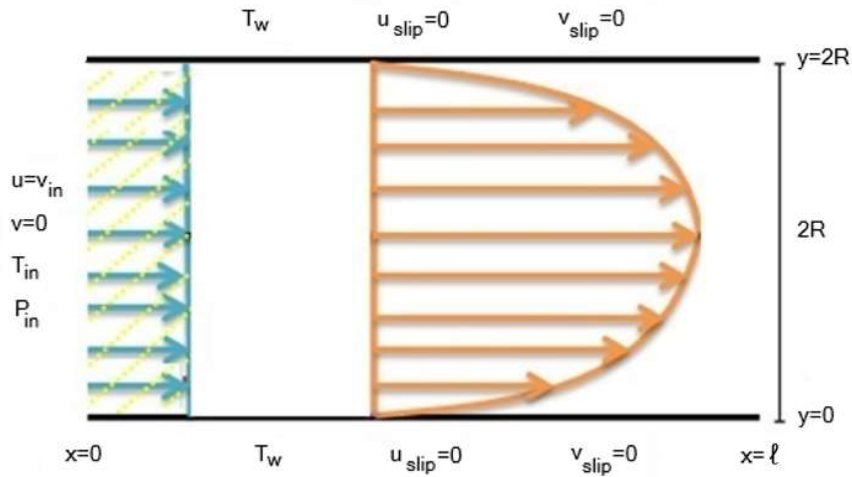


Figure 5.3 Velocity, temperature, and pressure of fluid at pipe inlet /
Velocity and temperature of fluid over inner surface of pipe

CHAPTER 6

Dimensionless Numerical Model

6.1 Introduction

To solve Navier–Stokes equations, they must be simplified for each specific case by removing the terms of low significance. Under non-Newtonian flow conditions, given the relatively high viscosity of the fluid, inertia will remain negligible, and its corresponding term in Navier–Stokes equations can be ignored.

On the other hand, dimensionless equations governing the flow can be written by defining dimensionless numbers and variables and placing them in the equations (Al-Zahrani and Al-Fariss, 1998; Iktisanov and Sakhabutdinov, 1999). Using dimensionless equations results in:

- A flow that is a function of dimensionless numbers and variables
- Flow variables will be bounded to the 0–1 range
- After solving the dimensionless equations governing the problem, the relations presented for the dimensionless variables can be used to obtain the main flow variables

6.2 Dimensionless Numbers

By considering heat loss between the pipe interior surface and its centerline, and momentum flows entering the differential fluid volume, the dimensionless numbers of Reynolds, Brinkman, and Prandtl are introduced to the dimensionless equations governing the problem. In other words, the flow is a function of the mechanism, heat loss, and momentum flows entering the differential volume of the fluid.

6.2.1 Generalized Reynolds Number

As stated previously, according to the flow model used to describe the fluid behavior, various theories for calculating the Reynolds number are proposed. The value of the Reynolds number for a Power-law fluid flowing in pipes, channels and between parallel plates, in addition to the flow behavior index, depends on other parameters such as velocity, density and, dimensions of the flow path. For the present study, the following relation defines the generalized Reynolds number:

$$Re = \frac{\rho \cdot (v_{in})^{2-n} \cdot (2R)^n}{\mu} \quad (6.1)$$

Where v_{in} is the entry velocity of the Power-law crude oil with flow behavior index n , viscosity μ and density ρ which enters a horizontal pipe with diameter $2R$ (Madlener *et al.*, 2009).

6.2.2 Prandtl Number

The Prandtl number is defined as the ratio of momentum diffusivity to thermal diffusivity. The momentum diffusivity tells us the material's resistance to shear-flows (different layers of the flow travel with different velocities) in relation to density. The Prandtl number is given as:

$$Pr = \frac{\text{Viscous diffusion rate}}{\text{Thermal diffusion rate}}$$

For the present study, the following relation defines the Prandtl number:

$$Pr = \frac{\mu \cdot C_p \cdot (v_{in})^{n-1}}{K (2R)^{n-1}} \quad (6.2)$$

Where v_{in} is the entry velocity of the Power-law crude oil with flow behavior index n , viscosity μ , thermal conductivity C_p , and specific heat capacity K which enters a horizontal pipe with diameter $2R$ (Coulson and Richardson, 1999).

Since the Prandtl number is only a function of the fluid properties, therefore, it can be found in fluid specification tables along with such properties as viscosity, thermal conductivity, and specific heat capacity. Some researchers suggest the following range for Prandtl number:

Table 6.1 Prandtl number ranges for some fluids (Coulson and Richardson, 1999)

Fluid	Range
Gases	0.7-1.0
Water	1-10
Liquid metals	0.001-0.03
Oils	50-2000

6.2.3 Brinkman Number

Heat loss takes place as a result of the stresses exerted on the fluid. The ratio of heat dissipated to heat transferred between the fluid and the pipe wall is known as the Brinkman number.

Different definitions have been proposed for Brinkman number, but under the assumed boundary condition, the number can be defined by the following equation (Brodkey and Hershey 1988; Pontes, 2012).

$$\text{Br} = \frac{\mu \cdot (v_{\text{in}})^{n-1}}{(2R)^{n-1} (T_w - T) K} \quad (6.3)$$

Where v_{in} is the entry velocity of the Power-law crude oil with flow behavior index n , viscosity μ , specific heat capacity K , and temperature T which enters a horizontal pipe with diameter $2R$ and wall temperature T_w . Since $T > T_w$, so Br is negative.

6.3 Dimensionless Variables

The dimensionless quantities below are used to write the dimensionless form of the equations governing the flow (Al-Zahrani, 1977). Substituting the units of the components of the variables reveals them all dimensionless.

$$x^* = \frac{x}{\ell} \quad (6.4)$$

$$y^* = \frac{y}{2R} \quad (6.5)$$

$$t^* = \frac{t \cdot v_{\text{in}}}{\ell} \quad (6.6)$$

$$u^* = \frac{u}{v_{\text{in}}} \quad (6.7)$$

$$v^* = \frac{v}{v_{\text{in}}} \quad (6.8)$$

$$P^* = \frac{P}{P_{\text{in}}} \quad (6.9)$$

$$C_p^* = \frac{C_p}{C_{p_{\text{in}}}} \quad (6.10)$$

$$\rho^* = \frac{\rho}{\rho_{\text{in}}} \quad (6.11)$$

$$\mu^* = \frac{\mu}{\mu_{in}} \quad (6.12)$$

$$K^* = \frac{K}{K_{in}} \quad (6.13)$$

$$\theta = \frac{T - T_w}{T_{in} - T_w} \quad (6.14)$$

Where the variables in the relations above are as follows:

Table 6.2 Variables of relations (6.4) to (6.14)

C_P	Specific heat capacity	T_w	Pipe wall temperature	μ_{in}	Fluid viscosity at pipe inlet
C_{Pin}	Fluid specific heat capacity at pipe inlet	T	Time	μ^*	Dimensionless apparent viscosity
C^*_P	Dimensionless specific heat capacity	u	Fluid velocity in x-direction	ρ	Density
K	Thermal conductivity	u^*	Dimensionless fluid velocity in x-direction	ρ_{in}	Fluid density at pipe inlet
K_{in}	Fluid thermal conductivity at pipe inlet	v	Fluid velocity in y-direction	ρ^*	Dimensionless density
K^*	Dimensionless thermal conductivity	v_{in}	Fluid velocity at pipe inlet or entry velocity of fluid		
ℓ	Pipe length	v^*	Dimensionless fluid velocity in y-direction		
P	Fluid pressure	x	Distance on longitudinal axis (horizontal)		
P_{in}	Fluid pressure at pipe inlet	x^*	Dimensionless distance on longitudinal axis (horizontal)		
P^*	Dimensionless fluid pressure	y	Distance on transverse axis (vertical)		
$2R$	Pipe diameter	y^*	Dimensionless distance on transverse axis (vertical)		
T	Fluid temperature	θ	Dimensionless temperature		
T_{in}	Fluid temperature at pipe inlet	μ	Apparent viscosity		

6.4 Dimensionless Form of Governing Equations

The dimensionless form of the governing equations is obtained as follows by introducing the quantities mentioned above and dimensionless numbers. The dimensionless continuity equation:

$$\frac{\partial u^*}{\partial x^*} + \frac{\partial v^*}{\partial y^*} = 0 \quad (6.15)$$

The dimensionless momentum equations:

$$\frac{\partial u^*}{\partial t^*} + \frac{\partial u^{*2}}{\partial x^*} + \frac{\partial(u^* \cdot v^*)}{\partial y^*} = \frac{\mu^*}{\text{Re}} \left(\frac{\partial}{\partial x^*} \left(\frac{\partial u^*}{\partial x^*} \right) + \frac{\partial}{\partial y^*} \left(\frac{\partial v^*}{\partial y^*} \right) \right) - \frac{\partial P^*}{\partial x^*} \quad (6.16)$$

$$\frac{\partial v^*}{\partial t^*} + \frac{\partial v^{*2}}{\partial y^*} + \frac{\partial(v^* \cdot u^*)}{\partial x^*} = \frac{\mu^*}{\text{Re}} \left(\frac{\partial}{\partial y^*} \left(\frac{\partial v^*}{\partial y^*} \right) + \frac{\partial}{\partial x^*} \left(\frac{\partial u^*}{\partial x^*} \right) \right) - \frac{\partial P^*}{\partial y^*} \quad (6.17)$$

The dimensionless energy equation:

$$\begin{aligned} \frac{\partial \theta}{\partial t^*} + \frac{\partial(u^* \cdot \theta)}{\partial x^*} + \frac{\partial(v^* \cdot \theta)}{\partial y^*} &= \frac{1}{\text{Re} \cdot \text{Pr}} \cdot \frac{K^*}{C_p^*} \left(\left(\frac{\partial \theta}{\partial x^*} \right)^2 + \left(\frac{\partial \theta}{\partial y^*} \right)^2 \right) \\ &- \frac{\text{Br}}{\text{Re} \cdot \text{Pr}} \cdot \frac{\mu^*}{C_p^*} \left(2 \left(\left(\frac{\partial u^*}{\partial x^*} \right)^2 + \left(\frac{\partial v^*}{\partial y^*} \right)^2 \right) + \left(\frac{\partial u^*}{\partial y^*} + \frac{\partial v^*}{\partial x^*} \right)^2 \right) \end{aligned} \quad (6.18)$$

The dimensionless governing equations are presented in Eqs. (6.15) through (6.18). According to these equations, one must note that the Brinkman number appears only in the last term on the right side of the dimensionless energy equation and has no impact on dimensionless continuity and momentum equations. Furthermore, according to Eq. (6.18), the dimensionless temperature gradient depends on the dimensionless velocity gradient of the fluid.

6.5 Modified Governing Dimensionless Equations

By taking into account the assumptions for viscosity, thermal conductivity and specific heat capacity for each reference crude oil in Eqs. (6.10), (6.12) and (6.13), the governing dimensionless equations Eqs. (6.15) through (6.18) are modified into Eqs. (6.19) through (6.22).

$$\frac{\partial u^*}{\partial x^*} + \frac{\partial v^*}{\partial y^*} = 0 \quad (6.19)$$

$$\frac{\partial u^*}{\partial t^*} + \frac{\partial u^{*2}}{\partial x^*} + \frac{\partial(u^*.v^*)}{\partial y^*} = \frac{1}{\text{Re}} \left(\frac{\partial}{\partial x^*} \left(\frac{\partial u^*}{\partial x^*} \right) + \frac{\partial}{\partial y^*} \left(\frac{\partial v^*}{\partial y^*} \right) \right) - \frac{\partial P^*}{\partial x^*} \quad (6.20)$$

$$\frac{\partial v^*}{\partial t^*} + \frac{\partial v^{*2}}{\partial y^*} + \frac{\partial(v^*.u^*)}{\partial x^*} = \frac{1}{\text{Re}} \left(\frac{\partial}{\partial y^*} \left(\frac{\partial v^*}{\partial y^*} \right) + \frac{\partial}{\partial x^*} \left(\frac{\partial u^*}{\partial x^*} \right) \right) - \frac{\partial P^*}{\partial y^*} \quad (6.21)$$

The modified dimensionless energy equation:

$$\begin{aligned} \frac{\partial \theta}{\partial t^*} + \frac{\partial(u^*.\theta)}{\partial x^*} + \frac{\partial(v^*.\theta)}{\partial y^*} = \frac{1}{\text{Re.Pr}} \left(\left(\frac{\partial \theta}{\partial x^*} \right)^2 + \left(\frac{\partial \theta}{\partial y^*} \right)^2 \right) \\ - \frac{\text{Br}}{\text{Re.Pr}} \left(2 \left(\left(\frac{\partial u^*}{\partial x^*} \right)^2 + \left(\frac{\partial v^*}{\partial y^*} \right)^2 \right) + \left(\frac{\partial u^*}{\partial y^*} + \frac{\partial v^*}{\partial x^*} \right)^2 \right) \end{aligned} \quad (6.22)$$

6.6 Dimensionless Initial and Boundary Conditions

Given that $0 \leq x \leq \ell$ and $0 \leq y \leq 2R$, based on Eqs. (6.4) and (6.5), the variables are bounded between 0 and 1 after nondimensionalization, based on Eqs. (6.7), (6.8), (6.9) and (6.14), the dimensionless initial and boundary conditions can be written as follows:

$$x^* = 0 \quad \begin{cases} u^* = 1 \\ v^* = 0 \\ \theta = 1 \\ P^* = 1 \end{cases} \quad \text{and} \quad \begin{cases} y^* = 0 \\ y^* = 1 \end{cases} \quad \begin{cases} u^* = 0 \\ v^* = 0 \\ \theta = 0 \end{cases} \quad (6.23)$$

CHAPTER 7

Computational Fluid Dynamics (CFD) Technique

7.1 Introduction

To avoid the calculation complexities and duplicate explanations in the numerical methods ahead, the simplified form of the dimensionless variables is used in the dimensionless equations and the dimensionless initial and boundary conditions, for example, $x^* \rightarrow x$, therefore, Eqs. (6.19) through (6.22) are written as follows:

$$\frac{\partial u}{\partial x} + \frac{\partial v}{\partial y} = 0 \quad (7.1)$$

$$\frac{\partial u}{\partial t} + \frac{\partial u^2}{\partial x} + \frac{\partial(u.v)}{\partial y} = \frac{1}{\text{Re}} \left(\frac{\partial}{\partial x} \left(\frac{\partial u}{\partial x} \right) + \frac{\partial}{\partial y} \left(\frac{\partial v}{\partial y} \right) \right) - \frac{\partial P}{\partial x} \quad (7.2)$$

$$\frac{\partial v}{\partial t} + \frac{\partial v^2}{\partial y} + \frac{\partial(v.u)}{\partial x} = \frac{1}{\text{Re}} \left(\frac{\partial}{\partial y} \left(\frac{\partial v}{\partial y} \right) + \frac{\partial}{\partial x} \left(\frac{\partial u}{\partial x} \right) \right) - \frac{\partial P}{\partial y} \quad (7.3)$$

$$\begin{aligned} \frac{\partial \theta}{\partial t} + \frac{\partial(u.\theta)}{\partial x} + \frac{\partial(v.\theta)}{\partial y} = & \frac{1}{\text{Re.Pr}} \cdot \left(\left(\frac{\partial \theta}{\partial x} \right)^2 + \left(\frac{\partial \theta}{\partial y} \right)^2 \right) \\ & - \frac{\text{Br}}{\text{Re.Pr}} \cdot \left(2 \left(\left(\frac{\partial u}{\partial x} \right)^2 + \left(\frac{\partial v}{\partial y} \right)^2 \right) + \left(\frac{\partial u}{\partial y} + \frac{\partial v}{\partial x} \right)^2 \right) \end{aligned} \quad (7.4)$$

Moreover, the dimensionless initial and boundary conditions can be written:

$$x=0 \quad \begin{cases} u = 1 \\ v = 0 \\ \theta = 1 \\ P = 1 \end{cases} \quad \text{and} \quad \begin{cases} y = 0 \\ y = 1 \end{cases} \quad \begin{cases} u = 0 \\ v = 0 \\ \theta = 0 \end{cases} \quad (7.5)$$

Based on Eqs. (7.2) and (7.3), velocity and pressure depend strongly on each other. On the other hand, the velocities should satisfy Eq. (7.1).

Eq. (7.4) also indicates the dependence of temperature and velocity. Therefore, analytical and simultaneous solving of non-dimensional equations is very difficult due to the dependence of flow variables.

In solving these equations, one of the numerical techniques of Computational Fluid Dynamics (CFD) is used, and accordingly, velocity, pressure, and temperature are approximated in the computational field.

CFD techniques have the capacity for analyzing systems with flowing fluids, heat transfer, and else, and offer unique advantages in comparison with experimental methods. Finite-difference, Finite-element, and Finite-volume methods are some interesting examples of CFD techniques. These methods are different in their estimations of unknown flow variables and the discretization process but, in general, involve the following steps:

- Unknown variables are estimated using simple functions
- The integral equations resulting from the integration of the governing partial differential equations are discretized by substituting the estimations and carrying out the required mathematical operations
- Solving the system of algebraic equations obtained in the previous step by an iterative solution method

7.2 Finite-Volume Method

The main attraction of the finite-volume method is the explicit relation between the numerical algorithm and the general rule of physical conservation that facilitates the comprehension of the concepts for the user in comparison with other CFD techniques. Moreover, integration of the governing equations on all control volumes (CVs) or meshes are a distinct feature of this particular method.

Each CV contains a node at the center that preserves the flow data. **Fig. 7.1** shows a three-dimensional general CV with a general node Plc. In this figure, B, S, E, M, R, and C are the neighbors of the general node.

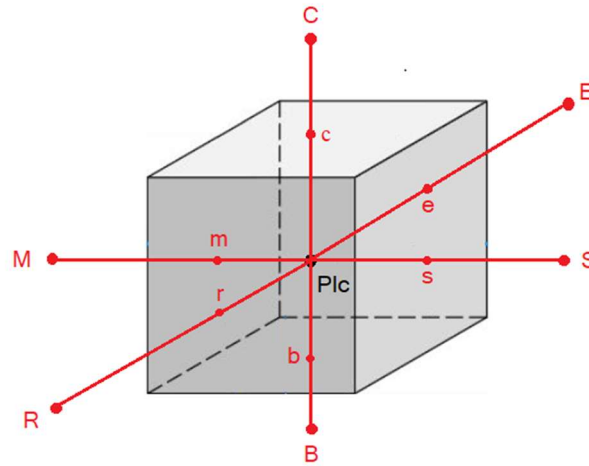


Figure 7.1 General three-dimensional CV and location of nodes neighboring general node

The finite-volume method begins with the transfer of the computational or solution domain to a computational grid. The continuous computational domain must be discretized into several CVs provided that, they do not interfere and fill the entire domain together.

Next, the terms of each integral equation obtained from partial differential equations are approximated over the general CV, discretizing the equations by substituting their terms with approximates.

Given the dependence of the pressure and temperature on the velocity, it can be concluded that the velocity variable plays a key role in the approximation of the other two variables. Therefore, at first, the SIMPLE algorithm is used to find the correct relation between pressure and velocity (pressure–velocity coupling algorithm). Accordingly, the pressure and velocity of the reference crude oil are estimated overall the general CV. By approximating the flow velocity on the general CV and inserting it into the discrete energy equation, the fluid temperature can be easily estimated on the CV.

In the following, the approximations obtained on the general CV are expanded over the computational grid. This is carried out by solving the resulting system of algebraic equations by line-by-line or Tri-Diagonal Matrix Algorithm (TDMA) method.

An attractive feature of the finite-volume method is that the results, including the unknown variables, apply to all CVs and, therefore, the entire computational domain.

7.2.1 Computational Domain Discretization

The following must be taken into account when discretizing the computational domain.

- The accuracy of a numerical method depends on the number of CVs in the grid. More CVs lead to higher accuracy of calculations. However, computational cost and time increase in proportion to the rise in the number of CVs.
- When establishing a computational grid, first, the faces of CVs must be determined, then, the nodes must be placed at the centers of CVs.
- Considering the steep velocity and temperature gradients near the inner surface of the wall compared to other regions, smaller CVs and closer nodes are assumed (**Fig. 7.2**).
- The faces of CVs take place at the boundaries of the computational grid and not the nodes.

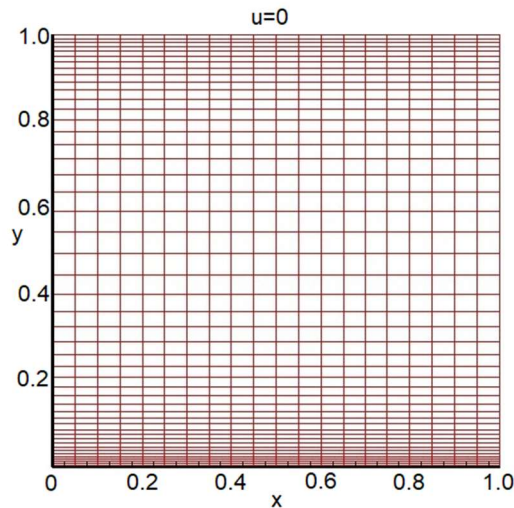


Figure 7.2 Computational domain discretization

7.3 General Equation

As mentioned earlier, the next step in the finite-volume method following the discretization of the computational domain is discretizing every term of integral equations obtained from the integration of partial differential Eqs. (7.1) through (7.4) on the computational grid. Accordingly, to present a unified method, the general form of the equations is presented before integration. In

doing so, it will suffice to make the following replacements in the said equations:

- Replace ℓ , u , v and θ with ϕ
- Replace zero, $\frac{1}{Re}$, $\frac{1}{Re}$ and $\frac{1}{Re \cdot Pr}$ with Γ
- Replace zero, $-\frac{\partial P}{\partial x}$, $-\frac{\partial P}{\partial y}$ and $-\frac{Br}{Re \cdot Pr} \left(2 \left(\left(\frac{\partial u}{\partial x} \right)^2 + \left(\frac{\partial v}{\partial y} \right)^2 \right) + \left(\frac{\partial u}{\partial y} + \frac{\partial v}{\partial x} \right)^2 \right)$ with S_ϕ

Eqs. (7.1) through (7.4) will be written as follows which is the general form of the equations.

$$\frac{\partial \phi}{\partial t} + \text{div}(\phi \mathbf{u}) = \text{div}(\Gamma \text{grad}(\phi)) + S_\phi \quad (7.6)$$

Eqs. (7.1) through (7.4) can be derived from the general equation; in other words, these equations are special forms of the general equation. Eq. (7.6) is also referred to the ϕ transfer equation where ϕ denotes the global variable, Γ represents diffusivity and S_ϕ is the source term. Furthermore, $\frac{\partial \phi}{\partial t}$ denotes the transient term and is equal to the increasing rate of the property ϕ in the CV.

In Eq. (7.6), $\text{div}(\phi \mathbf{u})$ is the convective term and equals the net flow rate ϕ outside the CV. Moreover, $\text{div}(\Gamma \text{grad}(\phi))$ is the diffusion term and is the increasing rate of ϕ through diffusion in the CV and S_ϕ represents the source and equals the increasing rate of ϕ as a result of the source in the CV.

In the heat transfer between the reference crude oil and the pipe wall, under conditions where the fluid temperature experiences a slow decline, the interaction rate between paraffin molecules, crystal nucleation, increased interconnection between paraffin molecules and their growth (clustering) are mitigated and smaller and more uniform paraffin crystals are formed (see Section 1.5.1). Put differently, the increase in viscosity is slow enough for it to be convenient to assume a steady model for momentum and energy equations. In other words, the time-dependent terms can be omitted in Eqs. (5.23), (5.24) and (5.28). Accordingly, the time-dependent terms are also omitted in Eqs. (7.2), (7.3) and (7.4).

Given the assumption of steady flow, Eq. (7.6) in the convection-diffusion problem loses its transient term and is, thus, written as:

$$\text{div}(\phi \cdot \mathbf{u}) = \text{div}(\Gamma \text{grad}(\phi)) + S_\phi \quad (7.7)$$

7.3.1 Integration of General Equation

To investigate the changes in the general property ϕ from Eq. (7.7) on any CV, the variable general fluxes ϕ must be taken into account on the CV to determine its change inside the CV based on its variation on CV boundaries. Therefore, the volumetric integral must be transformed into the surface integral with the help of Gauss's divergence theorem. For \vec{a} , the theory states:

$$\int_{CV} \text{div}(\vec{a}) dv = \int_A \vec{n} \cdot \vec{a} dA \quad (7.8)$$

The vector \vec{a} is the perpendicular vector to the area dA and its direction is outside. The area A implies all surface areas encompassing the CV.

Eq. (7.8) states that the divergence integral of the vector \vec{a} in a CV is the sum of vector components \vec{a} normal to the surfaces encompassing the volume on all boundaries.

7.3.1.1 Discretization of Convective Term Integral

Gauss's divergence theorem is employed to transform the volumetric integral of the convective term:

$$\int_{CV} \text{div}(\phi \vec{u}) dv = \int_A \vec{n} \cdot (\phi \vec{u}) dA \quad (7.9)$$

$$\begin{aligned} &= (\phi u)_e A_e - (\phi u)_r A_r + (\phi v)_c A_c - (\phi v)_b A_b + (\phi w)_s A_s - (\phi w)_m A_m \\ &= (u)_e A_e \phi_e - (u)_r A_r \phi_r + (v)_c A_c \phi_c - (v)_b A_b \phi_b + (w)_s A_s \phi_s - (w)_m A_m \phi_m \end{aligned}$$

As evident in the above integration, a term containing the global variable ϕ appeared in each face of the CV ($\phi_e, \phi_r, \phi_c, \phi_b, \phi_s$ and ϕ_m). However, one must be noted that the global variable ϕ is stored in the nodes of the CV, not on its faces. The essential problem of the discretizing convection sections is calculating ϕ transferred from the faces of the CV and the convective flux passing these boundaries.

Based on **Fig. 7.1**, the several methods exist for estimating the global variable ϕ including Central Difference and Upwind schemes.

In the central difference, the global variable ϕ is estimated on the faces of the CV by linear interpolation. However, a serious shortcoming of this scheme lies in its inability to determine the flow, as it takes into account the effects of all neighbors of the general point Plc in the calculation of the diffusive-convective flux. Furthermore, in a strong west-east flow, the central difference scheme transfers equal shares from west and east to Plc, this is not convenient, as Plc must receive a more significant impact from the western node in such cases. Therefore, such a function yields inaccurate results.

In the upwind scheme, the direction of the flow is used to determine its magnitude on the cell surface. The convected ϕ on the surface of the CV is assumed to equal ϕ at the node upwind of Plc. In the west-east direction:

$$\phi_r = \phi_R \quad (7.10)$$

$$\phi_e = \phi_{Plc} \quad (7.11)$$

Accordingly, the general values ϕ are substituted in the integrated equation. Thanks to its simplicity, the upwind scheme is extensively employed in typical CFD tasks and can be easily expanded to any coordinate direction in multi-dimensional problems.

7.3.1.2 Discretization of Diffusion Term Integral

The volumetric integral of the diffusion term is replaced with a surface integral as discussed earlier:

$$\begin{aligned} \int_{CV} \text{div}(\Gamma \text{grad } \phi) dv &= \int_A \vec{n} \cdot (\Gamma \text{grad } \phi) dA \quad (7.12) \\ &= (\Gamma \frac{\partial \phi}{\partial x})_e A_e - (\Gamma \frac{\partial \phi}{\partial x})_r A_r + (\Gamma \frac{\partial \phi}{\partial y})_c A_c - (\Gamma \frac{\partial \phi}{\partial y})_b A_b + (\Gamma \frac{\partial \phi}{\partial z})_s A_s - (\Gamma \frac{\partial \phi}{\partial z})_m A_m = \\ &= \frac{\Gamma_e A_e}{(\delta x)_{Plc.E}} (\frac{\partial \phi}{\partial x})_e - \frac{\Gamma_r A_r}{(\delta x)_{R.Plc}} (\frac{\partial \phi}{\partial x})_r - \frac{\Gamma_c A_c}{(\delta x)_{Plc.C}} (\frac{\partial \phi}{\partial y})_c - \frac{\Gamma_b A_b}{(\delta x)_{B.Plc}} (\frac{\partial \phi}{\partial y})_b - \frac{\Gamma_s A_s}{(\delta x)_{Plc.S}} (\frac{\partial \phi}{\partial z})_s - \\ &\quad - \frac{\Gamma_m A_m}{(\delta x)_{S.Plc}} (\frac{\partial \phi}{\partial z})_m \end{aligned}$$

7.3.1.3 Discretization of Source Term Integral

The integral of the source term is as follows:

$$\int_{CV} S_{\phi} dv = \bar{S} \Delta v \quad (7.13)$$

by linearizing the source term:

$$\int_{CV} S_{\phi} dv = S_u + S_{Plc} \phi_{Plc} \quad (7.14)$$

Up to this point, the terms on either side of Eq. (7.7) have been integrated on the CV in three dimensions. For the sake of simplicity, the following two factors are introduced:

$$D = \frac{\Gamma}{\delta x} A \quad \text{Diffusivity} \quad (7.15)$$

$$F = u \cdot A \quad \text{Convective mass flux} \quad (7.16)$$

The above two factors are rewritten below for each face:

$$F_e = u_e \cdot A_e \quad F_r = u_r \cdot A_r \quad (7.17)$$

$$F_b = u_b \cdot A_b \quad F_c = u_c \cdot A_c \quad (7.18)$$

$$F_m = u_m \cdot A_m \quad F_s = u_s \cdot A_s \quad (7.19)$$

$$D_e = \frac{\Gamma_e}{(\delta x)_{Plc.E}} A_e \quad D_r = \frac{\Gamma_r}{(\delta x)_{R.Plc}} A_r \quad (7.20)$$

$$D_c = \frac{\Gamma_c}{(\delta x)_{Plc.C}} A_c \quad D_b = \frac{\Gamma_b}{(\delta x)_{B.Plc}} A_b \quad (7.21)$$

$$D_s = \frac{\Gamma_s}{(\delta x)_{Plc.S}} A_s \quad D_m = \frac{\Gamma_m}{(\delta x)_{M.Plc}} A_m \quad (7.22)$$

Next definition is the convection ratio to diffusion in the flow, which defines the Péclet number:

$$Pe = \frac{F}{D} \quad (7.23)$$

The Péclet number is rewritten for every face of the element, for example:

$$Pe_e = \frac{F_e}{D_e} \quad (7.24)$$

Now, considering Eq. (7.7), the integrated terms, and the new factors introduced above, the following general form is obtained after factorization of ϕ :

$$a_{Plc} \phi_{Plc} = a_E \phi_E + a_R \phi_R + a_S \phi_S + a_M \phi_M + a_C \phi_C + a_B \phi_B \quad (7.25)$$

which the factors of a_E , a_R , a_S , a_M , a_C and a_B are defined as follows:

$$a_E = D_e A (|Pe_e| + \max(-F_e, 0)) \quad (7.26)$$

$$a_R = D_r A(|Pe_r|) + \max(-F_r, 0) \quad (7.27)$$

$$a_S = D_s A(|Pe_s|) + \max(-F_s, 0) \quad (7.28)$$

$$a_M = D_m A(|Pe_m|) + \max(-F_m, 0) \quad (7.29)$$

$$a_C = D_c A(|Pe_c|) + \max(-F_c, 0) \quad (7.30)$$

$$a_B = D_b A(|Pe_b|) + \max(-F_b, 0) \quad (7.31)$$

which the function $A(|Pe|)$ would be:

$$A(|Pe_e|) = \max(0, (1 - 0.1|Pe_e|)^5) \quad (7.32)$$

$$A(|Pe_r|) = \max(0, (1 - 0.1|Pe_r|)^5) \quad (7.33)$$

$$A(|Pe_s|) = \max(0, (1 - 0.1|Pe_s|)^5) \quad (7.34)$$

$$A(|Pe_m|) = \max(0, (1 - 0.1|Pe_m|)^5) \quad (7.35)$$

$$A(|Pe_c|) = \max(0, (1 - 0.1|Pe_c|)^5) \quad (7.36)$$

$$A(|Pe_b|) = \max(0, (1 - 0.1|Pe_b|)^5) \quad (7.37)$$

The above functions can be used for all Péclet numbers (positive, negative and zero).

Eq. (7.25) is used as the basis for computer programming. In other words, the dimensionless velocity, pressure, and temperature of the flow are calculated in every CV using this equation.

7.3.2 SIMPLE Algorithm

The calculation of the temperature is not as complicated as calculating the velocity and pressure. The calculation of the temperature can only be calculated by having the flow velocity values on the general CV. By introducing the estimated dimensionless flow velocity to Eq. (7.25), the temperature of the fluid can be approximated on the general CV. For this purpose, the relation between the general node and its neighbors is obtained based on the general node Plc and by introducing the relations from the previous section to Eq. (7.25). The new relation, which is based on the vector components of the coordinate system (that is i , j and k), can be applied to all CVs using the programmed loop. Thus, a system of algebraic equations is obtained that can be solved by a TDMA approach.

In the case of computing the pressure and velocity on the general CV, the subject is slightly different. As discussed in the previous section, the momentum and continuity equations have complicated combinations for all velocity components that appear in the continuity equation in addition to momentum equations. The pressure and velocity are coupled in the momentum equations, and no separate equation is available for obtaining the pressure. If the pressure gradient is known, the velocities can be obtained from the momentum equations without any difficulty. However, often that is not the case in reality.

The combination of the pressure and velocity imposes the condition where, if the correct pressure is applied to the momentum equations, the resulting velocity satisfies the continuity equation. In this case, the continuity equation is the key to the relation between the velocity and pressure. The pressure is calculated by a coupling method such as the SIMPLE algorithm or its modified versions. These methods are based on employing the continuity equation to obtain the pressure distribution (Patankar, 1980). This algorithm is used in the present study to couple the equations.

The SIMPLE algorithm starts with an initial guess of the velocity and pressure. The guess is then used to solve the momentum equations. If the speculated pressure is correct, the velocities should satisfy the continuity equation. Otherwise, the pressure and velocity will be corrected drawing on a special formulation that is readily presented replacing the results with the initial guess and solving the equations again. The process iterates until the results satisfy the continuity equation. This algorithm requires storage to be set for the velocities, which can be done by using collocated or non-collocated grids.

7.3.2.1 Collocated Grid

Collocated grids facilitate applying the initial and boundary conditions in complex geometries. **Fig. 7.3** shows a collocated grid that can be used to calculate all variables on the general node and its neighbors.

Considering **Fig. 7.4**, if the pressure is determined on e and r by linear interpolation, to determine the pressure gradient $\frac{\partial P}{\partial x}$ at the general node Plc, one can write in the momentum equation in the x-direction (Patankar, 1980):

$$\frac{\partial P}{\partial x} = \frac{P_e - P_r}{\delta x} = \frac{\left(\frac{P_E - P_{Plc}}{2}\right) - \left(\frac{P_R - P_{Plc}}{2}\right)}{\delta x} = \left(\frac{P_E - P_R}{2\delta x}\right) \quad (7.38)$$

similarly, for the momentum equation in the y-direction, the pressure gradient $\frac{\partial P}{\partial y}$ is:

$$\frac{\partial P}{\partial y} = \left(\frac{P_S - P_M}{2\delta y}\right) \quad (7.39)$$

As evident, the pressure at the central node Plc appears in Eq. (7.38) and Eq. (7.39). By substituting P_E and P_R in Eq. (7.38) and P_S and P_M , it is revealed that all the pressure gradients vanish even under the severe pressure fluctuations. The non-uniform pressure appears as uniform in the discrete equations.

It is clear that if the velocities are defined in the nodes of the scalar grid, the pressure effect does not appear in the discrete momentum equations. One solution to this problem is to use a non-collocated grid for the velocity components.

7.3.2.2 Non-Collocated Grid

Fig. 7.5 illustrates two velocities CVs (u and v) along with the sequence of their corresponding nodes (u_E , u_R , v_S , and v_M). As evident, the nodes corresponding to the velocities CVs are located on the faces of the pressure CV.

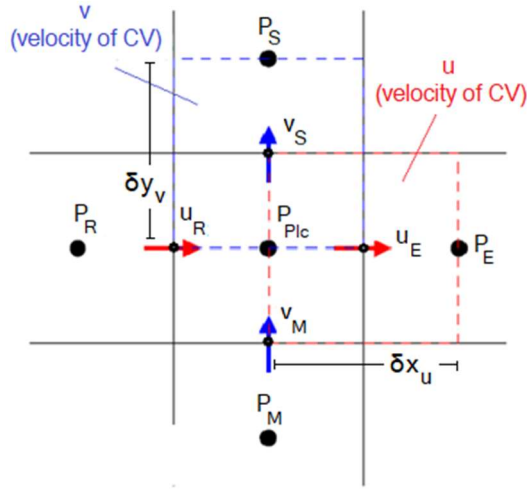


Figure 7.5 Non-collocated grid and location of velocity and pressure CVs

In the non-collocated structure, the pressure gradient $\frac{\partial P}{\partial x}$, is expanded by the relation below:

$$\frac{\partial P}{\partial x} = \frac{P_{Plc} - P_R}{\delta x_u} \quad (7.40)$$

where δx_u represents the width of the velocity CV of u . Similarly:

$$\frac{\partial P}{\partial y} = \frac{P_{Plc} - P_M}{\delta y_v} \quad (7.41)$$

where δy_v represents the width of the velocity CV of v .

7.3.2.3 Corrected Pressure and Velocity

By considering a non-collocated grid of CVs (**Fig. 7.6**), the speculative pressure P_{spec} , the speculative velocity u_{spec} in x -direction and the speculative velocity v_{spec} in y -direction are assumed.

Since the used variables in the equations ahead are dimensionless, so according to Eq. (6.9), the speculative pressure at the pipe inlet can be considered as below:

$$P_{spec}=1 \quad (7.42)$$

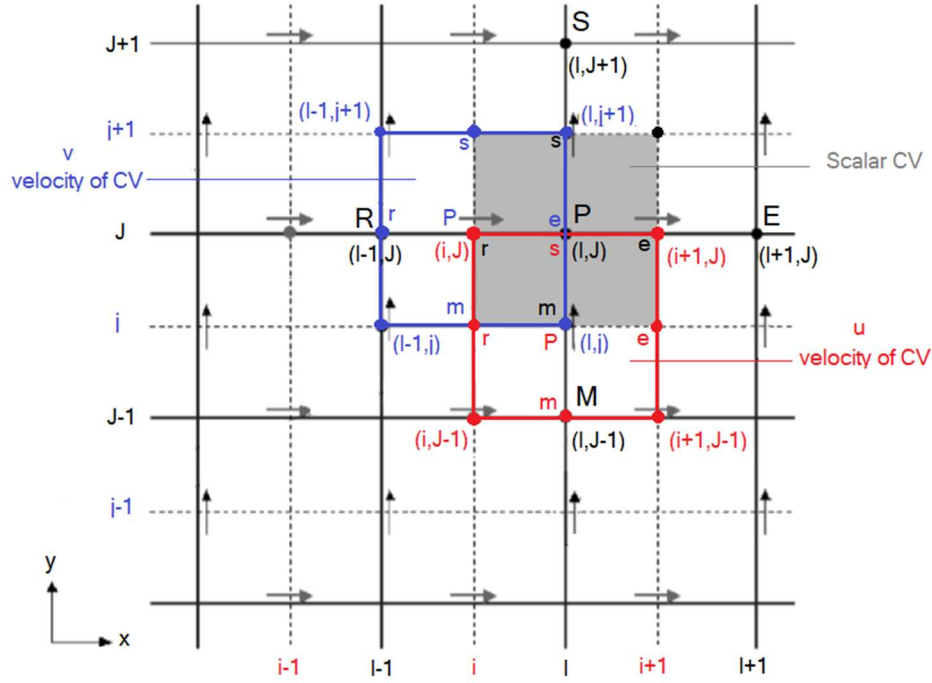


Figure 7.6 Velocity CVs in a non-collocated grid

Eqs. (7.43) and (7.44) can be written based on the speculative pressure and velocities as follows:

$$a_{Plc}(i, J)u_{spec}(i, J) = \sum a_k u_{spec,k} + (P_{spec,I-1,J} - P_{spec,I,J})A_{i,J} \quad (7.43)$$

$$a_{Plc}(I, j)v_{spec}(I, j) = \sum a_k v_{spec,k} + (P_{spec,I,J-1} - P_{spec,I,J})A_{I,j} \quad (7.44)$$

the speculative velocities u_{spec} and v_{spec} are obtained by solving the equations above. Now, the following equation is introduced:

$$\dot{P} = P - P_{spec} \quad (7.45)$$

The above equation is referred to as the pressure-correction equation where \dot{P} is the modified pressure. Similarly, the following relations are established between the modified velocity and the speculative velocity:

$$u' = u - u_{spec} \quad (7.46)$$

$$v' = v - v_{spec} \quad (7.47)$$

The modified velocity can be obtained by substituting the modified pressure in the momentum equations. If Eqs. (7.46) and (7.47) are deducted from the discrete velocity equations to

substitute Eqs. (7.45), (7.46) and (7.47), the discrete modified velocity equations are changed as follows:

$$u'_{i,J} = d_{i,J}(P'_{I-1,J} - P'_{I,J}) \quad (7.48)$$

$$v'_{I,j} = d_{I,j}(P'_{I,J-1} - P'_{I,J}) \quad (7.49)$$

Where:

$$d_{i,J} = \frac{A_{i,J}}{a_{i,J}} \quad \text{and} \quad d_{I,j} = \frac{A_{I,j}}{a_{I,j}} \quad (7.50)$$

Eqs. (7.48) and (7.49) are substituted in Eqs. (7.46) and (7.47) to have:

$$u_{i,J} = u_{\text{spec},i,J} + d_{i,J}(P'_{I-1,J} - P'_{I,J}) \quad (7.51)$$

$$v_{I,j} = v_{\text{spec},I,j} + d_{I,j}(P'_{I,J-1} - P'_{I,J}) \quad (7.52)$$

The continuity equation has the following form:

$$((uA)_{i+1,J} - (uA)_{i,J}) + ((uA)_{I,j+1} - (uA)_{I,j}) = 0 \quad (7.53)$$

The velocities resulted from Eqs. (7.51) and (7.52) are substituted in Eq. (7.53):

$$a_{I,J}P'_{I,J} = a_{I+1,J}P'_{I+1,J} + a_{I-1,J}P'_{I-1,J} + a_{I,J+1}P'_{I,J+1} + a_{I,J-1}P'_{I,J-1} \quad (7.54)$$

The above discrete equation is used to modify the pressure \dot{P} , which is, in fact, Eq. (7.25). Besides, Eq. (7.54) tends to diverge unless a new modified pressure P^{new} is obtained in iterations using the equation below:

$$P^{\text{new}} = P_{\text{spec}} + \alpha_P \dot{P} \quad (7.55)$$

Where α_P is the under-relaxation factor of pressure.

If α_P is 1, then the speculative pressure is improved by Eq. (7.45) but for 0, it remains unchanged. If the factor falls in the 0–1 range, a fraction of the modified pressure \dot{P} can be added to the speculative pressure P_{spec} . Moreover, the components of the new modified velocity can be obtained from the following relations:

$$u^{\text{new}} = \alpha_u u + (1 - \alpha_u) u^{(n-1)} \quad (7.56)$$

$$v^{\text{new}} = \alpha_v v + (1 - \alpha_v) v^{(n-1)} \quad (7.57)$$

where $u^{(n-1)}$ and $v^{(n-1)}$ are the results at (n-1)th iteration. The extreme values of α can yield fluctuating or even repetitive and divergent results, whereas small values lead to slow

convergence.

7.3.3 Tri-Diagonal Matrix Algorithm

As discussed in previous sections, in the calculation of the velocity, pressure and temperature of the fluid, the relation between the general node P_{lc} as the basis and its neighbor nodes is determined by Eq. (7.25).

To compute the flow variables on all nodes from the computational grid, it is needed to operate line by line. Given its cost-effectiveness and that, it requires a minimalistic level of memory for data storage; the Tri-Diagonal Matrix Algorithm (TDMA) is common in CFD programs. The TDMA is a direct method for solving one-dimensional problems but can also be used in two and three-dimensional problems through line-by-line iteration.

The dimensional initial and boundary conditions (Eqs. (7.5)) govern the boundaries $x=0$ (at the pipe inlet) and $y=0$ (on the pip wall). Since ϕ can be any of the dimensionless flow variables, so for a computational gride with CVs number of $m \times m$, the relations below can be written based on vector components of the coordinate system (i,j) :

$$\phi_{i,1} = 0 \quad i = 1, \dots, m + 1 \quad (7.58)$$

$$\phi_{i,m+1} = 0 \quad i = 1, \dots, m + 1 \quad (7.59)$$

$$\phi_{1,j} = 0 \text{ or } 1 \quad j = 1, \dots, m + 1 \quad (7.60)$$

The TDMA can be used through line-by-line iteration, therefore, $\phi_{i,j}$ is written for (i,j) as follows:

$$\phi_{i,j} = \frac{a_{i,j+1}}{a_{i,j}} \phi_{i,j+1} + \frac{a_{i,j-1}}{a_{i,j}} \phi_{i,j-1} \quad i = 2, \dots, m \text{ and } j = 2, \dots, m \quad (7.61)$$

Now, the below variables are defined:

$$\lambda_{i,j} = a_{i,j+1} \quad (7.62)$$

$$\omega_{i,j} = a_{i,j} \quad (7.63)$$

$$\beta_{i,j} = a_{i,j-1} \quad (7.64)$$

Eq. (7.61) can be rewritten as follows:

$$\phi_{i,j} = \frac{\lambda_{i,j}}{\omega_{i,j}} \phi_{i,j+1} + \frac{\beta_{i,j}}{\omega_{i,j}} \phi_{i,j-1} \quad (7.65)$$

Through progressive elimination process and by using the second equation ($j=2$) of the system (Eq. (7.65)), $\varphi_{i,2}$ is substituted in the third equation ($j=3$) to obtain:

$$\varphi_{i,3} = \left(\frac{\lambda_{i,3}}{\omega_{i,3} - \beta_{i,3} \frac{\lambda_{i,2}}{\omega_{i,2}}} \right) \varphi_{i,4} + \left(\frac{\beta_{i,3} \left(\frac{\beta_{i,2}}{\omega_{i,2i}} \varphi_{i,1} \right)}{\omega_{i,3} - \beta_{i,3} \frac{\lambda_{i,2}}{\omega_{i,2}}} \right) \quad (7.66)$$

The equation above is rewritten as follows:

$$\varphi_{i,3} = \left(\frac{\lambda_{i,3}}{\omega_{i,3} - \beta_{i,3} \frac{\lambda_{i,2}}{\omega_{i,2}}} \right) \varphi_{i,4} + \left(\frac{\beta_{i,3} \psi_{i,2}}{\omega_{i,3} - \beta_{i,3} \xi_{i,2}} \right) \quad (7.67)$$

where:

$$\xi_{i,2} = \frac{\lambda_{i,2}}{\omega_{i,2}} \quad (7.68)$$

$$\psi_{i,2} = \frac{\beta_{i,2}}{\omega_{i,2}} \omega_{i,1} \quad (7.69)$$

Assuming:

$$\psi_{i,3} = \frac{\beta_{i,3} \psi_{i,2}}{\omega_{i,3} - \beta_{i,3} \xi_{i,2}} \quad \text{and} \quad \xi_{i,j} = \frac{\lambda_{i,3}}{\omega_{i,3} - \beta_{i,3} \xi_{i,2}} \quad (7.70)$$

Eq. (7.67) becomes:

$$\lambda_{i,3} = \xi_{i,3} \lambda_{i,4} + \psi_{i,3} \quad (7.71)$$

In general, the equation can be written as follows:

$$\lambda_{i,j} = \xi_{i,j} \lambda_{i,j+1} + \psi_{i,j} \quad (7.72)$$

In the progressive elimination process, the equations above are used to remove $\varphi_{i,j}$ from the j th equation in the system of Eq. (7.65). Furthermore:

$$\psi_{i,j} = \frac{\beta_{i,j} \psi_{i,j-1}}{\omega_{i,j} - \beta_{i,j} \xi_{i,j-1}} \quad \text{and} \quad \xi_{i,j} = \frac{\lambda_{i,j}}{\omega_{i,j} - \beta_{i,j} \xi_{i,j-1}} \quad (7.73)$$

At the boundaries ($j=1$ and $j=m+1$), which can be employed as follows:

$$\xi_{i,j} = 0 \quad \text{and} \quad \psi_{i,1} = \lambda_{i,1} \quad (7.74)$$

$$\xi_{i,m+1} = 0 \quad \text{and} \quad \psi_{i,m+1} = \lambda_{i,m+1} \quad (7.75)$$

7.4 Flowchart for Solving Equations by SIMPLE and TDMA Algorithms

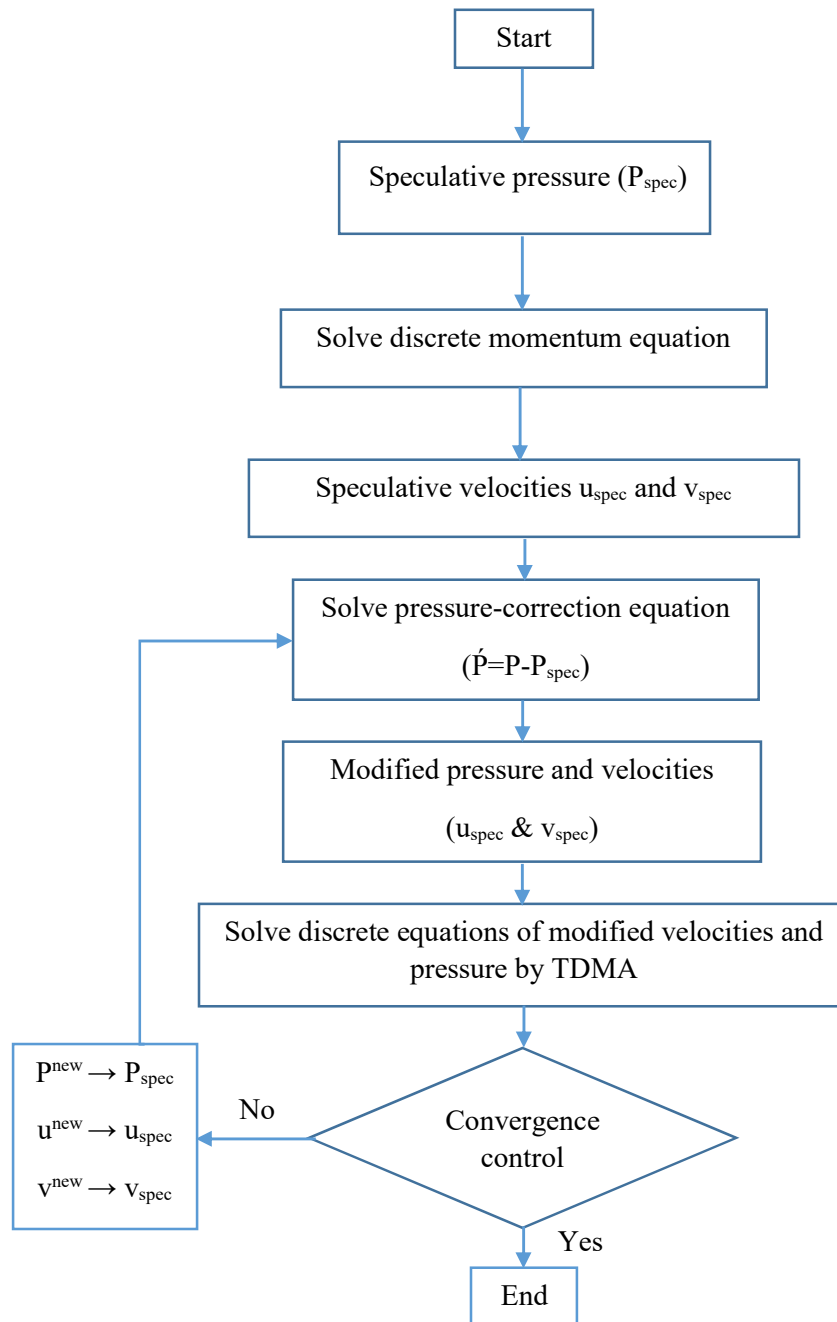


Figure 7.7 Flowchart for Solving Equations by SIMPLE and TDMA Algorithms

CHAPTER 8

Velocity, Pressure and Temperature Distributions

8.1 Input Data

Under steady state, Eqs. (7.1) through (7.4) can be written as follows:

$$\frac{\partial u}{\partial x} + \frac{\partial v}{\partial y} = 0 \quad (8.1)$$

$$\frac{\partial u^2}{\partial x} + \frac{\partial (u.v)}{\partial y} = \frac{1}{\text{Re}} \left(\frac{\partial}{\partial x} \left(\frac{\partial u}{\partial x} \right) + \frac{\partial}{\partial y} \left(\frac{\partial v}{\partial y} \right) \right) - \frac{\partial P}{\partial x} \quad (8.2)$$

$$\frac{\partial v^2}{\partial y} + \frac{\partial (v.u)}{\partial x} = \frac{1}{\text{Re}} \left(\frac{\partial}{\partial y} \left(\frac{\partial v}{\partial y} \right) + \frac{\partial}{\partial x} \left(\frac{\partial u}{\partial x} \right) \right) - \frac{\partial P}{\partial y} \quad (8.3)$$

$$\frac{\partial (u.\theta)}{\partial x} + \frac{\partial (v.\theta)}{\partial y} = \frac{1}{\text{Re.Pr}} \left[\left(\frac{\partial \theta}{\partial x} \right)^2 + \left(\frac{\partial \theta}{\partial y} \right)^2 \right] - \frac{\text{Br}}{\text{Re.Pr}} \left[2 \left(\left(\frac{\partial u}{\partial x} \right)^2 + \left(\frac{\partial v}{\partial y} \right)^2 \right) + \left(\frac{\partial u}{\partial y} + \frac{\partial v}{\partial x} \right)^2 \right] \quad (8.4)$$

In the following, to solve the above equations and obtain the dimensionless velocity, pressure and temperature for each reference crude oil sample in the computational grid by CFD technique, it is necessary to estimate Re, Pr, and Br along the pipe by Eqs. (6.1) through (6.3) for each fluid. Accordingly, taking into account the pipe specifications including $2R=21$ cm and $\ell=300$ cm the following input data are required:

Table 8.1 Input data

Reference crude oil	Density (ρ) (gr/cm ³)	Viscosity (μ) (Pa.s)	Entry velocity (v_{in}) (cm/s)	Temperature (T_w) (°C)	Specific heat capacity (K) (W/m °C)	Thermal conductivity (C_p) (J/g °C)	Calculated	
							Re	Pr
A	0.87	0.09	10	22	0.13	1.83	2019	1.27
B	0.89	0.20	10	22	0.14	1.90	649	3.93

It must be noted that the last term on the right side of Eq. (8.4) will be 0 due to the lack of heat loss on the centerline, where Br is 0 (Chhabra *et al.*, 2008).

Because of the heat loss, Br is not 0 in the area between the interior surface and the centerline. Given the above input data and Eq. (6.14), Br appears in the last term on the right side of Eq. (8.4) based on the relations below:

$$Br = -0.71/4\theta \quad \text{for the reference crude oil A} \quad (8.5)$$

$$Br = -2.07/4\theta \quad \text{for the reference crude oil B} \quad (8.6)$$

Under the dimensionless boundary condition, CFD calculations for each reference crude oil are based on Eqs. (8.1) through (8.4).

8.2 Convergence and Rate of Solution

A numerical solution has been developed in an attempt to determine the distribution of velocity, pressure, and temperature of the reference crude oil on a non-collocated computational grid by CFD technique according to the preceding chapter where an under-relaxation factor is used to prevent the solution divergence.

Applying the under-relaxation factor affects the convergence and rate of the solution. Lowering the factor down to 0.05 does not have a significant impact on the convergence and only reduces the rate of the solution.

By increasing the factor, it is unlikely that the discussed parameters (velocity, pressure, and temperature) can be optimized but it should be noted that with this increase, the solution does not tend to diverge. The under-relaxation factor is assumed at 0.15.

In addition to the under-relaxation factor, the number of CVs must also be optimized to prevent considerable computational error on the one hand and high computational costs on the other. It must be noted that a sub-optimal number of CVs exacerbates the error, whereas too many of them result in excess computational costs.

8.2.1 Optimal Number of CVs

To determine the optimal number of CVs, first the computational domain is discretized into an assumed number of CVs, then, it suffices to calculate the velocity of reference crude oil sample B on the centerline (**Table 8.2**). As shown in **Table 8.2**, the velocity distribution does not change significantly on the centerline by increasing CVs above a certain number.

As previously mentioned, the flow variables are dimensionless. Therefore, the dimensionless velocity at the start of the centerline (the pipe inlet) is known and equal to 1.

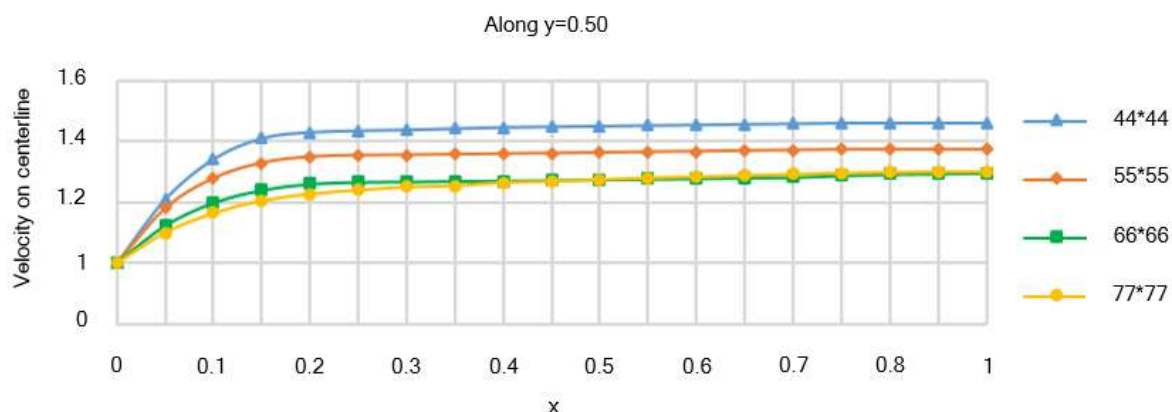


Figure 8.1 Velocity distribution of reference crude oil B on centerline from start to pipe end against number of CVs

As evident, the curves gradually unite as the number of CVs increases. Also, reaching the end of the centerline and from (about) $x=0.95$ to the next, the fluid velocity reaches its maximum value based on each of the number of CVs assumed. Moreover, the maximum velocity of reference crude oil sample B on the centerline for different numbers of CVs is as follows:

Table 8.2 Number of CVs in calculations

Reference crude oil B	Number of CVs			
	44×44	55×55	66×66	77×77
u_{\max} on centerline	1.46	1.37	1.29	1.33

Increasing the number of CVs above 66×66 does not result in considerable improvement. Therefore, to achieve higher calculation accuracy, the highest number of CVs (77×77) is taken as optimal.

8.3 Distributions of Velocity, Pressure and Temperature

What is important to researchers in the oil sector is to be able to predict the rheology of the fluid (that is its velocity, pressure, and temperature) at sections of the transmission pipeline under heat transfer between the fluid and the pipe wall.

8.3.1 Distribution of Flow Velocity

In this section, the dimensionless velocity distribution between the centerline and the inner surface of the pipe is calculated at two sections on either end, taking into account that the pipe wall temperature, affected by the ambient temperature, remains lower than the fluid temperature. The results are presented under the dimensionless initial and boundary conditions. It must be noted that in the calculations, velocity is a dimensionless parameter and its maximum value is 1 at the inlet.

8.3.1.1 Dimensionless Velocity Distribution at Pipe Inlet

As evident from **Tables 8.3-4**, in the inlet region and near the inner surface of the pipe, the flow velocity approaches 0 but increases further away, reaching 1.10 and 1.24 on the centerline ($y=0.5$) for the reference crude oils samples B and A, respectively.

The numerical results for the dimensionless velocity distribution in the flow between the inner surface and the centerline of the pipe are shown in **Table 8.3** and **Fig. 8.2** at multiple points near the inlet.

Table 8.3 Calculated results for dimensionless velocity of reference crude oil B between inner surface and centerline of pipe at multiple points in inlet region

	y					
	0	0.1	0.2	0.3	0.4	0.5
Velocity	0	1.08	1.10	1.10	1.10	1.10

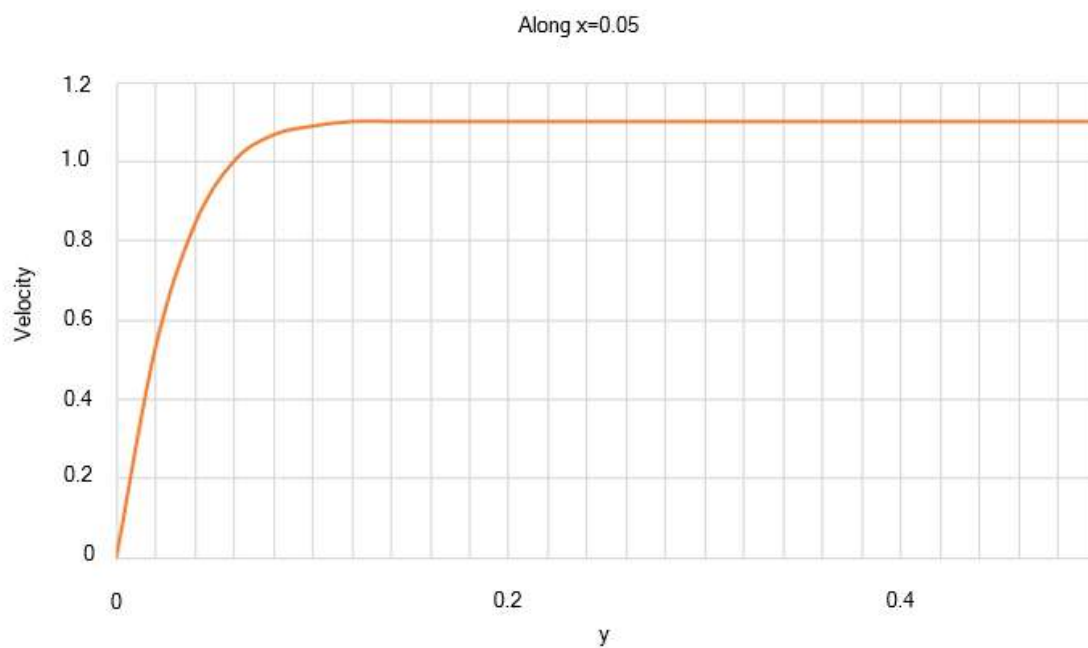


Figure 8.2 Dimensionless velocity distribution near inlet from inner surface to centerline in reference crude oil B

The numerical results for the dimensionless velocity distribution in the flow between the inner surface and the centerline of the pipe are shown in **Table 8.4** and **Fig. 8.3** at multiple points near the inlet.

Table 8.4 Numerical results for dimensionless velocity of reference crude oil A between inner surface and centerline of pipe at multiple points in inlet region

	y					
	0	0.1	0.2	0.3	0.4	0.5
Velocity	0	1.05	1.23	1.24	1.24	1.24

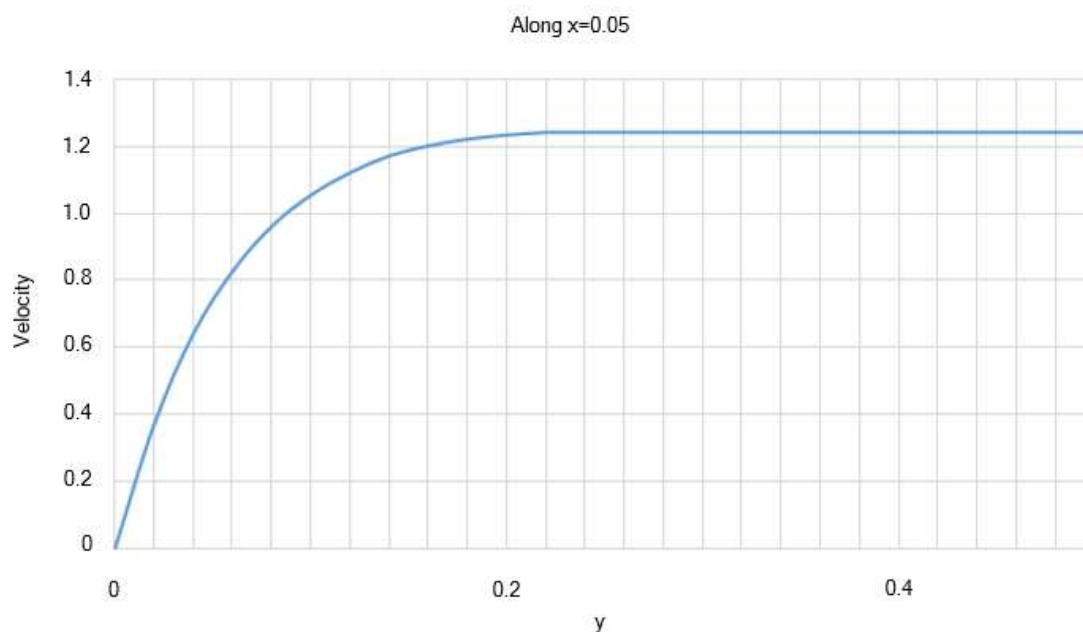


Figure 8.3 Dimensionless velocity distribution near inlet from inner surface to centerline in reference crude oil A

According to **Figs. 8.2-3**, in the vicinity of the pipe wall, the slope of the temperature curve is steeper for sample B than sample A. In other words, the velocity gradient of crude oil sample B is sharper than that of sample A in this region. Further away from the pipe wall, the velocity gradients of both crude oils samples A and B decline until vanished. The velocity gradient of reference crude oil sample B vanishes in the $y > 0.1$ region, whereas that of sample A is practically 0 for $y > 0.2$. In fact, in comparison with crude oil sample A, the flow of sample B reaches its maximum velocity at a closer distance from the pipe wall.

8.3.1.2 Dimensionless Velocity Distribution near Pipe End

As evident from **Tables 8.5-6**, at the pipe end, the flow velocity approached 0 near the inner surface of the pipe but increased further away, reaching 1.33 and 1.48 on the centerline for reference crude oils samples B and A, respectively.

The numerical results for the dimensionless velocity distribution in the flow between the inner surface and centerline of the pipe are shown in **Table 8.5** and **Fig. 8.4** at multiple points near the

pipe end.

Table 8.5 Numerical results for dimensionless velocity of reference crude oil B between inner surface and centerline of pipe at multiple points near pipe end

		y				
		0	0.1	0.2	0.3	0.4
Velocity	0	0	1.02	1.29	1.33	1.33

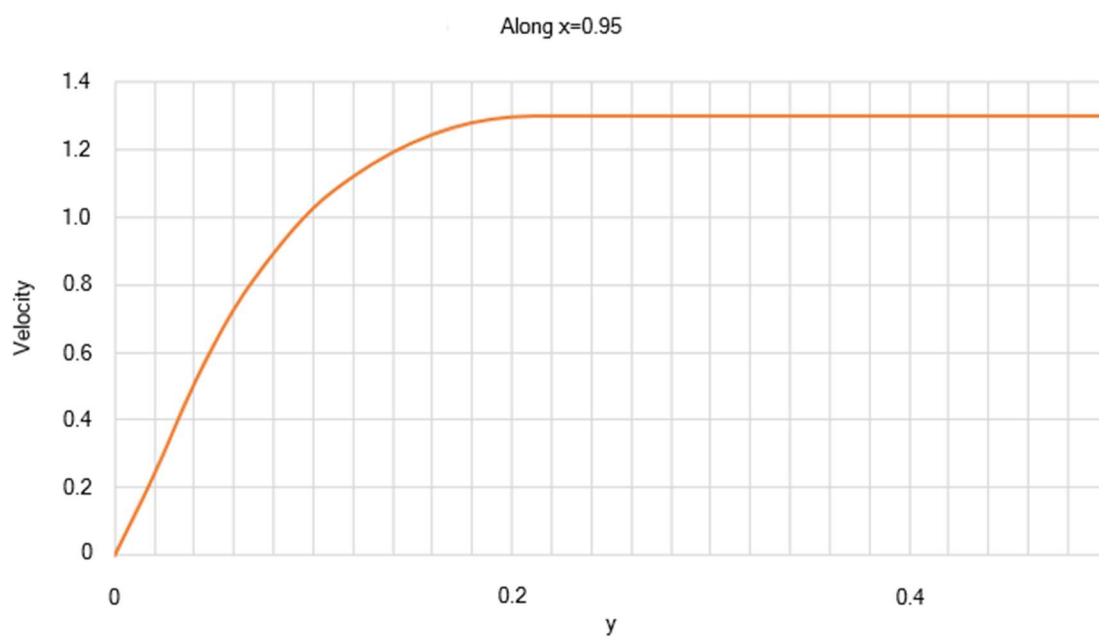


Figure 8.4 Dimensionless velocity distribution at pipe end from inner surface to centerline in reference crude oil B

The numerical results for the dimensionless velocity distribution in the flow between the wall and the centerline are shown in **Table 8.6** and **Fig. 8.5** at multiple points near the pipe end.

Table 8.6 Numerical results for dimensionless velocity of reference crude oil A between inner surface and centerline of pipe at multiple points near pipe end

	y					
	0	0.1	0.2	0.3	0.4	0.5
Velocity	0	0.92	1.42	1.48	1.48	1.48

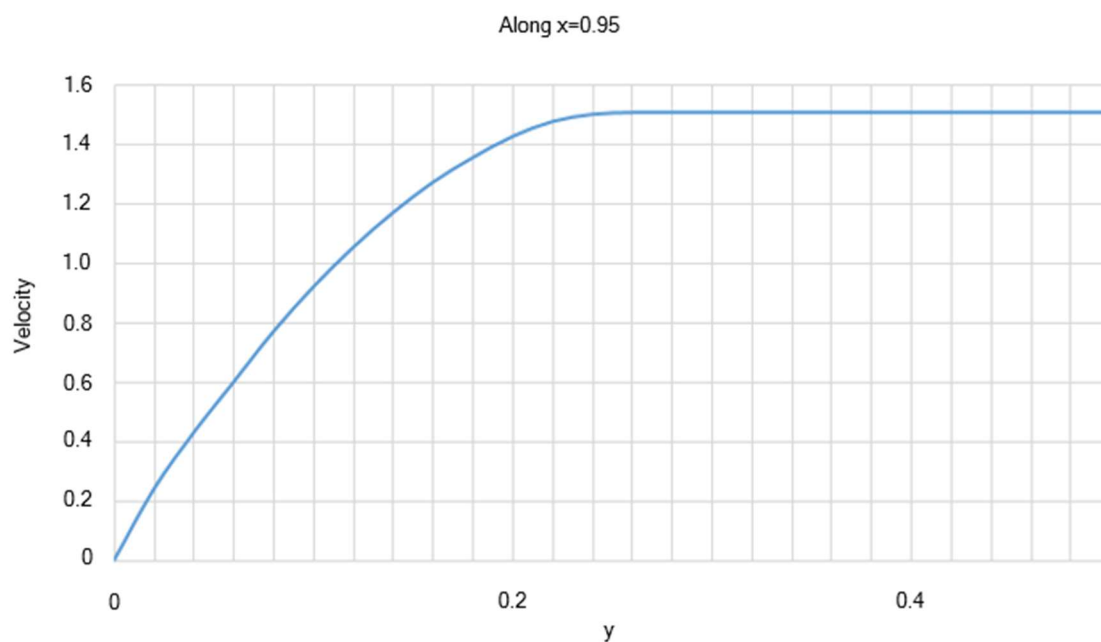


Figure 8.5 Dimensionless velocity distribution near pipe end from inner surface to centerline in reference crude oil A

According to **Figs. 8.4-5**, in the vicinity of the pipe wall, the slope of the velocity curve is slightly steeper for sample B than sample A. In other words, the velocity gradient of crude oil sample B is marginally sharper than that of sample A in this region. Further away from the pipe wall, the velocity gradients of both crude oils samples A and B decline until eliminated. The velocity gradient of reference crude oil sample B vanishes in the $y > 0.2$ region, whereas that of sample A is practically 0 for $y > 0.24$. In fact, in comparison with crude oil sample A, the flow of sample B reaches its maximum velocity in a closer distance from the pipe wall.

8.3.1.3 Effect of Flow Behavior Index and Reynolds Number on Dimensionless Velocity Distribution in Inlet Region

As evident from **Table 8.7**, at the intersection of two curves, that is $y=0.11$, the velocity gradient of crude oil sample B vanishes as the flow velocity is maximized. Meanwhile, the flow of crude oil sample A has an increasing velocity gradient at the same point.

The numerical results for the dimensionless velocity distribution for both crude oils samples A and B between the wall and the centerline are shown in **Table 8.7** and **Fig. 8.6** at multiple points in the inlet region.

Table 8.7 Comparison of numerical results for dimensionless velocities of reference crude oils A and B between inner surface and centerline of pipe at multiple points in inlet region

		y					
		0	0.1	0.2	0.3	0.4	0.5
Crude	B	0	1.08	1.10	1.10	1.10	1.10
Oil	A	0	1.05	1.23	1.24	1.24	1.24

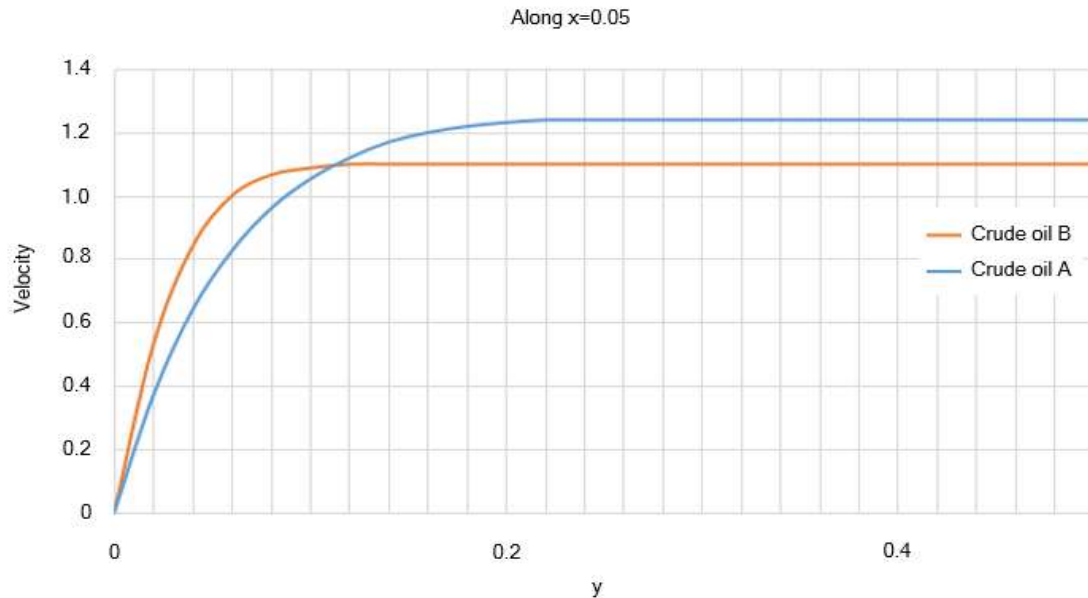


Figure 8.6 Comparison of dimensionless velocity distribution of reference crude oils A and B in pipe inlet region, between pipe wall and centerline

According to **Table 8.7** and **Fig. 8.6**, the crude oil sample A features a higher maximum velocity than the crude oil sample B in the inlet region. In this section of the pipe, the flow of crude oil sample B has a maximum velocity of 1.1 whereas the crude oil sample A features a maximum velocity of 1.24. In other words, at this cross-section, the closer the behavior index of the paraffinic crude oil to 0.5, the lower the maximum velocity of the flow. Since the Reynolds number is a function of the flow behavior index, it can be concluded that in the inlet region, the flow of the reference crude oil with higher Reynolds number also has lower velocity.

8.3.1.4 Effect of Flow Behavior Index and Reynolds Number on Dimensionless Velocity Distribution near Pipe End

As evident from **Table 8.8**, at the intersection of the two curves ($y=0.15$), the velocity gradient of crude oil sample B vanishes as the flow velocity approaches its peak. Meanwhile, the flow of crude oil sample A has an increasing velocity gradient at the same point.

The numerical results for the dimensionless velocity distribution for both crude oils samples A and B from an area in the vicinity of the pipe wall to the centerline are shown in **Table 8.8** and **Fig. 8.7** at multiple points near the pipe end.

Table 8.8 Comparison of numerical results for dimensionless velocities of reference crude oils A and B from an area in the vicinity of inner surface to centerline at multiple points at pipe end

		y					
		0	0.1	0.2	0.3	0.4	0.5
Crude	B	0	1.02	1.29	1.33	1.33	1.33
Oil	A	0	0.92	1.42	1.48	1.48	1.48

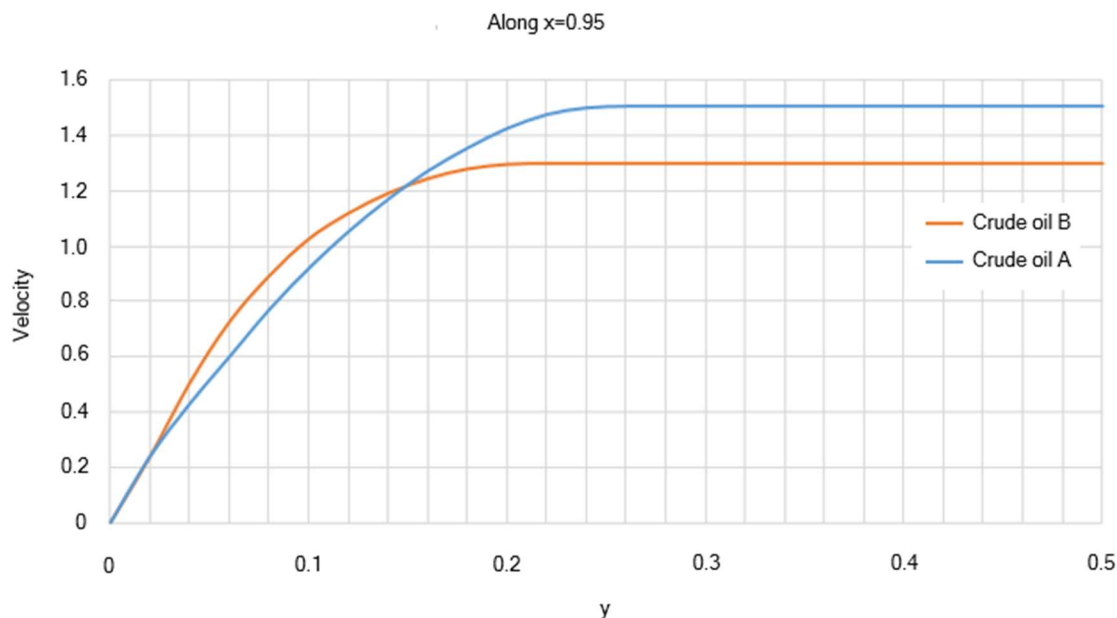


Figure 8.7 Comparison of dimensionless velocity distribution of reference crude oils A and B near pipe end, between pipe wall and centerline

According to **Table 8.8** and **Fig. 8.7**, crude oil sample A features a higher maximum velocity than sample B at the pipe end. In this pipe section, the flow of crude oil sample B has a maximum velocity of 1.33, whereas crude oil sample A features a maximum velocity of 1.48. In other words, at this cross-section, the closer the behavior index of the paraffinic crude oil to 0.50, the lower the maximum velocity of the flow. Since the Reynolds number is a function of the flow behavior index, it can be concluded that at the pipe end, the reference oil flow with higher Reynolds number also has lower velocity.

8.3.2 Dimensionless Pressure Distribution

The results from previous sections are suggestive of the decline in flow velocity in spite of the steeper velocity gradient near the inner surface of the pipe as a result of the heat transfer to the pipe wall and the higher flow velocity further toward the centerline where velocity is at maximum. Put differently, the lower flow velocity near the pipe wall is indicative of a pressure drop in the region.

The dimensionless pressure is calculated for both reference crude oils samples across the pipe and near its inner surface. It must be noted that maximum dimensionless pressure ($=1$) takes place at the inlet.

The numerical results for the dimensionless pressure in the vicinity of the pipe wall are shown in **Table 8.9** and **Fig. 8.8** at multiple points along the pipe.

Table 8.9 Numerical results for dimensionless pressure of reference crude oil B near pipe wall at multiple points along pipe

	x							
	0	0.05	0.25	0.5	0.7	0.8	0.9	1
Pressure	1	0.74	0.47	0.40	0.37	0.36	0.35	0.34

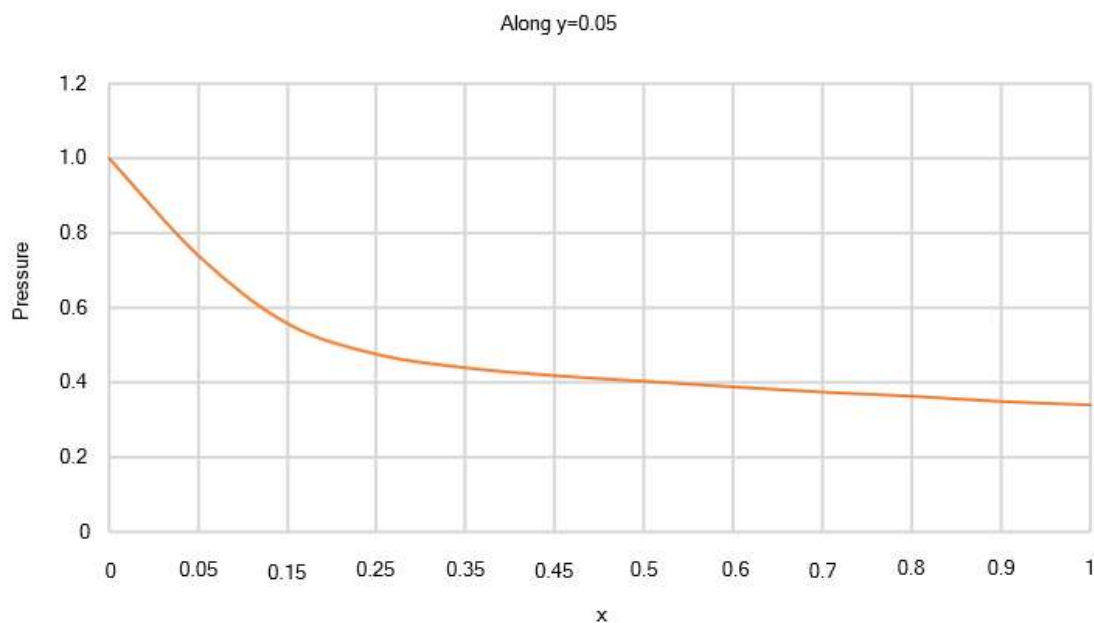


Figure 8.8 Dimensionless pressure distribution along pipe running reference crude oil B

As evident from **Table 8.9** and **Fig. 8.8**, the pressure drop in the flow is considerable for $x \leq 0.45$. The flow pressure drop decreases for $x > 0.45$ as at the pipe end, the flow pressure is minimized, reaching 0.34.

The numerical results for the dimensionless pressure in the vicinity of the pipe wall are shown in **Table 8.10** and **Fig. 8.9** at multiple points along the pipe.

Table 8.10 Numerical results for dimensionless pressure of reference crude oil A near pipe wall at multiple points along pipe

	x							
	0	0.05	0.25	0.5	0.7	0.8	0.9	1
Pressure	1	0.80	0.60	0.49	0.45	0.44	0.43	0.42

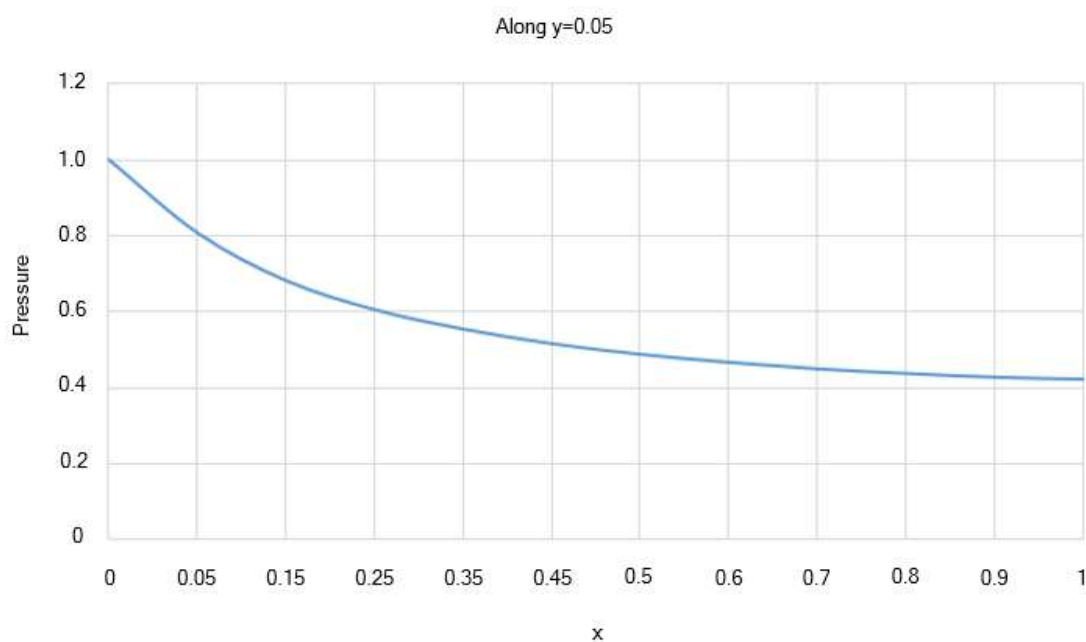


Figure 8.9 Dimensionless pressure distribution along pipe running reference crude oil A

As evident from **Table 8.10** and **Fig. 8.9**, flow pressure drop is significant for $x \leq 0.5$. The flow pressure drop decreases for $x > 0.5$ as at the pipe end, the flow pressure is minimized, reaching 0.42.

8.3.2.1 Effect of Flow Behavior Index and Reynolds Number on Dimensionless

Pressure Distribution

The numerical results for the dimensionless pressure distribution in the flow of reference crude oils samples A and B in the vicinity of the pipe wall are shown in **Table 8.11** and **Fig. 8.10** at multiple points along the pipe.

Table 8.11 Comparison of numerical results for dimensionless pressures of reference crude oils A and B in the vicinity of inner surface of pipe at multiple points along pipe

		x							
		0	0.05	0.25	0.5	0.7	0.8	0.9	1
Crude Oil	B	1	0.74	0.47	0.4	0.37	0.36	0.35	0.34
	A	1	0.80	0.60	0.49	0.45	0.44	0.43	0.42

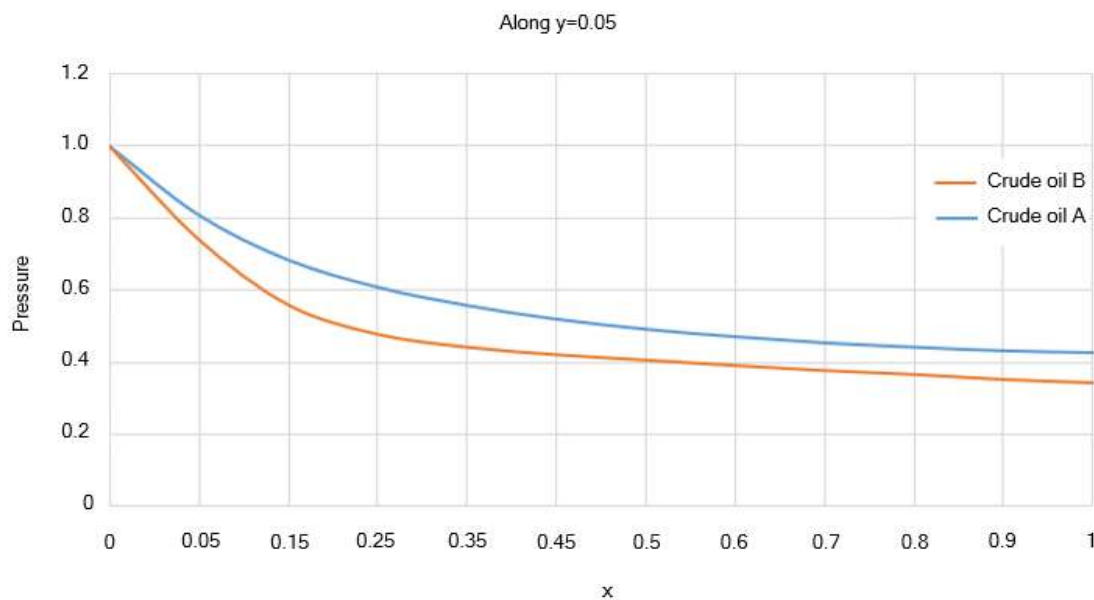


Figure 8.10 Comparison of dimensionless pressure in flow of reference crude oils A and B near wall and along pipe

As shown in **Table 8.11** and **Fig. 8.10**, the reference crude oil sample B features a more substantial pressure drop than the sample A along the pipe and in the vicinity of its wall. The pipe running the reference crude oil sample B features a pressure drop of 0.65 across its length,

whereas the pressure drop is at 0.57 across the flow of the reference crude oil sample A. In other words, the closer the behavior index of the paraffinic crude oil to 0.50, the higher the pressure drop along the pipe. Since the Reynolds number is a function of the flow behavior index, it can be concluded that in the vicinity of the pipe wall, the flow of the reference crude oil with lower Reynolds number also has a higher-pressure drop.

In fact, near the inner surface of the pipe, the pressure drop is more considerable with the reference crude oil sample B due to its higher viscosity than the sample A. Put differently, the higher viscosity of the reference crude oil sample B increases its resistance against the exerted stresses, as well as the pressure drop across the flow.

8.3.3 Distribution of Dimensionless Temperature

The dimensionless energy equation for each reference crude oil sample (Eq. (8.4)), is solved by employing the dimensionless flow velocity calculated through solving the dimensionless continuity and momentum equations in every CV of the computational grid and considering the dimensionless boundary condition. The numerical results are shown in **Figs. 8.11-18**.

Eq. (6.14) shows that $0 \leq \theta \leq 1$ also, based on the dimensionless initial and boundary conditions, θ is 0 over the inner surface of the pipe.

8.3.3.1 Dimensionless Temperature Distribution in Inlet Region and near Pipe Wall for Flow of Reference Crude Oil Sample B

As evident from **Table 8.12**, in the inlet region for $0.24 \leq y$, the temperature gradient decreases and approaches 0. In other words, the dimensionless temperature of the fluid approaches a developed state. In this region, the stresses exerted on the fluid begin to disappear with the temperature gradient vanishing.

The numerical results for the dimensionless temperature distribution in the flow of reference crude oil sample B in the vicinity of the pipe wall at multiple points along the pipe are shown in **Table 8.12** and **Fig. 8.11**.

Table 8.12 Numerical results for temperature distribution of reference crude oil sample B near pipe wall, at multiple points in inlet region

y	0	0.04	0.08	0.12	0.16	0.2	0.24
θ	0	0.12	0.29	0.45	0.57	0.65	0.67

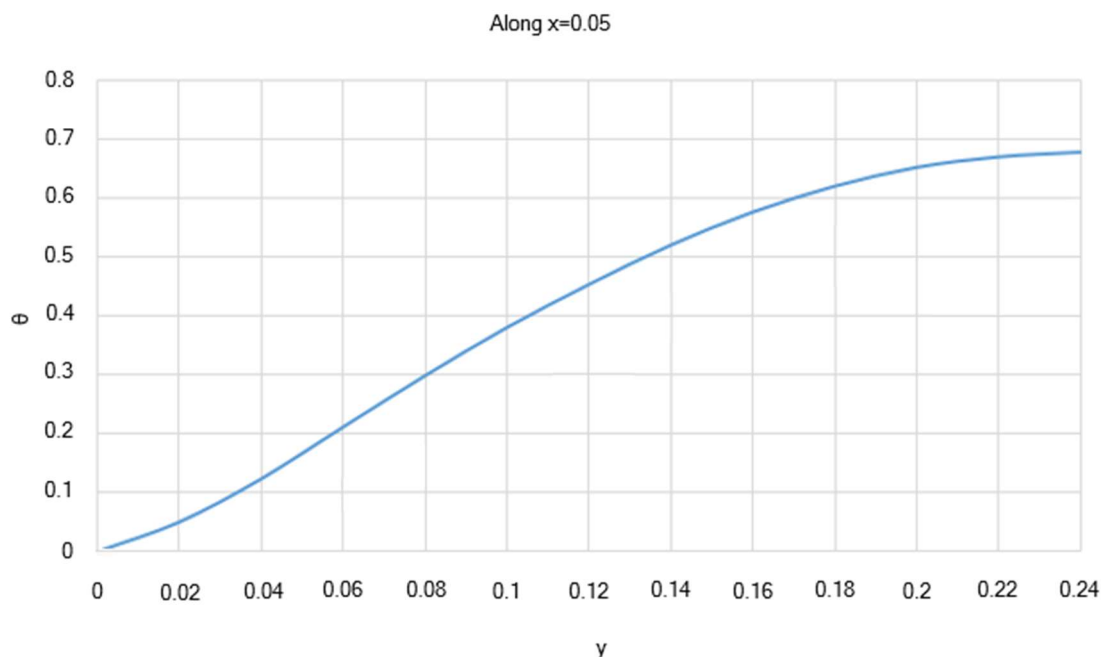


Figure 8.11 Dimensionless temperature distribution for reference crude oil sample B in inlet region and near pipe wall

Table 8.12 and **Fig. 8.11** show that, the variations range of dimensionless temperature is limited to $0 \leq \theta \leq 0.7$.

8.3.3.2 Dimensionless Temperature Distribution at End and near Pipe Wall for Flow of Reference Crude Oil Sample B

As evident from **Table 8.13**, near the pipe end in the $0.24 \leq y$ region, the temperature gradient decreases and approaches 0. In other words, the temperature of the fluid approaches a developed state. In this region, the stresses exerted on the fluid begin to disappear with the temperature gradient vanishing.

The numerical results for the dimensionless temperature distribution in the flow of reference crude oil sample B in the vicinity of the pipe wall at multiple points near the pipe end are shown in **Table 8.13** and **Fig. 8.12**.

Table 8.13 Numerical results for temperature distribution in reference crude oil sample B near pipe wall, at multiple points near pipe end

y	0	0.04	0.08	0.12	0.16	0.2	0.24
θ	0	0.06	0.19	0.34	0.48	0.55	0.58

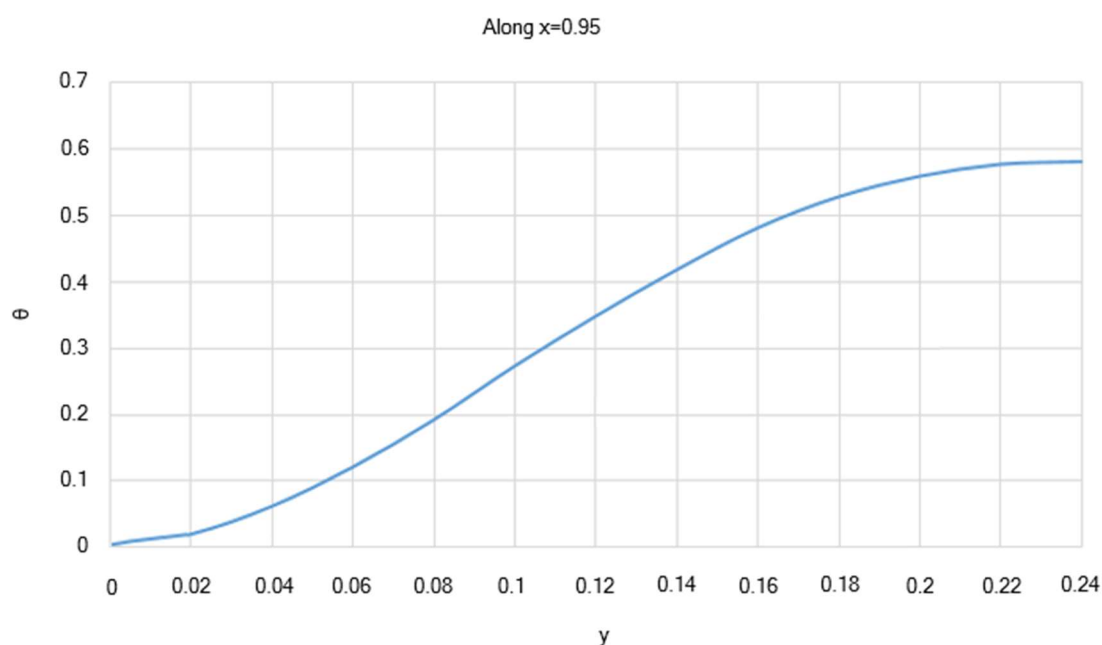


Figure 8.12 Temperature distribution for reference crude oil sample B in pipe end region and near inner surface

Table 8.13 and **Fig. 8.12** show that, the variations range of dimensionless temperature is limited to $0 \leq \theta \leq 0.6$.

8.3.3.3 Dimensionless Temperature Distribution in Inlet Region and near Pipe Wall for Flow of Reference Crude Oil Sample A

As evident from **Table 8.14**, in the inlet region for $0.24 \leq y$, the temperature gradient decreases and approaches 0. In other words, the dimensionless temperature of the fluid approaches a developed state. In this region, the stresses exerted on the fluid begin to disappear with the temperature gradient vanishing.

The numerical results for the dimensionless temperature distribution in the flow of crude oil sample A in the vicinity of the pipe wall at multiple points along the pipe are shown in **Table 8.14** and **Fig. 8.13**.

Table 8.14 Numerical results for temperature distribution of reference crude oil sample A near pipe wall, at multiple points in inlet region

y	0	0.04	0.08	0.12	0.16	0.2	0.24
θ	0	0.15	0.25	0.31	0.36	0.39	0.40

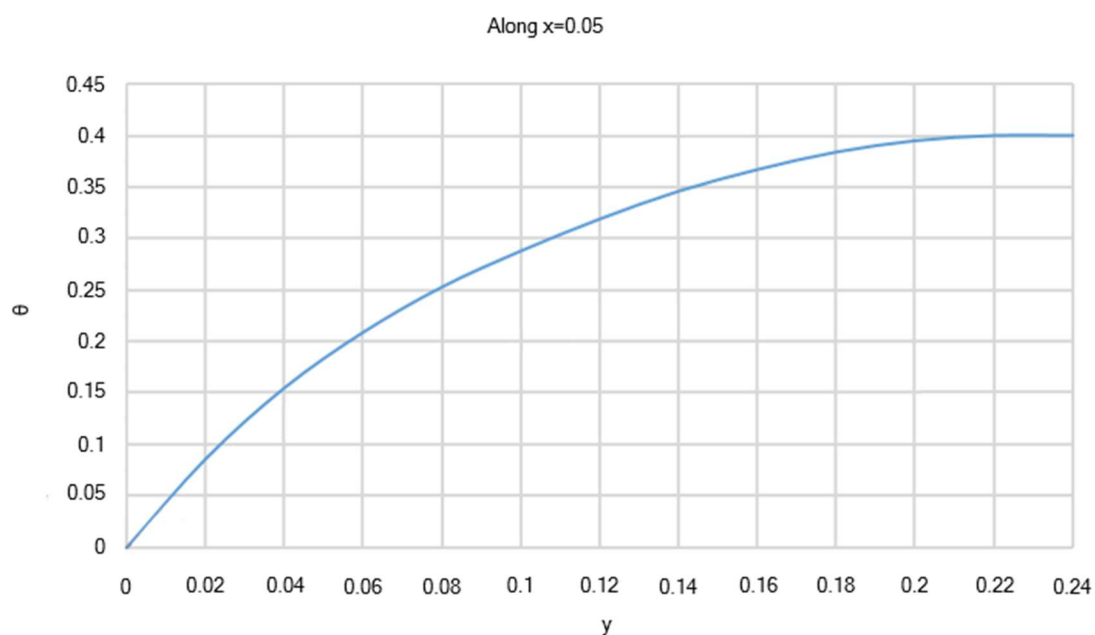


Figure 8.13 Temperature distribution for reference crude oil sample A in inlet region and near inner surface of pipe wall

Table 8.14 and **Fig. 8.13** show that, the variations range of dimensionless temperature is

limited to $0 \leq \theta \leq 0.4$.

8.3.3.4 Dimensionless Temperature Distribution in Pipe End Region and near Pipe Wall for Flow of Reference Crude Oil Sample A

As evident from **Table 8.15**, near the pipe end in the $0.24 \leq y$ region, the temperature gradient decreases and approaches 0. In other words, the temperature of the fluid approaches a developed state. In this region, the stresses exerted on the fluid begin to disappear with the temperature gradient vanishing.

The numerical results for the dimensionless temperature distribution in the flow of crude oil sample A in the vicinity of the pipe wall at multiple points near the pipe end are shown in **Table 8.15** and **Fig. 8.14**.

Table 8.15 Numerical results for temperature distribution of reference crude oil sample A near pipe wall, at multiple points near pipe end

y	0	0.04	0.08	0.12	0.16	0.2	0.24
θ	0	0.07	0.12	0.16	0.18	0.20	0.20

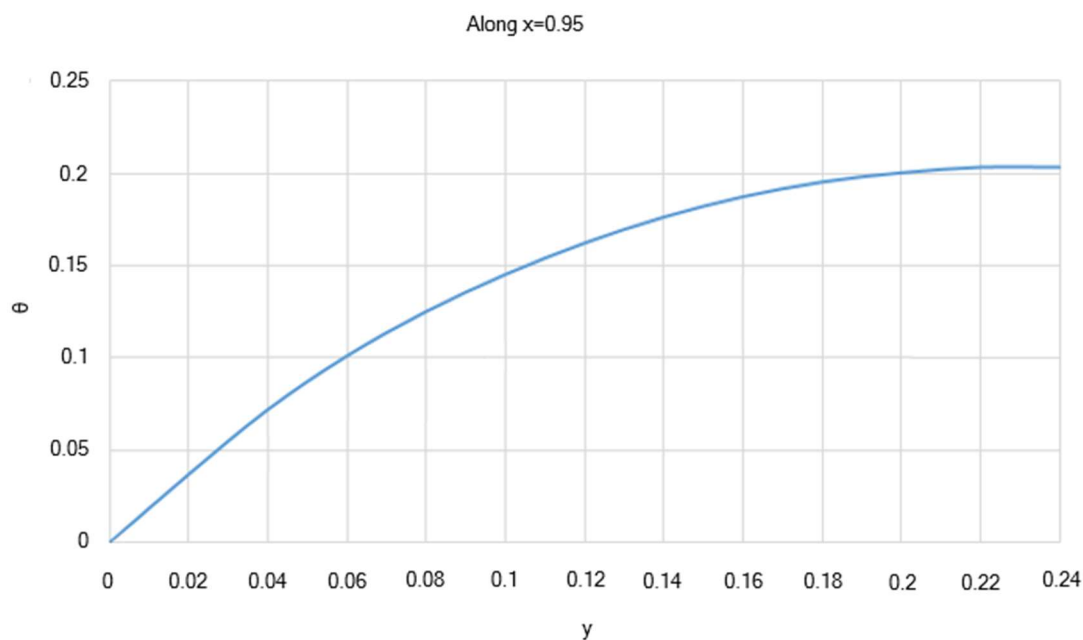


Figure 8.14 Temperature distribution for reference crude oil sample A in pipe end region and near inner surface

Table 8.15 and **Fig. 8.14** show that, the variations range of dimensionless temperature is limited to $0 \leq \theta \leq 0.2$.

8.3.3.5 Effect of Flow Behavior Index and Reynold Number on Dimensionless Temperature Distribution

As evident from **Table 8.16**, near the inlet and in the $y \leq 0.06$ region, that is between the wall and $y=0.06$ (the intersection of the two curves); the dimensionless temperature gradient is steeper for crude oil sample A than for sample B. In other words, the temperature of crude oil sample A, decreases at a lower rate than sample B in the said region.

The reference crude oil flow with a lower Reynolds number is faced with a lower temperature decrease near the inlet and in the $y \leq 0.06$ region.

The numerical results for the dimensionless temperature distribution in the reference crude oils samples A and B from an area in the vicinity of the pipe wall to the centerline at multiple points in the inlet region of the pipe are shown in **Table 8.16** and **Fig. 8.15**.

Table 8.16 Comparison of numerical results for dimensionless temperature distribution of reference crude oils A and B between inner surface and centerline of pipe at multiple points in inlet region

		y						
		0	0.04	0.08	0.12	0.16	0.2	0.24
Crude	B	0	0.12	0.29	0.45	0.57	0.65	0.67
Oil	A	0	0.15	0.25	0.31	0.36	0.39	0.40

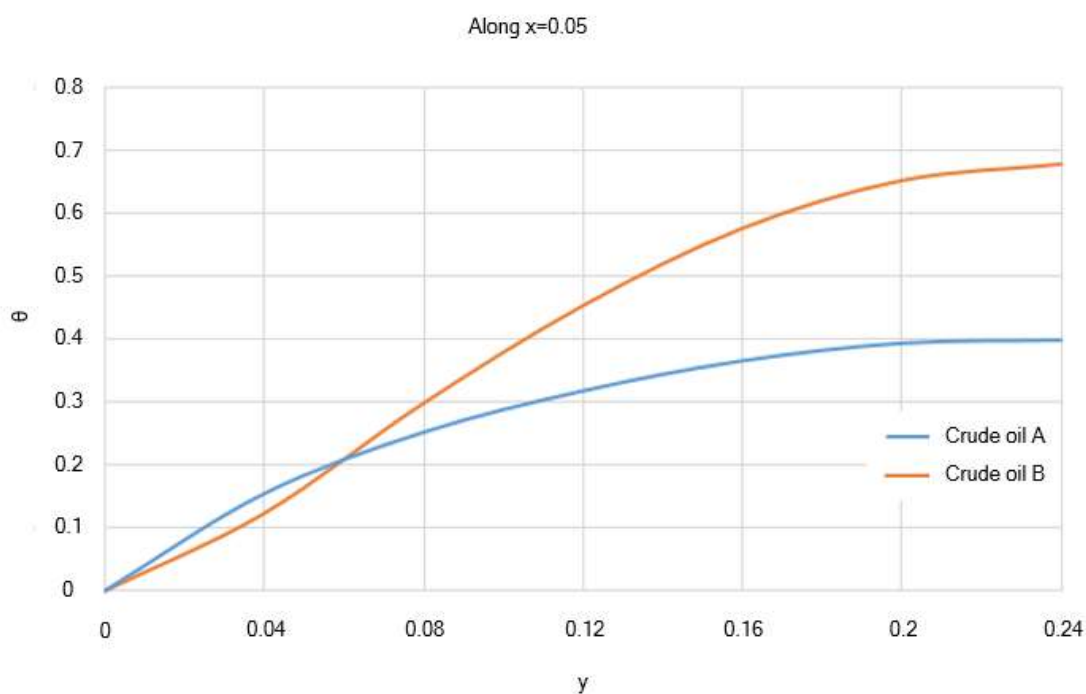


Figure 8.15 Comparison of dimensionless temperature distribution of reference crude oils A and B in pipe inlet region, between pipe wall and centerline

As shown in **Fig. 8.15**, further away from the intersection of the two curves ($0.06 < y \leq 0.24$), the dimensionless temperature gradient of reference crude oil sample B exhibits a considerable rise. In other words, the temperature gradient of reference crude oil sample B is intensified compared with that of sample A.

As evident from **Table 8.17**, near the pipe end in the $y \leq 0.05$ region, that is between the wall and $y=0.05$ (the intersection of the two curves), the dimensionless temperature gradient is steeper for reference crude oil sample A than for sample B. Put differently, the temperature of reference crude oil sample A decreases at a lower rate than sample B in the said region.

The reference crude oil flow with a lower Reynolds number is faced with a lower temperature decrease near the pipe end and in the $y \leq 0.05$ region.

The numerical results for the dimensionless temperature distribution in the reference crude oils samples A and B from an area in the vicinity of the pipe wall to the centerline at multiple points near the pipe end are shown in **Table 8.17** and **Fig. 8.16**.

Table 8.17 Comparison of numerical results for dimensionless temperature distribution of reference crude oils A and B from an area in the vicinity of inner surface to centerline at multiple points at pipe end

		y						
		0	0.04	0.08	0.12	0.16	0.2	0.24
Crude	B	0	0.06	0.19	0.34	0.48	0.55	0.58
Oil	A	0	0.07	0.12	0.16	0.18	0.20	0.20

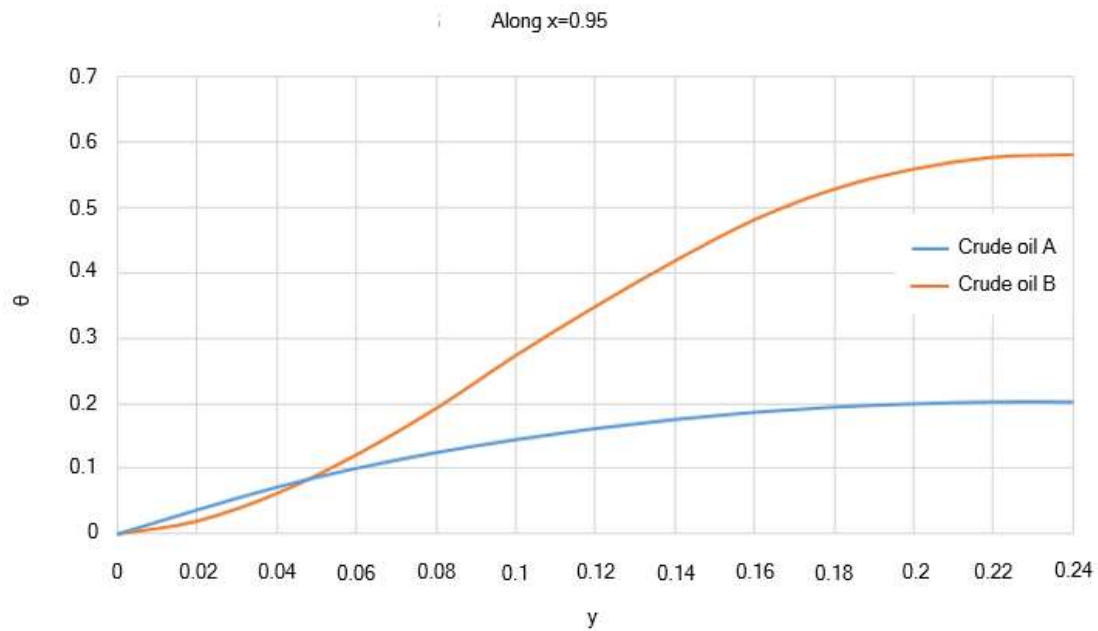


Figure 8.16 Comparison of dimensionless temperature distribution in reference crude oils A and B near pipe end, between wall and centerline

Fig. 8.16 shows that, further away from the intersection of the two curves ($0.05 < y \leq 0.24$), the dimensionless temperature gradient of reference crude oil sample B exhibits a considerable rise. In other words, the temperature gradient of reference crude oil sample B is intensified compared with that of sample A.

CHAPTER 9

Validity of Numerical Model

9.1 Introduction

The validity of the proposed model including the validity of all assumptions, input parameters, numerical methods, and the computer code written in MATLAB is determined by comparing numerical results of this study with those in the literature under the same governing conditions. Accordingly, while confirming the accuracy of numerical results, it will be shown that the proposed model benefits from the integrated capabilities of several models.

9.2 Validity of Numerical Model

The number of studies compared is limited considering structural equations, flow path, flow mechanism, flow behavior index, shear rate range and initial and boundary conditions. To examine the validity of the numerical model in this study, the results are compared with those obtained from the studies of Skelland (1967), Chhabra *et al.* (2008) and Etemad *et al.* (1994) for the same systems.

To ensure the performance of the numerical model, the fully developed flow of the reference crude oils A and B is respectively studied with the flow behavior index 0.99 and 0.5.

It is noteworthy that Skelland (1967), Chhabra *et al.* (2008) and Etemad *et al.* (1994) ignored the heat loss. As previously mentioned, the heat loss in the energy equation affects the temperature distribution of a Power-law fluid flowing in a pipe. The heat loss on the centerline is 0 and can thus be ignored ($Br=0$). In this case, the last term can be deleted from the right-hand side of the energy equation and its dimensionless form. The dimensionless numerical results of this study are compared with those in these three studies.

9.2.1 Velocity of Power-law Crude Oil

Skelland (1967) studied the maximum dimensionless velocity of a Power-law fluid on the centerline. As shown in **Table 9.1**, the numerical results of the present study on each of the reference crude oils samples at the cross-section of $x=0.95$ on the centerline, are compared with those obtained from Skelland's study.

Table 9.1 Comparison of maximum dimensionless velocities of reference crude oils A and B on centerline between present study and those obtained from Skelland's study

Reference crude oil	Present study	Skelland
A	1.48	1.5
B	1.33	1.3

Table 9.1 indicates the nearly identical results of both studies with a maximum precision of ± 0.03 . Since in the Skelland's study, the heat transfer of a fully developed flow is studied, therefore, it can be claimed that the region $0.095 \leq x$ is located in a fully developed region of fluid flow.

9.2.2 Temperature of Power-law Crude Oil

Chhabra *et al.* (2008) studied the heat transfer in a fully developed flow of a Power-law fluid. They ignored the heat loss in their study, presented the relation between thermal conductivity, specific heat capacity, pressure, and fluid velocity at each point (x, r) (Eq. (2.1)).

As stated in the literature, using Eq. (6.14) and dimensionless temperature, Eq. (2.1) can be rewritten as follows, which solved by Bird *et al.* (1987) by separation of variables for given values in the range of $0 \leq n \leq 1$.

$$u \frac{\partial \theta}{\partial x} = \frac{K}{r C_p} \frac{\partial}{\partial r} \left(r \frac{\partial \theta}{\partial r} \right) \quad (9.1)$$

Given the numerical results of the present study, the purpose is to compare the results of two studies at the cross-section $x=0.95$. Since in the Chhabra *et al.*'s study, the heat loss is ignored, so under the comparison conditions, the CVs of the computational grid is limited to the centerline. **Table 9.2** compares the dimensionless temperatures calculated by the present study with those obtained from the Chhabra *et al.*'s study.

Table 9.2 Comparison of dimensionless temperatures of reference crude oils A and B on centerline between present study and those obtained from Chhabra *et al.*'s study

Reference crude oil	Present study	Chhabra <i>et al.</i>
A	0.27	0.24
B	0.66	0.62

Table 9.2 indicates the nearly identical results of both studies with a maximum precision of +0.04. Since Chhabra *et al.* (2008) studied the heat transfer in a fully developed flow, therefore, it can be claimed that the region $0.95 \leq x$ is located in a fully developed region of the fluid flow.

9.2.3 Pressure Drop in Flow of Power-law Crude Oil

Since in the present study, the two-dimensional flow of the Power-law crude oils is considered, so the numerical results can be compared with those obtained from the Etemad *et al.*'s study for the same system.

The Etemad *et al.*'s study focuses on a certain range of the flow behavior index, within which the index 0.99 is not included. Therefore, in this section, the comparison of the results of both studies is limited to the reference crude oil B with $Re=649$.

Fig. 9.1 and **Table 9.3** compare the dimensionless pressure drop of reference crude oil B in the vicinity of the wall/plate inner surface ($y=0.05$) obtained in this study with those obtained from the Etemad *et al.*'s study in horizontal mode:

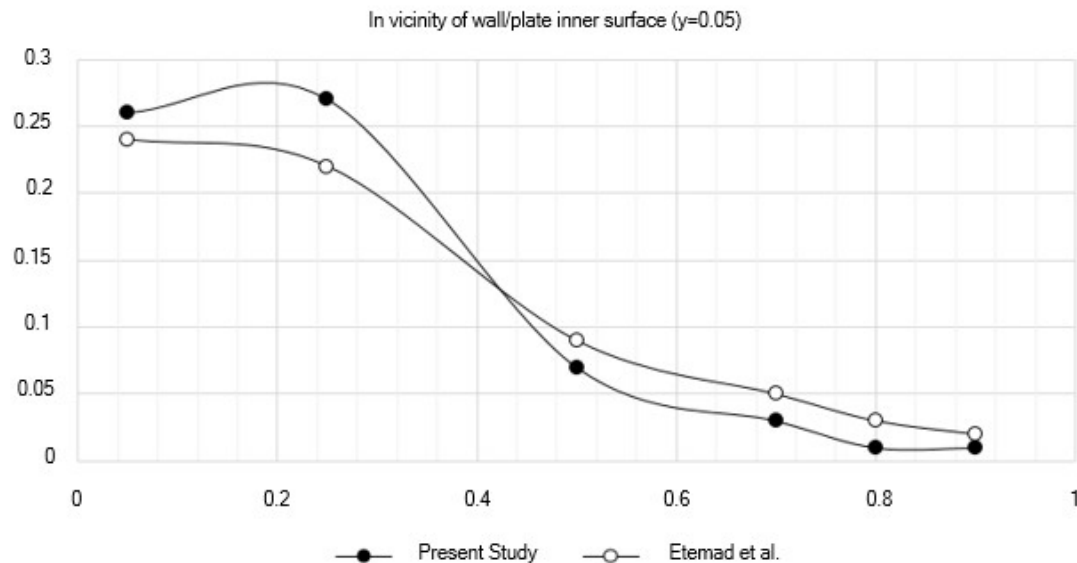


Figure 9.1 Comparison of dimensionless pressure drop of reference crude oil sample B in the vicinity of inner surface of pipe wall from present study with dimensionless pressure drop in the vicinity of plate inner surface from Etemad *et al.*'s study

Table 9.3 Comparison of dimensionless pressure drop of reference crude oil B in the vicinity of wall/plate inner surface between present study and those obtained from Etemad *et al.*'s study

	x					
	0.05	0.25	0.5	0.7	0.8	0.9
Present study	0.26	0.27	0.07	0.03	0.01	0.01
Etemad <i>et al.</i>	0.24	0.22	0.09	0.05	0.03	0.02

Table 9.3 indicates the nearly identical results of both studies with a maximum precision of ± 0.05 . As shown in **Tables 9.1-3**, the nearly identical results indicate that the proposed numerical model in the present study, has the integrated capabilities of the models proposed in all three studies of Skelland, Chhabra *et al.* and Etemad *et al.*

CHAPTER 10

Conclusions and Recommendations

Based on the available samples, two types of paraffinic crude oils with different paraffin contents (7 and 25 wt.%) were studied as reference crude oils to fulfill the followings:

- To analyze the impact of paraffin content on the rheological behavior of paraffinic crude oil
- To present a numerical model to estimate the velocity, pressure, and temperature of paraffinic crude oil flow in a pipeline
- To analyze the effect of paraffin content on the velocity, pressure, and temperature of paraffinic crude oil in different areas of the flow path
- To investigate the numerical model validity and accuracy

10.1 Experimental Conclusions

The most important experimental conclusions can be summarized as follows:

1. Based on the shear-rotary rheometry tests, there is a significant difference between the rheological behavior of reference crude oils A and B in the shear rate range of $100\text{--}600\text{ s}^{-1}$ at temperatures 22 and 26 °C.
2. The flow curves of each reference crude oil at 26 and 22 °C indicate the presence of a paraffinic network. The existence of this network at both temperatures indicates that the cloud point of each reference crude oil can be estimated at least 26 °C ($26\text{ °C} \leq \text{Cloud point}$). As temperature decreases from 26 to 22 °C, the strength of this network increases (especially in the reference crude oil B) and results in a more viscosity.
3. The shear stress increases by increasing the paraffin content.
4. The viscosity of reference crude oil B decreases by increasing the shear rate while the shear rate does not significantly change the viscosity of reference crude oil A.
5. The thermal conductivity and specific heat capacity of the reference crude oils samples are not significantly sensitive to temperature variations from 26 to 22 °C.

10.2 Numerical Conclusions

A numerical model based on the rheological behavior of reference crude oils samples, the relation between mass transfer and heat transfer and by taking into account heat loss, has been presented for calculating the velocity, pressure and temperature distributions along the pipe. This numerical model has the integrated capabilities of the models proposed in all studies of Skelland, Chhabra *et al.* and Etemad *et al.* In this regard, the most important conclusions can be summarized as follows:

- 1- To solve the numerical model, an under-relaxation factor has been used. Applying the under-relaxation factor affects the convergence and rate of the solution. Lowering the factor down to 0.05 does not have a significant impact on the convergence and only reduces the rate of solution, but by increasing the factor to 0.15, the solution tends to convergence.
- 2- The number of CVs has been also optimized to prevent considerable computational error on one hand and high computational costs on the other. To determine the optimal number of CVs, the maximum dimensionless velocity of reference crude oil B on the centerline of pipe has been calculated based on the given number of CVs (44×44 , 55×55 , 66×66 and 77×77). As the number of CVs increases, the maximum dimensionless velocity of reference crude oil sample B on the centerline gradually unite for different numbers of CVs. The increase in the number of CVs above 66×66 does not result in a considerable improvement. Therefore, the highest number of CVs (77×77) is taken as optimal.
- 3- The optimal number of CVs (77×77) has been used to discretize the computational domain, accordingly by applying a CFD technique, the desired numerical model has been solved and the dimensionless velocity, pressure, and temperature of each reference crude oil have been calculated.

If the CVs number of 44×44 is considered to discretize the computational domain, then the dimensionless velocity of reference crude oil B will be 1.46. This result, in comparison with the dimensionless velocity obtained from the Skelland's study for the same system, is faced with the precision ± 0.16 . Applying the CVs number of 44×44 results in increasing the error of result compared to conditions where the CVs number of

77×77 (with the precision +0.03) is applied.

Considering the CVs number of 44×44 to discretize the computational domain, the dimensionless pressure drop of reference crude oil B in the vicinity of the pipe wall and at the points $x=0.05$, 0.5 and 0.9 are, respectively, 0.19, 0.06 and 0.01. These results, in comparison with the dimensionless pressure drop obtained from the Etemad *et al.*'s study for the same system, are, respectively, faced with the precision -0.05, -0.03 and -0.01. Applying the CVs number of 44×44 results in increasing the error of result compared to conditions where the CVs number of 77×77 (with the precision +0.02, -0.02 and -0.01) is applied.

Considering the CVs number of 44×44, the dimensionless temperatures of reference crude oils A and B on the centerline of the pipe are, respectively, 0.19 and 0.58. These results, in comparison with the dimensionless temperature obtained from the Chhabra *et al.*'s study for the same system, are faced with the precision -0.05, and -0.04. Applying the CVs number of 44×44 results in increasing the error of result compared to conditions where the CVs number of 77×77 (with the precision +0.03 and +0.04) is applied.

- 4- For the reference crude oils samples, A and B, near the inner surface, at the pipe inlet (the flow is developing) and at the pipe end (the flow is fully developed) the dimensionless velocity approaches 0 but increases on the centerline ($y=0.50$).
- 5- In the vicinity of the pipe wall, the velocity gradient of the crude oil sample B is sharper than that of sample A in this region. Further away from the pipe wall, the velocity gradients of both reference crude oils samples A and B decline until vanished. In fact, in comparison with the reference crude oil sample A, the flow of sample B reaches its maximum velocity at a closer distance from the pipe wall.
- 6- The reference crude oil sample A features a higher maximum velocity than sample B in the inlet region. In other words, at this cross-section, the closer the behavior index of the paraffinic crude oil to 0.50, the lower the maximum velocity of the flow. Since Reynolds number is a function of the flow behavior index, so in the pipe inlet region, the flow of reference oil with higher Reynolds number has lower velocity.
- 7- The reference crude oil sample A features a higher maximum velocity than sample B at

the pipe end. In other words, at the pipe end, the flow of reference crude oil with higher Reynolds number has lower velocity.

- 8- The decline in the flow velocity in spite of the steeper velocity gradient near the inner surface of the pipe as a result of heat transfer to the pipe wall and the higher flow velocity further toward the centerline where velocity is at maximum. Put differently, the lower velocity of the flow near the pipe wall is indicative of a pressure drop in the region.
- 9- The reference crude oil sample B features a more substantial pressure drop than sample A along the pipe and in the vicinity of its wall. In other words, near the inner surface of the pipe, the flow of the reference crude oil with lower Reynolds number and higher Prantle number has a higher-pressure drop.

Near the inner surface of the pipe, the pressure drop is more considerable with the reference crude oil sample B due to its higher viscosity than the sample A. Put differently; the higher viscosity of the crude oil sample B increases its resistance against the exerted stresses, as well as the pressure drop across the flow.

- 10- In the inlet region, the dimensionless temperatures of reference crude oils samples B and A approach a developed state. In this region, the stresses exerted on the fluid begin to disappear with the temperature gradient vanishing.
- 11- Comparison of the dimensionless temperatures of reference crude oils B and A in the pipe inlet region, between the pipe wall and centerline indicates that in the $y \leq 0.06$ region, the flow of reference crude oil with lower Reynolds number and higher Prantle number is faced with the lower temperature drop.
- 12- Comparison of the dimensionless temperatures of reference crude oils B and A near the pipe end, between the wall and centerline indicates that in the $y \leq 0.05$ region, the flow of reference crude oil with lower Reynolds number and higher Prantle number is faced with the lower temperature drop.

Based on this study, it is recommended to:

1. Experimental study on the rheological behavior of reference crude oils in a wider temperature range.

2. Estimation of Power-law indices for reference crude oils (in terms of paraffin content) at several temperatures and determination of a suitable regression relation for estimating these indices at a given temperature.
3. Error / statistical analysis according to Chapter 3 results.
4. Using Herschel-Bulkley and Bingham plastic equations to study the rheological behaviors of reference crude oils in pipe and comparison of results with those obtained in this study.
5. Study of unsteady flow of reference crude oils, i.e. fluid flow kinetics in pipe.
6. Numerical modeling of reference crude oils flow in pipe in Polar or Spherical coordinates.

REFERENCES

- Abulencia, J.P. and Theodore, L., 2009, Fluid flow for the practicing chemical engineer (Essential Engineering Calculations Series). John Wiley & Sons, New York.
- Adeyanju, O. and Oyekunle, L., 2012, An experimental study of rheological properties of Nigerian paraffinic crude oil. *Petroleum Science and Technology*, 3:1102-1111.
- Agarwal, K.M., Purohit, R.C., Surianarayanan, M., Joshi, G.C. and Krishna, R., 1989, Influence of waxes on the flow properties of Bombay high crude. *Fuel*, 68:937-939.
- Agrawal, K.M., Purohit, R.C. and Joshi, G.C., 1994, Rheological properties of Bombay high crude oil in relation to its n-alkane components. *Fuel Science and Technology Intl.*, 12: 9.
- Ajayi, E.O., 2013, Evaluation of methods of controlled wax deposition and loosening for oil and gas production. Norwegian university of science and technology: Trondheim, Norway, 143-152.
- Ajienka, J.A. and Ikoku, C.U., 1991, The effect of temperature on the rheology of paraffinic crude oils. SPE 23605 Technical Publications.
- Ajienka, J.A. and Ikoku, C.U., 1995, Criteria for the design of paraffinic crude oil pipelines: maximum pump (horse power) Pressure requirement. *J. Pet. Science. Eng.*, 13: 87-94.
- Aksel, Nuri and Heymann, 2007, Non-Newtonian flows. Springer handbook of experimental fluid mechanics. Berlin: Springer Science+Business Media, Inc, ISBN 978-3-540-25141-5.
- Al-Fariss, T.F., Jang, L.K., *et al.*, 1993, A new correlation for the viscosity of paraffin oils. *J. Pet. Sci. Eng.*, 10:139-44.
- Al-Zahrani, S.M., 1977, A generalized rheological model for shear thinning fluids. *J. Pet. Sci. Eng.*, 17: 211-215.
- Al-Zahrani, S.M. and Al-Fariss, T.F., 1998, A general model for the viscosity of paraffin oils. *Chem. Eng. Proc.*, 37: 433-437.
- Alboudwarej, H., Kempton, E. and Huo, Z., 2006, Flow-assurance aspects of subsea systems design for production of paraffinic crude oils. SPE Annual Technical Conference, San Antonio, Texas, U.S.A.
- Ansari, A.M., Sylvester, N.D., Sarica, C., Shoham, O. and Brill, J.P., 1994, A comprehensive mechanistic model for upward two-phase flow in wellbores. *SPE J. Production and*
- Assael, M.J., Dix, M., Lucas, A. and Wakeham, W.A., 1981, Absolute determination of the

- thermal conductivity of the noble gases and two of their binary mixtures. J. Chem. Soc., Faraday Trans. 77(1): 439-464.
- Backhurst, J.R., Harker, J.H., Coulson, J.M. and Richardson, J.F., 1999, Chemical engineering: Fluid flow, Heat transfer and mass transfer .Elsevier, 1(6): 928.
- Barnes, H.A., Hutton, J.F. and Walters, K., 1991, An introduction to rheology. Elsevier: Amsterdam.
- Barnes, H.A. , 1999, The yield stress review. J. non-Newtonian Fluid Mech, 81: 133-178.
- Beggs, H.D. and Robinson, J.R., 1975, Estimating the viscosity of crude oil systems. JPT, 1140-1141.
- Bejan, A. and Sciubba, E., 1992, The optimize spacing of plates cooled by forced convection. internat, J. Heat mass transfer, 35: 3259-3262.
- Bennison, T., (2-4 Dec)1998, Prediction of heavy oil viscosity. IBC Heavy Oil Field Development Conference, London.
- Bird, R.B., Armsrtong, R.C. and Hassager, O., 1987, Dynamics of polymeric liquids, Vol. 1, Fluid Dynamics, 2nd edition, Wiley New York.
- Bishop, A.N., Philip, R.P., Allen, J. and Ruble, T.E., 1995. Donoslia-San Sebastian, Spain.
- Brill, J.P. and Beggs, H.D., 1988, Two-phase flow in pipes. University of Tulsa, 6th. Ed.
- Brill, J.P. and Mukerjee, H., 1999, Multiphase flow in wells. SPE Monograph.
- Brodkey, R.S. and Hershey, H.C., 1988, Transport phenomena: A unified approach. Brodkey Publishing, 333, ISBN 978-0-9726635-9-5.
- Chandaa, D., Sarmaha, A., Borthakura, R A., Raoa, K.V., Subrahmanyama, B. and Das, H.C., 1998, Combined effect of asphaltenes and flow improvers on the rheological behavior of Indian paraffinic crude oil. Fuel, 77 (11): 1163-1167.
- Chang, C., Boger, D.V. and Nguyen, Q.D., 1998, The yielding of paraffinic crude oils. Industrial & Engineering Chemistry Research, 37(4): 1559-1551.
- Chang, P.Y., *et al.*, 1998, Heat transfer mechanism for non-Newtonian Fluid 2:1 Rectangular duct. Int. J. Heat Transfer 41: 3841-3856.
- Chhabra, R.P. and Richardson, J.F., 2008, Non-Newtonian flow and applied rheology. R.P.C.F. Richardson, Editor., Butterworth-Heinemann: Oxford,1-55.
- Clifford, A.A., Kestin, J., Wakeham, W.A., 1980, Further contribution to the theory of the transient hot-wire technique for thermal conductivity measurements. Physica, 100 (2): 370-374.
- Coulson, J.M., Richardson, J.F., 1999, Chemical Engineering. Elsevier, 1(6), ISBN 978-0-

7506-4444-0.

- De Castro, C.A. Nieto, Calado, J.C.G., Wakeham, W. A., 1976, An apparatus to measure the thermal conductivity of liquids. *Journal of Physics E: Scient. Inst.* 9: 1073-1080.
- De Castro, C.A. Nieto, Calado, J.C.G., Wakeham, W. A., 1977, Absolute measurements of the thermal conductivity of liquids using a transient hot-wire technique. Cezarilanyan, A. ed. *Proceedings of the seventh symposium on thermophysical properties*, Gaithersburg, Maryland, New York, ASME, 730-738.
- De Groot, J.J., Kestin, J., Sookiazian, H., 1974, Instrument to measure the thermal conductivity of gases. *Physica*, 75: 454-482.
- De Groot, J.J., Kestin, J., Sookiazian, H., 1978, The thermal conductivity of four monatomic gases as a function of density near room temperature. *Physica*, 92: 117-144.
- Dutta, A. and Mashelkar, R.A., 1987. *Adv. Heat Transf*, 18:161.
- Edwin, N., Stewart and Warren, E., 2007, *Transport phenomena*. Wiley. ISBN 9780470115398. OCLC 288965242.
- El-Gamal, I.M., 1998, Combined effects of shear and flow improvers: The optimum solution for handling paraffin crudes below pour point. *Colloids and Surfaces A: Physicochemical and Engineering Aspects*, 135 (1–3): 283-291.
- El-Gamal, I.M., Gad, E.A.M., 1998, Low temperature rheological behavior of Umbarka paraffin crude and influence of flow improver. *Colloids and Surfaces A: Physicochemical and Engineering Aspects*, 131(1–3): 181-191.
- Elsharkawy, A.M., Al-Sahhaf, T.A., Fahim, M.A. and Al-Zabbai, W., 1999, Determination and prediction of wax deposition from Kuwaiti crude oils. SPE Paper No. 54006, Presented at Latin American and Caribbean Oil Engineering Conference held in Caracas, Venezuela.
- Ely, J. F. and Hanley, J. M., 1981, Prediction of transport properties. 1. Viscosity of fluids and mixtures. *Industrial & Engineering Chemistry Fundamentals*, 20: 323-332.
- Etemad, S. Gh., Mujumadar, A.S. and Huang, B., 1994, Effects of variable viscosity on laminar convection heat transfer of a Power-law fluid. *Int. J. Heat Mass Transfer*, 38 (2): 2225-2238.
- Fernandez-Lozano, J.A. and Rodriguez, Y.M., 1984, Rheological and conductometric properties of two different crude oils and of their fractions. *Industrial & Engineering Chemistry Process Design and Development*, 23(1), DOI: 10.1021/i200024a019.
- Flores, A. F., 1991, Heat transfer to Power-law fluids flowing in pipes ducts with viscous

- heat generation. *Chemical Eng. Science*, 113:837-842.
- Ford, P.E., Ells, J.W., Russel, R.J., 1965, Pipelining high pour point crude. *Oil Gas J.*, 10: 107-109.
- Ford, P.E., Ells, J.W., Russel, R.J., 1965, Pipelining high pour point crude. *Oil Gas J.*, 10: 183-189.
- Gilby, G.W., 1993, *Chemicals in the oil industry*, 108-113.
- Glaser, O., 1980, Generalized Pressure–Volume–Temperature correlations for crude oil system. *Journal of Oil Technology*, 32 (5): 785-795.
- Guo, L., Wang, Y., Shi, S., Yu, X. and Chen, X., 2015, Study on properties of paraffinic crude oil based on hysteresis loop area. *Engineering*, 7 (7): 469.
- Haarman, J.W., 1969. Thesis. Technische Hogeschool, Delft.
- Hamilton, R.L. and Crosser, K., 1962, Thermal conductivity of heterogeneous two-component systems. *Industrial & Engineering Chemistry Fundamentals*, 1:187-191.
- Hammami, A., Ratulowski, J., Coutinho, J.A.P., 2003, Cloud points: Can we measure or model them. *Oil Science and Technology*, 21(3-4): 345-358.
- Hamouda, A.A. and Davidsen, S., 1995, An approach for simulation of paraffin deposition in pipelines as a function of flow characteristics with a reference to Teesside oil. *Society of Oil Engineers, SPE28966*, 213-224.
- Hartenett, J.P. and Kostic, M., 1989, Heat transfer to Newtonian and non-Newtonian fluids in rectangular ducts. *Adv. Heat transfer*, 19:247-356.
- Healy, J.J., De Groot, J.J. and Kestin, J., 1976, The theory of the transient hot-wire method for measuring thermal conductivity. *Physica*, 82(2): 392-408.
- Iktisanov, V.A. and Sakhabutdinov, K.G., 1999, Rheological studies of paraffin-base oil at different temperatures. *Colloid Journal*, 61(6):719-722.
- Irani, C. and Zajac, J., 1982, Handling of high pour point west african crude oils. *J. Pet. Technol.*
- Jaafar, A., Bhaskoro, P., Sariman, M. and Rozlee, R., 2014, Rheological investigation on the effect of shear and time dependent behavior of paraffinic crude oil. In *MATEC Web of Conferences*. EDP Sciences.
- Johnson, S.E., Svrcek, W.Y., Mehrotra, A.K., 1987, Viscosity prediction of Athabasca bitumen using the extended principle of corresponding states. *Ind. Eng. Chem. Res.*, 26: 2290.
- Kandwal, V.C., Agrawal, K.M., Nautiyal, P. and Khan, H. U., 2000, Paraffin deposition and

- viscosity temperature behavior of Assam crude oil. *Pet. Sci. Tech*, 18(7,8): 755-769.
- Kané, M., Djabourov, M. and Volle, J. L., 2004, Rheology and structure of paraffinic crude oils in quiescent and under shearing conditions. *Fuel*, 83(11,12): 1591-1605.
- Kaya, A.S., 1998, Comprehensive mechanistic modeling of two-phase flow in deviated wells. MS Thesis. University of Tulsa. Tulsa, OK.
- Kestin, J., Paul, R., Clifford, A.A., Wakeham, W.A., 1980, Absolute determination of the thermal conductivity of the noble gases at room temperature up to 35 MPa. *Physica*, 2: 349-369.
- Kestin, J., Wakeham, W.A.A., 1978, Contribution to the theory of the transient hot-wire technique for thermal conductivity measurements. *Physica*. 92A(1,2): 102-116.
- Khan, H.U., Agrawal, K.M., Anwar, M., Nautiyal, S.P. and Rawat, B.S., 1998, Role of composition on the viscosity and shear stress temperature behavior of some lube oil base stocks. *Pet. Sci. Tech.*, 16(1,2).
- Kirsanov, E.A., Remizov, S.V., 1999, Application of the Casson model to paraffinic crude oil. *Rheol Acta*, 38: 172.
- Li, H., Zhang, J., Song, C. and Sun, G., 2015, The influence of the heating temperature on the yield stress and pour point of paraffinic crude oils. *Journal of Oil Science and Engineering*, 135: 476-483.
- Lira-Galeana, C., Firoozabadi, A. and Prausnitz, J.M., 1996, Thermodynamics of wax precipitation in oil mixtures. *AIChE Journal*, 42(1): 239-248.
- Lorenzini, G., Biserni, C., 2004, Numerical investigation on mixed convection in non-newtonian fluid inside a vertical duct. *International Journal of thermal sciences*, 43: 1153-1160.
- Lorge, O., Djabourov, M. and Brucy, F., 1997, Crystallisation and gelation of paraffinic crude oils under flowing conditions. *Oil & Gas Science and Technology*, 52(2): 235-239.
- Madlener, K., Frey, B. and Ciezki, H. K., 2009, Generalized Reynolds number for non-Newtonian fluids. *EDP Sciences*, 1: 237-250.
- Majeed, A., Bringedal, B. and Overa, S., 1990, Model Calculates Wax Deposition for North Sea Oils. *Oil Gas J*, 63-69.
- Mani, N., 1971, Precise determination of the thermal conductivity of fluids using absolute transient hot-wire technique. Thesis. University of Calgary. Calgary, Alberta, Canada.
- Menashe, J., Wakeham, W.A., 2010, Absolute measurements of the thermal conductivity of

- liquids of pressures up to 500 MPa. *Berichte der Bunsengesellschaft für physikalische Chemie*, 86(6):541-545.
- Mishra, P. and Tripathi, G., 1971. *Chem. Eng. Sci.*, 26:915.
- Mozes, G., Freund, M., Csikos, R., Keszthelyi, S, 1982, Chemical crystallographical, and Physical Properties of liquid paraffins and paraffins waxes, in paraffin product, properties, technologies, applications. Mozes, G, ED, Elsevier Scientific, New York.
- Musser, BJ. and Kilpatrick, P.K., 1998. *Energy & Fuels*, 12:715-721.
- Naderi, G., Shokoohi, S., 2014, *Rheology*, 199.
- Oliemans, R.V.A., 1994, Multiphase science and technology for oil / gas production and transport. SPE Paper 27958. University of Tulsa Centennial Oil Engineering Symposium.
- Parsoil company: <http://www.parsoilco.com/fa/home/index.asp>.
- Patankar, S.V., 1980, Numerical heat transfer and fluid flow. Mc Graw-Hill.
- Pedersen, K.S., Christensen, P.L., 2006, Phase behavior of oil reservoir fluid , 82, 230 and 233.
- Pedersen, K.S., Fredenslund, Aa., 1987, An improved corresponding states model for the prediction of oil and gas viscosities and thermal conductivities. *Chem. Eng. Sci.*, 42: 182-186.
- Pedersen, K.S., Skovborg, H.P., Ronningsen, H.P., 1991, Wax precipitation from north sea crude oil. *Energy fuels*, 5:924-932.
- Pittman, J.F.T., 1968, Fluid thermal conductivity determination by the transient line source method. Thesis. University of London.
- Pontes., J., 2012, Computational heat and mass transfer – CHMT 2001-. Editora E-papers, 113, ISBN 978-85-87922-44-1.
- Reid, R.C., Prausnitz, J.M. and Sherwood, T.K., 1977, The properties of gases and liquids. McGraw-Hill, New York.
- Rønningsen, H.P., Bjørndal, B., Hansen, A.B. and Pedersen, W.B., 1991, Crystallization and dissolution temperatures and Newtonian and non-Newtonian flow properties. *Energy & Fuels*, 5: 895-908.
- Ryan, N.W. and Johnson, M.M., 1959. *AIChE J.*, 5 : 433.
- Silva, J.B, 1992, Analytical solutions to simultaneously developing laminar flow inside channels. *Int. J. Heat Transfer*, 887-895.
- Singh, P., Venkatesan, R., Fogler, H.S. and Nagarajan, N., 2000, Formation and aging of

- incipient thin film wax-oil gels. *AJChE Journal*, 46 (5):1059-1074.
- Skelland, A. H. P., 1967, *Non-Newtonian flow and heat transfer*. Wiley, New York.
- Srivastava, S.P.J., 1993. *Phys Chem Solids*, 54:639-648.
- Togrul, H. and Arslan, N., 2004, Mathematical model for prediction of apparent viscosity of molasses. *Journal of Food Engineering*, 62(3): 281-289.
- Touloukian, Y.S., 1970, *Thermophysical properties of matter*. IFI/Plenum, New York, Washington, Vols.2 and 3.
- Turner, W.R., 1971. *Ind Eng Chem Prod Res Dev*, 10:238-246.
- Van Der Geest, C., Guersoni, V.C.B., Merino-Garcia, D. and Bannwart, A.C., 2015, A modified elasto-viscoplastic model for two commercial gelled paraffinic crude oils. *Rheologica Acta*, 54(6): 545-561.
- Venkatesan, R., Singh, P., Fogler, H.S., 2002, Delineating pour point and gelation temperature of paraffinic crude oils. *SPE Journal*, 7(4), DOI: 10.2118/72237-PA.
- Wardhaugh, L.T. and Boger, D.V., 1991, Flow characteristics of paraffinic crude oils: Application to pipeline design. *AICHE. J.*, 37 (6):871-885.
- Won, K.W., 1986, Continuous Thermodynamics for solid-liquid equilibria: Wax formation from heavy hydrocarbon mixtures fluid phase equilib, 30: 265-279.
- Xiao, J.J., Shoham, O. and Brill, J.P., 1990, A comprehensive mechanistic model for two-phase flow in pipelines. SPE 20631 presented at the SPE Annual Technical Conference and Exhibition, New Orleans, LA.
- Yu, W., France, D.M., Routbort, J.L., Choi, S., 2008, Review and comparison of nanofluid thermal conductivity and heat transfer enhancements. *Heat Transfer. Eng.*, 29:432–60.
- Zeller, R. C. and Pohl, R. O., 1971, Thermal conductivity and Specific heat of noncrystalline solids. *Phys. Rev. B*, 4, 2029–2041.
- Zhang, J. and Liu, X., 2008, Some advances in crude oil rheology and its application. *Journal of Central South University of Technology*, 15: 288-292.
- Zuo, J.Y., Zhang, D.D. and Ng, H.J., 2001, An improved thermodynamic model for wax precipitation from oil fluids. *Chem. Eng. Sci.*, 56:6941-6947.